RADAR ANALYSIS AND MAPPING OF MIGRATORY BIRD STOPOVER USE IN NORTH CAROLINA

FINAL REPORT FOR COOPERATIVE AGREEMENT WM-0293

Prepared for
North Carolina Wildlife Resources Commission

Jeffrey Buler, Assistant Professor
Jaclyn Smolinsky, Research Associate
&
Kimberly Rivera, Undergraduate Student

Department of Entomology & Wildlife Ecology
University of Delaware
Newark, DE 19716

May 2016

Table of Contents

List of Figures

List of Tables

EXECUTIVE SUMMARY

Identifying important stopover habitats and areas for migratory birds in North Carolina and how bird stopover distributions have changed over time will contribute to several conservation priorities outlined in the North Carolina Action Plan. A unique tool in assessing migratory bird habitat use is the national network of weather surveillance radars. These radars detect nocturnally-migrating birds as they depart en masse from stopover areas and comprehensively measure their stopover distributions at the ground over broad spatio-temporal scales. Our objectives were to use data from 5 weather surveillance radars that cover portions of North Carolina to 1) map the spatio-temporal patterns of stopover use by birds within North Carolina during seven spring and five fall seasons between early years (2000-2003) and late years (2013-2015), 2) develop statistical models to predict stopover site use in areas not sampled by the radars and describe stopover habitat relationships, and 3) assess changes in migrant distributions over the last decade. Overall, 17.6% (748/4260) of radar sampling days were suitable for determining migrant landbird densities. For each suitable radar sampling day, we used instantaneous measures of vertically-integrated radar reflectivity (VIR; the relative emigrant density in the air from the ground to 1.5 km above ground) interpolated in time to the peak of bird nocturnal flight exodus to map relative emigrant bird stopover densities. We classified bird stopover use by the seasonal mean emigrant density (mean VIR) and coefficient of variation of emigrant density (CV VIR) to identify areas of consistently-high emigrant density. Radars provided direct comprehensive observations of the spatio-temporal patterns of stopover use of migrating birds across nearly a quarter of the land area within the state of North Carolina. We used Generalized Additive Models (GAM) to predict mean and CV VIR for each season by time period. Modeling analysis revealed that consistently high emigrant stopover densities occurred in landscapes with greater forest cover (pine and hardwood), greater urban cover, less agriculture, and with greater proximity to the coast. Habitats with greater NDVI and canopy height harbored greater emigrant densities. These observations can serve as a baseline of the status and aggregate distribution of migratory landbird species, many of which are of conservation concern, and may facilitate long-term monitoring and fill critical data gaps.

Between 2001 and 2011, the net change in land use/cover was 7.8% of the total land area within 100 km of the five radars. Landscape change was primarily due to urbanization, deforestation and afforestation. Across the state, emigrant stopover density changes between were most closely related to geographical location rather than landscape-scale or local-scale land cover changes. Migrant densities have increased at both the extreme western portion of the state and in areas close to the coast. Additionally, migrant densities have declined in both seasons in the southern portion of the state. Declines in emigrant density were also observed with increased urbanization and deforestation. Future research should be focused on better understanding changes in migrant distributions over longer time scales (e.g., the radar data archive began in1995 for most radars) and with greater frequency (e.g., annually) within landscapes with high turn-over (i.e., regions with active timber industry) in order to address questions about behavioral shifts in habitat use and population regulation patterns in response to landscape-change, weather, and climate drivers.

INTRODUCTION

Most conservation efforts for migratory landbirds in North America have focused on protecting or enhancing breeding habitat. For many species, however, migration may be the period in the annual cycle when mortality is highest (e.g., Sillett and Holmes 2002) and can limit their populations (Newton 2004). Identifying important stopover sites, areas where birds rest and refuel along their route, is a critical step in development of a comprehensive regional conservation plan for migratory landbirds. All three major national bird conservation plans (Brown et al. 2001, Kushlan et al. 2002, Rich et al. 2004) recognize the importance of stopover habitat, and acknowledge that in many cases habitat use during migration is poorly understood.

Understanding the long-term spatio-temporal dynamics of stopover use by migrating landbirds within North Carolina will contribute to several conservation priorities outlined in the North Carolina Wildlife Action Plan (North Carolina Wildlife Resources Commission 2005). These priorities include 1) establishing baseline status and distribution information for priority species that include migratory landbirds and their habitats to facilitate long-term monitoring and fill critical data gaps, 2) conducting research to resolve questions of life history, productivity, and mortality factors for priority species, and 3) identifying areas for habitat conservation and restoration through acquisition and easements.

The national network of weather surveillance radars (NEXRAD) allows for a spatially-explicit assessment of the importance of migratory stopover sites across large geographic areas by measuring the relative magnitude and temporal variability of bird density as they leave stopover sites to initiate nocturnal migratory flight (Bonter et al. 2009, Buler and Diehl 2009, Buler and Moore 2011, Buler and Dawson 2014). Sampling terrestrial distributions of birds is generally done with a single near-instantaneous radar scan for a given night at the lowest radar tilt angle sweep (Buler and Diehl 2009) at the initial onset of the aggregate *en masse* flights of

various birds species that synchronize their flight initiation to the position of the sun (Åkesson et al. 1996). This approach helps to preserve the geographic fidelity and structure in animal distributions (Buler et al. 2012). We used NEXRAD radars that provide coverage of North Carolina to achieve the following objectives:

1) Map the temporal and spatial patterns of stopover use by birds within North Carolina during fall and spring migration
2) Develop statistical models to predict stopover site use in areas not sampled by the radars and describe stopover habitat relationships
3) Assess historical changes in migrant distributions

METHODS

Objective 1: We downloaded from the NCEI (National Centers for Environmental Information) data collected by five NEXRAD radars (Figure 1) that cover portions of North Carolina during peak landbird migration for spring (1 April through 31 May) and fall (15 August through 7 November). Sampling years were chosen based on the availability of archived radar and LiDAR data. Much data was missing from the NCDC archive during spring 2000-2002. Therefore, we added two spring seasons to the dataset such that we used spring data from seven years (2000-2003 and 2013-2015) and fall data from five years (2000-2002 and 2013-2014).

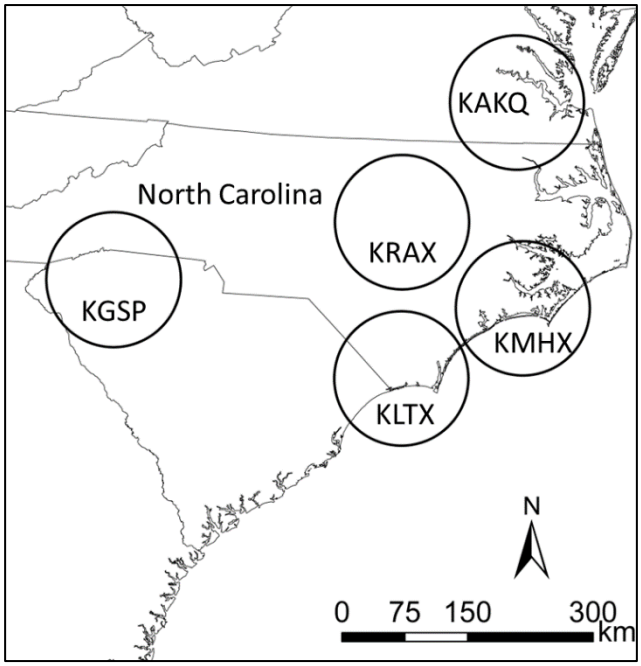

Figure 1. Coverage areas (80 km radius) of 5 NEXRAD radar stations (KAKQ: Norfolk, VA; KGSP: Greer, SC; KLTX: Wilmington, NC; KMHX: Morehead City, NC; KRAX: Raleigh, NC).

NEXRAD radars emit polarized, 10-cm (S band) electromagnetic waves, scanning the atmosphere at a varying number of tilt angles (e.g., 5 – 20 angles depending on the Volume Coverage Pattern). Radars emit 750 kW of energy at a 3 dB half beamwidth of 0.95°. The radar receives returned energy scattered back from objects within sampled volumes of airspace. The signal, or reflectivity, is measured in units of Z within a logarithmic scale to a half decibel in precision. Radar reflectivity is positively related to the density of birds in the air (Gauthreaux and Belser 1998, Larkin et al. 2002) and of migrant birds within stopover habitats (Buler and Diehl 2009). In addition to measuring reflectivity, the radars use Doppler technology to also measure radial velocity of objects, thus allowing us to determine the speed and direction of birds aloft. In 2008, all the NEXRAD radars underwent an upgrade in spatial resolution. Data prior to the upgrade, called 'legacy' format, has a 1km x 1° resolution in comparison to the newer 'super resolution' format, which is 250 m x 0.5°. Because the radars are designed for detecting precipitation, they function in two modes; 'precipitation' or 'clear air' mode. When in 'precipitation' mode, the radar scans the air approximately every six minutes, versus approximately every ten minute when operating in 'clear air' mode. With each scan, multiple sweeps are taken at varying tilt angles (from 0.5 to 19.5 degrees above the horizon). The lowest elevation scanned, at 0.5º above the horizon, is the most useful for detecting birds (i.e., emigrants) in flight as they depart stopover habitat.

We screened data at the 0.5º tilt angle around the time of evening civil twilight when many migrating landbirds depart daytime stopover sites in an abrupt exodos (Åkesson et al. 1996). We eliminated many nights due to precipitation, clutter or other types of nonbiological contamination following Buler and Dawson (2014). We identified whether reflectivity was dominated by birds or insects for each radar and sampling night by first estimating the mean

airspeeds of flying animals aloft based on a single radar sweep from the 2.5° tilt angle during the peak of nocturnal activity (~3 h after sunset). Data were processed using software WDSS-II, developed jointly between the Universities of Oklahoma and Delaware (Buler et al. 2012a) and MATLAB code from Farnsworth et al. (2014) following Buler and Diehl (2009). We sampled at the peak of nocturnal flight activity when most animals aloft should be in level horizontal flight and the radial velocity, a measure of only the horizontal component of movement relative to the radar, should best reflect their total velocity. We temporally interpolated (inverse-distance weighting) high-resolution data on winds aloft archived by the North American Regional Reanalysis (NARR) to the time of each radar sweep analyzed. These high-resolution modeled wind data are available in three-hour composites across the United States at approximately 0.3°resolution (i.e., as fine as 32 km). We used these data to determine air speeds (u and v wind components) at nine geopotential heights ranging from 650-1000mb within the 100-km range of a given radar. We vector-subtracted the wind velocity from the target ground velocity and then fit a sine function through velocities by azimuth (Browning and Wexler 1968) to calculate mean target airspeeds for each suitable sampling night. Following Larkin (1991), we considered nights with mean animal airspeeds < 5 m/s as insect-dominated. The remaining nights were considered bird-dominated and used in further analyses.

We constructed radial grid shapefiles of all radars that provide a georeferenced grid for displaying data within a GIS and for extracting other georeferenced data measures of ground elevation, land cover, and other landscape metrics used for modeling bird distributions. Individual sample volumes of radar data grids are 250-m in range by 0.5° wide in resolution, corresponding with the super resolution radar data. We assessed radar beam blockage and areas of persistent clutter around each radar by determining the frequency of detection of reflectivity

among individual sweeps for the 0.5° tilt angle. We mapped the standardized probability of reflectivity detection for each sample volume and identified sample volumes where 1) reflectivity was measured at a high frequency and with a mean magnitude greater than 1,000 Z as areas of persistent ground clutter and 2) reflectivity was infrequently measured regardless of magnitude as areas of partial beam blockage. Data from these sample volumes is excluded from analyses. Initially, we hoped to incorporate data from the KMRX (Knoxville, TN) radar but because the radar suffers from severe beam blockage due to mountainous topography, we eliminated it from our analyses.

For each suitable sampling night by radar, we interpolated radar data to an empirically determined sun angle at the point of maximum growth in mean total reflectivity among scans through time at the onset on nocturnal flight exodus (Figure 2). This allowed us to control for temporal sampling bias between radars and nights. We next used the "w2birddensity" tool in the WDSS-II software package to reduce measurement bias in reflectivity measures by estimating vertically-integrated radar reflectivity (VIR) from data at the 0.5° tilt angle. The VIR represents an approximation of the mean reflectivity from the ground to 1.5 km above ground within the column of airspace over the two-dimensional "footprint" of an individual sampling volume (Buler and Dawson 2014) that is measured in units of cm^2/ha.

We characterized bird stopover use across the migration period by the mean VIR (MN) and the mean coefficient of variation of VIR (CV) across all nights within seasons. Since the distribution of VIR among nights within a season is typically left-skewed, i.e. low-intensity migration nights heavily outweigh intense migration nights, we computed the geometric mean of VIR (hereafter referred to simply as mean VIR) as a measure of central tendency of emigrant density on a given day. "Important" stopover sites are identified as those areas with above-mean

(≥50th percentile) VIR, and further categorized as: 1) "consistently high density of emerging migrants" (CV ≤25th percentile and MN ≥75th percentile), or 2) "highly variable migrant density" (CV ≥75th percentile). We classified data at the local scale and combined data across radars to compute a regional classification for each season and period. Areas classified as consistently-high emigrant density are potentially important stopover sites for nocturnally migrating birds across North Carolina.

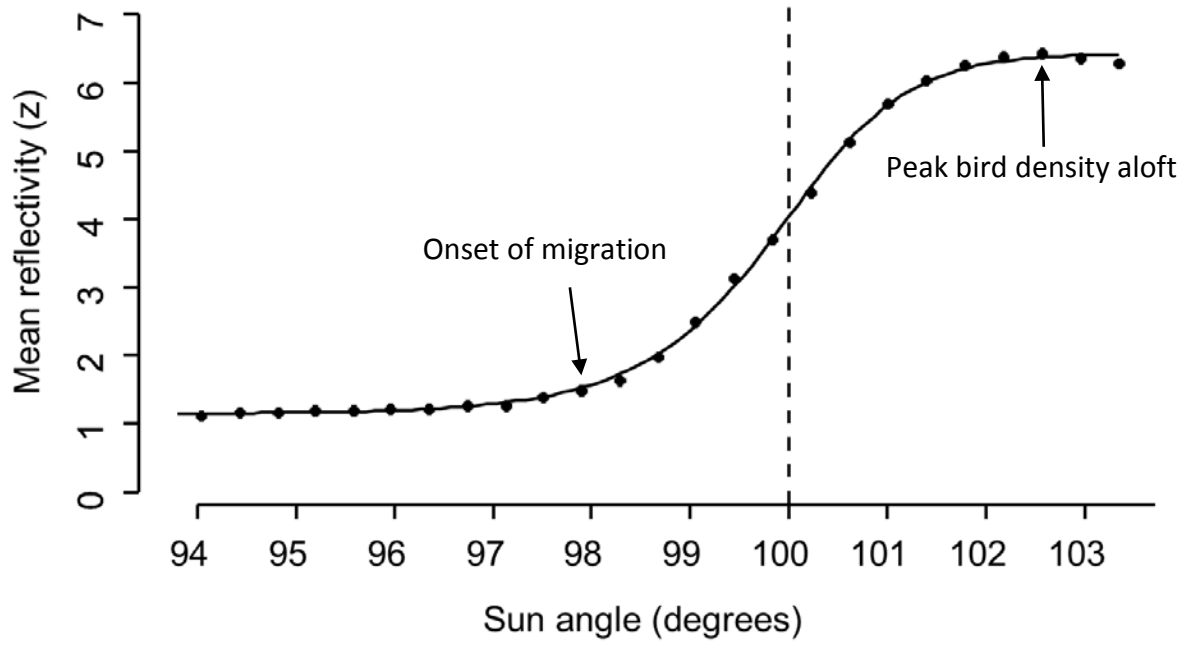

Figure 2. Example scatterplot of the increase in mean total reflectivity through time at the onset of a nocturnal bird-dominated flight. Vertical dashed line at the sun angle (100° [i.e., 10° below the horizon]) indicates where the point of the maximum rate of increase in reflectivity occurs. This would be the sun angle at which radar data were sampled for quantifying bird distributions aloft on this night.

Objective 2: Much of area of North Carolina is not sampled by NEXRAD radars. Therefore, we created statistical models to predict stopover use by migrants in these non-sampled areas. However, we were also interested in building models that could explain the pattern of stopover use within radar-sampled areas as well. The outcome variables we modeled included the seasonal geometric mean and CV of VIR for each season and time period. Spatially explicit models of ecological processes must contend with issues of spatial autocorrelation, over-fitting

imprecisely measured or non-uniformly sampled data and non-linear responses among variables (Valcu and Kempenaers 2010, Li 2016). We chose to address these modelling and data issues by using Generalized Additive Models (GAM); a semi-parametric extension of generalized linear models with assumptions that the marginal response functions are additive and that the components are smooth (Guisan et al. 2002). Typically, a reasonable balance must be maintained between the total number of observations and the total number of degrees of freedom used when fitting GAM models. However, given the extremely large samples sizes (n >30,000) for our models and the contiguous nature of the radar measures, degrees of freedom are of little concern. Instead, a greater concern is for overfitting models via the data-driven nature of GAMs, which led us to be conservative in choosing the maximum degrees of freedom for fitting spline functions to variables (max df = 10). Maintaining simpler response functions always improved their interpretation. We fits GAMs using the R package mgcv based on Wood (2011).

For the modelling analysis, we constructed a georeferenced polygon shapefile (i.e., grid) of over 130,000 square polygons covering the entire state, each with the dimensions of1 km x1 km. To help predict stopover in some areas along the north and south edges of the state, we included additional 1x1-km grid polygons to cover the extent of the KAKQ (Sterling, VA) radar to the north and the KGSP (Greenville, SC) radar to the south. The grid provides a framework in which to display predicted data and extract landscape information used to describe stopover habitat relationships across the state of North Carolina.

For each grid polygon, we computed a mean value for several predictor variables that characterize geographic position, landscape and local land cover composition, and other local characteristics (Figure 3). Whenever possible, we obtained data close in time to the radar data from early and late years because we were interested in comparing time periods. Predictor

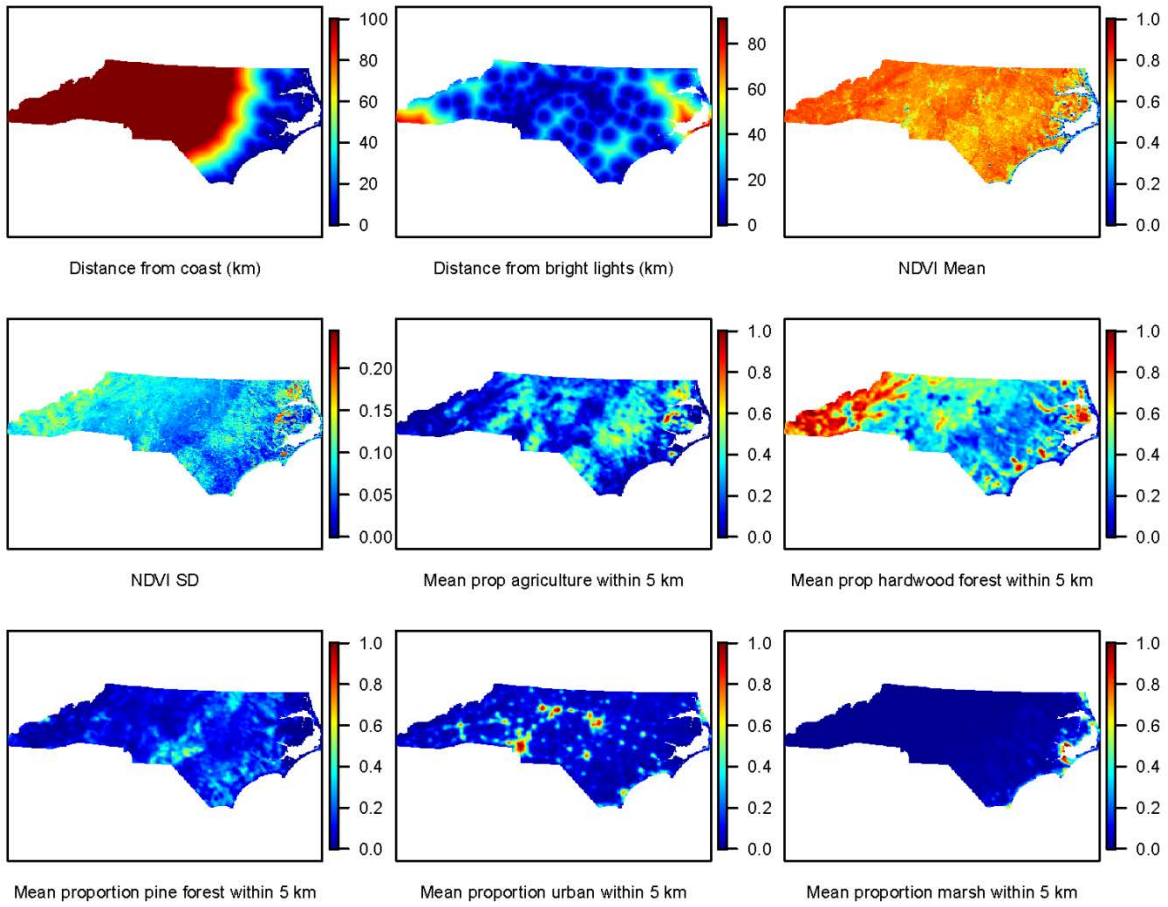

Figure 3. Example maps of some predictor variables used for modeling bird stopover densities measured within 1 square km polygons across North Carolina. These are a subset of predictors used for the fall season during late years.

variables included: geographic position (i.e. latitude, longitude, elevation relative to nearest radar), the amount of various land cover types (i.e., urban, agriculture, hardwood forest, pine forest, emergent marsh) at the local (within the 1-km grid polygon) and landscape (within 5-km surrounding the grid polygon) scale derived from the 2001 and 2011 National Land Cover Database (NLCD), mean and standard deviation of Normalized Difference Vegetation Index (NDVI) collected at 16-day intervals at 250 m resolution obtained from the Global Moderate-resolution Imaging Spectroradiometer (MODIS) for each season, mean and standard deviation of canopy height derived from LiDAR data supplied to us by US Fish and Wildlife Service, mean

level of night light brightness on the 0-63 index scale computed from cloud-free composites of Defense Meteorological Satellite Program-Operational Linescan System (DMSP-OLS) 30-arc second grids for the calendar years 2001 and 2013, and proximities to bright lights in 2001 and 2013 (i.e., index value ≥60 in the night light layer), coastline (up to 100 km from a coast), and radar location. Table 1 provides further information regarding the full suite of 21 variables considered for the predictive modeling. The variables denoting polygon position relative to the nearest radar (i.e. range and relative elevation) were used as "nuisance" variables in the predictive models to control for residual bias in VIR measures from the data processing algorithms. Within polygons containing suitable radar observations for building models, we found strong correlations ($r > 0.8$) between the mean and standard deviation of canopy heights and between night light intensity and the amount of urban development within 5 km. Therefore we dropped standard deviation of canopy height and night light intensity from further consideration. Additionally, we were unable to obtain canopy height data for the entire polygon grid of the state for the later years (i.e. 2014) because creation of the dataset is ongoing, and there were regions of the state grid where we had to censor canopy heights for the earlier year (i.e., 2001) dataset due to inaccurate data. Therefore, we did not use canopy height for building predictive models for mapping emigrant stopover densities. However, we did run GAM models including canopy height for the subset of grid polygons that had data for each time period to assess the value of canopy height in explaining emigrant stopover densities.

Table 1. Descriptions of predictor variables considered for building GAMs to predict mean and CV of emigrant stopover densities and measured within 1 km x 1km polygons across North Carolina. Short names appear in R analyses output.

Predictor type	Predictor description (units)	Predictor short name*
Geographic position	Latitude (UTM northing in km)	UTM_N
	Longitude (UTM easting in km)	UTM_E
	Ground elevation relative to nearest radar (m)	relelev
	Distance to coastline (km up to 100 km)	dcoast
	Distance to nearest radar (km)	Radar_dist
	Distance to nearest bright lights (km)	dst_lite_e (2001) light_dist (2013)
Landscape composition	Proportion of agriculture within 5 km	agyy5km
	Proportion of emergent marsh within 5 km	emrshyy5km
	Proportion of hardwood forest within 5 km	hwoodyy5km
	Proportion of pine forest within 5 km	pwoodyy5km
	Proportion of urban development within 5 km	urbanyy5km
Local characteristic	Mean canopy height (dm)	canht_yy
	Standard deviation of canopy height (dm)	canvar_yy
	Seasonal mean NDVI (index from 0-1)	ndvimeanst
	Seasonal standard deviation of NDVI	ndvistdst
	Night light intensity (index from 0 – 63)	lights_yy
Local composition	Proportion of agriculture (NLCD classes 81 & 82)	agyy
	Proportion of emergent marsh (NLCD class 95)	emarshyy
	Proportion of hardwood forest (NLCD classes 41 & 90)	hwoodyy
	Proportion of pine forest (NLCD classes 42& 42)	pwoodyy
	Proportion of urban development (NLCD classes 21-24)	urbanyy

* **s** = season; “f” for fall, “s” for spring: **t** = time period; “e” for early years, “l” for late years, **yy** = two number symbol for year; “01” for 2001 and “11” for 2011

Objective 3: To assess recent decadal changes in migrant distributions, we subtracted early year emigrant densities from late year emigrant densities for each season. We examined changes of emigrant densities at two slightly-different spatial scales; the native irregular sample-volumes and the regular 1-km grid polygons (i.e., aggregated sample volumes). We binned changes in emigrant densities of sample volumes into three categories to highlight areas with the most extreme changes. We identified sample volumes with the most extreme changes in VIR as either "decreased" (bottom 10^{th} percentile of distribution of change in mean VIR), or "increased" (top 10^{th} percentile of distribution of change in mean VIR). Sample volumes with a change in mean VIR within the inner 80^{th} quantile were classified as having "no change".

The Multi-Resolution Land Characteristics Consortium (MRLC) provided a NLCD land cover change map comparing 2001 and 2011 classified data from which we extracted areas of urbanization (change from non-urban to urban land use), deforestation (change from forest to non-forest land cover) and afforestation (change from non-forest to forest land cover). We determine how these types of land changes are associated with areas of greatest change in emigrant density at the sample volume scale.

To model changes in emigrant densities between early and late years by season at the 1 km grid polygon scale, we fit Boosted Regression Tree (BRT) models that combine statistical and machine learning methods into a single model framework to determine the most important predictors of emigrant densities. We considered 13 predictors to explain variability in the change of mean VIR between early and late years (Table 2). BRT models have an advantage over general linear models in that they can incorporate more complex response functions (i.e., threshold response), interactions among predictors, and do not rely on data conforming to specific distributions. We ran BRT models using the cross validation method provided by the

function gbm.step within the R package dismo (Hijmans et al. 2015). We used a tree depth of 5, a learning rate of 0.5 to get optimal fits within ~1000 trees, and a bag fraction of 0.5. We produced smoothed marginal response plots of the main effects of predictors to interpret the relationships with the response variable.

Table 2. Descriptions of predictor variables considered for building models to predict change in mean emigrant stopover densities between early and late years measured within 1 km x 1km polygons across North Carolina. Short names appear in R analyses output.

Predictor type	Predictor description (units)	Predictor short name*
Geographic position	Latitude (UTM northing in km)	UTM_N
	Longitude (UTM easting in km)	UTM_E
	Distance to coastline (km up to 100 km)	dcoast
	Change in distance to nearest bright lights from 2001 to 2013 (km)	diffdislight
Landscape composition	Change in proportion of agriculture within 5 km from 2001 to 2011	agchange5km
	Change in proportion of hardwood forest within 5 km from 2001 to 2011	hwoodchange5km
	Change in proportion of pine forest within 5 km from 2001 to 2011	pwoodchange5km
	Change in proportion of urban development within 5 km from 2001 to 2011	urbanchange5km
Local characteristic	Change in seasonal mean NDVI from early to late years (index from 0-1)	ndvichange**s**
	Change in night light intensity from 2001 to 2013 (index from 0 to 63)	lightchange
Local composition	Change in proportion of agriculture from 2001 to 2011	agchange
	Change in proportion of all forests from 2001 to 2011	forestchange
	Change in proportion of urban cover from 2001 to 2011	urbanchange

* **s** = season; "f" for fall, "s" for spring

RESULTS

Among all seasons and years, 17.6% of the days were considered suitable bird sampling days. Most data were eliminated due to precipitation, contaminating 38.4% of the data (Table 3). Although NCEI has archived radar data back into the early 1990's, much data was missing from the archive during the originally selected early years of this study (2000-2002). Additionally, we

had low sample sizes for late spring, mainly due to contamination by precipitation and clutter. We therefore added two seasons of spring data (2003 and 2015) to bolster the number of days used in our analyses.

Table 3. The number of days and type of classifications across five radars during the fall and spring migratory periods. (*Insufficient Data was predominantly due to no available data, the rest was attributed to data processing problems and no birds present).

Season	Radar	Classification					
		Bird Dominated	Anomalous Propagation	Clutter	Insect Dominated	Precipitation	*Insufficient Data
Fall	KAKQ	49	36	27	60	148	105
	KGSP	101	4	13	45	146	116
	KLTX	58	44	28	54	183	58
	KMHX	57	50	16	76	185	41
	KRAX	104	14	16	70	174	47
Spring	KAKQ	90	3	54	25	146	109
	KGSP	122	7	24	38	180	56
	KLTX	63	28	52	64	153	67
	KMHX	45	25	20	97	172	68
	KRAX	59	6	81	32	148	101
Total		748	217	331	561	1,635	768

On average, the 5 NEXRAD stations provided comprehensive measures of the stopover densities of emigrating birds for 22% of the land area within the state of North Carolina in a given season. We produced classified stopover use maps for each radar to elucidate local patterns of emigrant density (Appendix A). At this scale, we were able to see seasonal differences at nearly all the radars whereby concentrations of birds were more closely associated with coastal areas in the fall versus more inland concentrations in the spring. Patterns between the years were more variable although there were noticeable decreases in emigrant density at the two most coastal radars (KLTX and KMHX).

Fall: To better understand patterns of bird stopover distributions across the entire state, we also produced regionally classified maps for each season and time period. The early fall regional classification (Figure 4) shows high densities of emigrants occurring along large bodies

of water in addition to large forest and wetland habitats. Aside from the coast in KLTX, major waterways, primarily coastal rivers and surrounding wetlands, in both KLTX and KMHX were consistently visited in high densities. Notable forest patches that received high densities in North Carolina included Croatan National Forest in the domain of KMHX. Additionally, consistently high emigrant densities at the edge of the KGSP radar correspond to an area dominated by forest habitat. The early fall classification also shows a latitudinal gradient in emigrant density with those radars located further south showing higher emigrant densities.

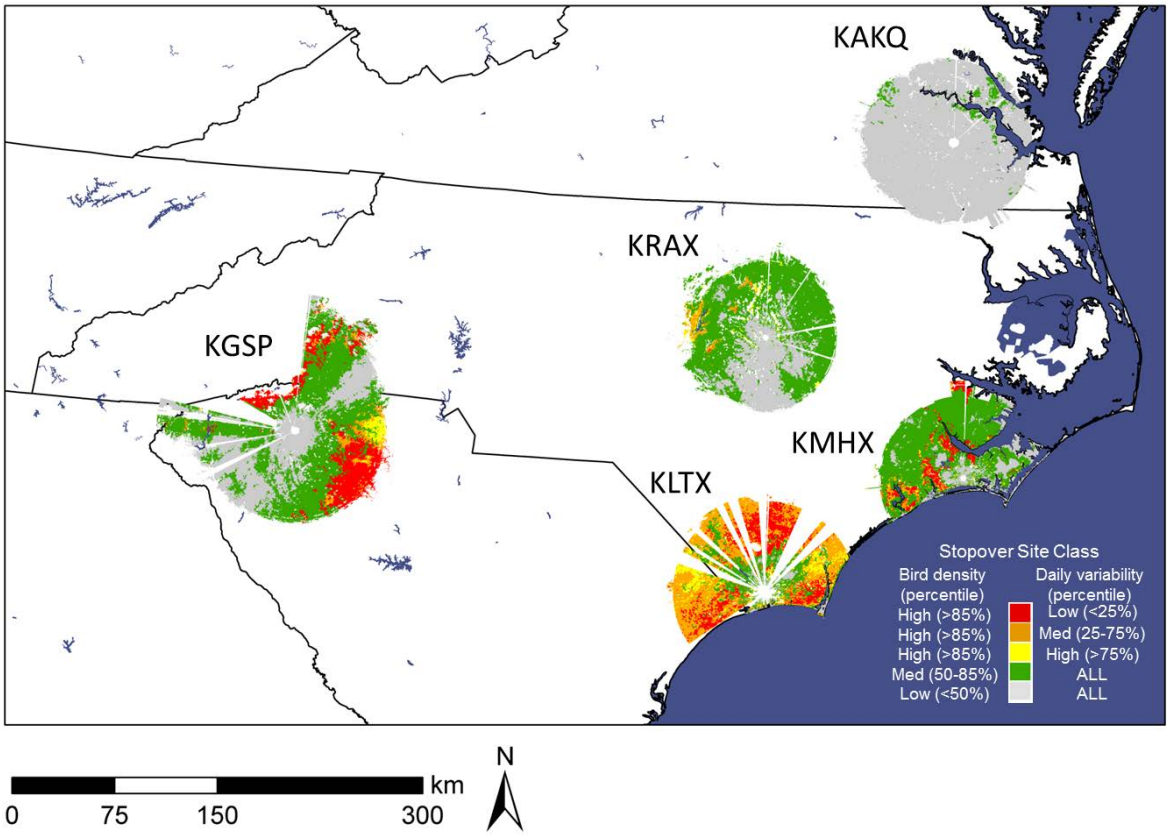

Figure 4. Mean bird density and daily variability regionally classified across five radars in the early fall years (2000-2002).

The late fall regionally classified map (Figure 5) shows that there are significant high emigrant densities with low variance along major water ways. This is most evident in the

KMHX imagery where the coastal rivers are bird dominated. This pattern holds true for both KRAX and KLTX radars. Birds also avoided major cities like Raleigh at KRAX.

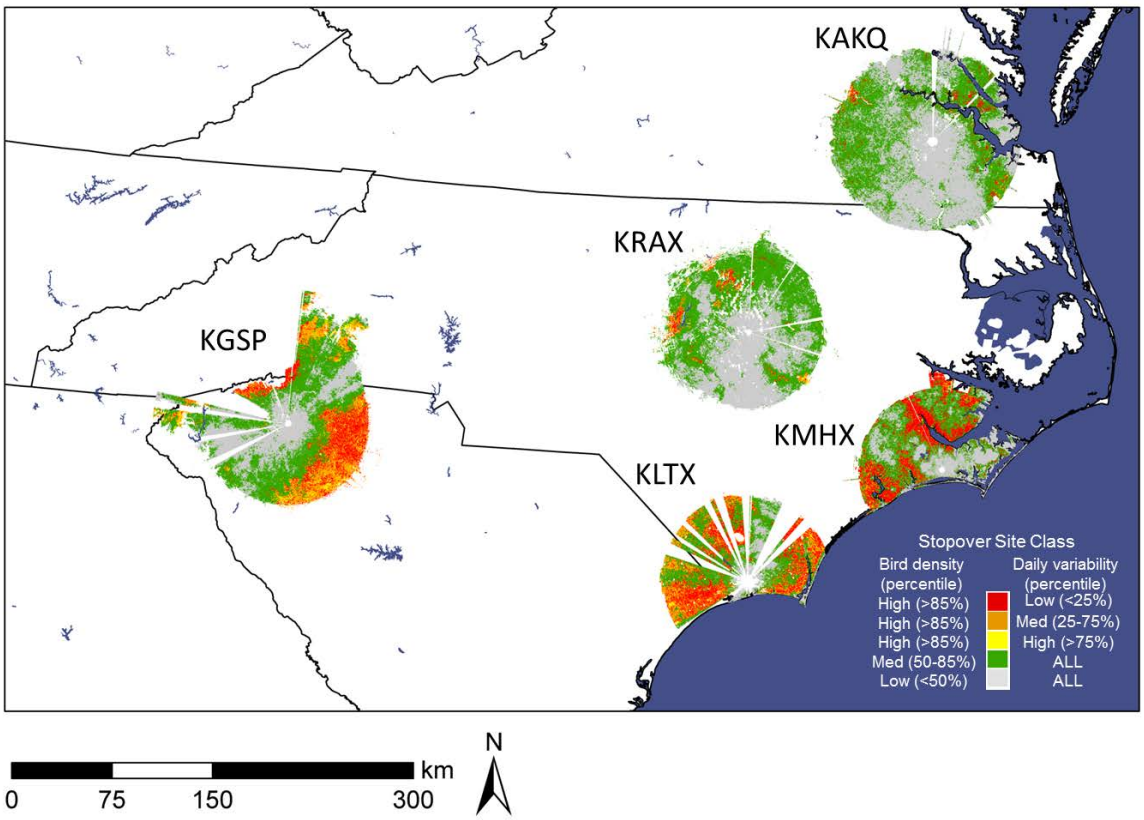

Figure 5. Mean bird density and daily variability regionally classified across five radars in the late fall years (2013-2014).

GAM models explained 81% and 47% of the deviance in the mean and CV VIR, respectively, for emigrants during early fall years (Appendix B.5 & B.6). The models indicate that the most important predictors include geographic location, NDVI, and landscape-scale emergent marsh habitat. Marginal response plots show that emigrant density was consistently higher at more southern latitudes, in close proximity to and at moderate distances from the coastline, with greater NDVI, and less emergent marsh in the surrounding landscape. The remainder of variables showed consistently higher densities of migrants with greater amounts of

hardwood forest, pine forest, and urban development, lesser amounts of agricultural land, and farther from brightly light areas. The maps of predicted classified bird stopover use during fall highlight consistent high emigrant density along forested coastal rivers and in the west within portions of South Mountains National Park and Pisgah National Forest (Figure 6). There is also broad high use of the southern portion of the state and variable use within Uwharrie National Forest for early years.

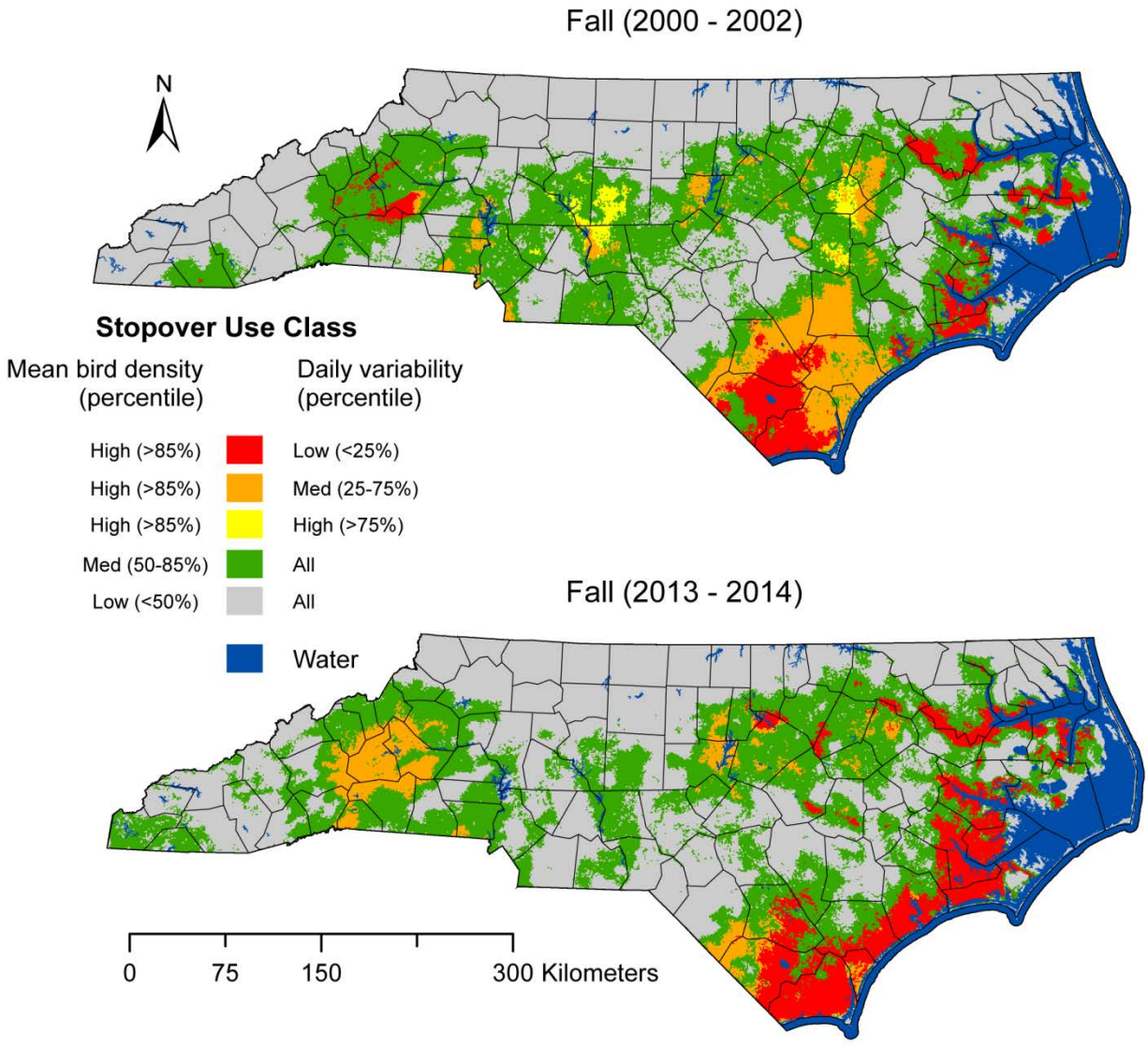

Figure 6. Classified stopover use maps based on predicted bird densities during fall of early (top panel) and late (bottom panel) years.

GAM models explained 72% and 45% of the deviance in the mean and CV VIR, respectively, for emigrants during late fall years (Appendix B.7 & B.8). For mean VIR, the most important predictors include geographic location, landscape-scale hardwood forest and distance from the coastline. Marginal response plots show that emigrant density was consistently higher at more southern latitudes, in close proximity to and at moderate distances from the coastline, and with greater hardwood forest in the surrounding landscape. The remainder of variables showed consistently higher densities of migrants with greater amounts of hardwood forest, pine forest, and urban development, and lesser amounts of agricultural land and emergent marsh, similar to the models from early fall. However, in later years, the response to proximity to brightly lit areas was reversed, such that emigrant densities were consistently greater closer to brightly lit areas.

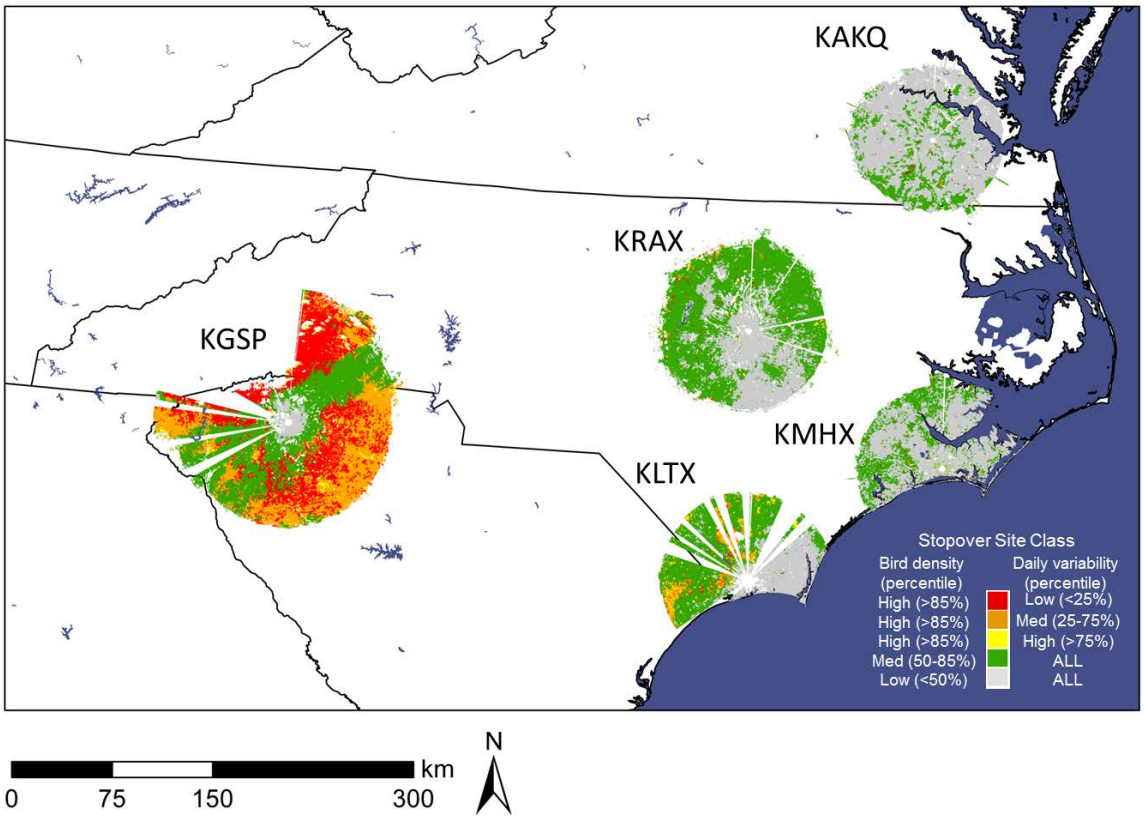

Figure 7. Mean bird density and daily variability regionally classified across five radars in the early spring years (2000-2003).

Spring: Observed bird stopover distributions during spring contrasted from those during fall in one major way; densities were greatest in the Appalachian Mountains rather than along the coasts (Figure 7). This pattern was particularly strong during the later years (Figure 8). Similar to fall, migrants showed greater densities in forested areas.

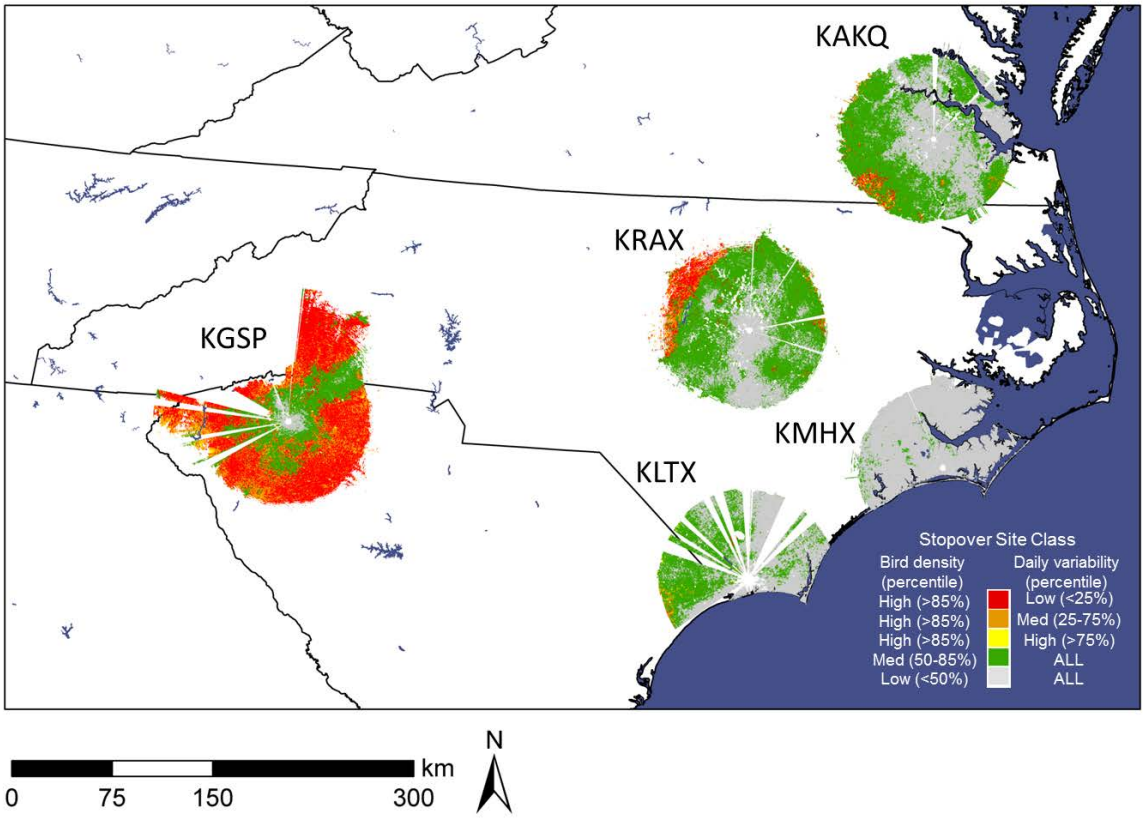

Figure 8. Mean bird density and daily variability regionally classified across five radars in the late spring years (2013-2015).

GAM models explained 80% and 33% of the deviance in the mean and CV VIR, respectively, for emigrants during early spring years (Appendix B.1 & B.2). The models indicate that the most important predictors include geographic location, NDVI, distance from bright lights and landscape-scale hardwood forest habitat. Marginal response plots show that emigrant

density was consistently higher at more western longitudes, farther away from bright areas, with greater mean and moderate SD of NDVI, and with more hardwood forest in the surrounding landscape. The remainder of variables showed consistently higher densities of migrants with greater amounts of pine forest, and urban development, lesser amounts of agricultural land. Differing from the early fall, early spring emigrant densities were consistently greater away from the coastline, yet also with greater amounts of emergent marsh in the surrounding landscape.

GAM models explained 86% and 56% of the deviance in the mean and CV VIR, respectively, for emigrants during late spring years (Appendix B.3 & B.4). The most important predictors were similar to early spring. Marginal response plots during later years were nearly identical to the earlier years. However, in later years, the response to proximity to brightly lit areas was reversed, such that emigrant densities were consistently greater closer to brightly lit areas (just as it was for late years in the fall).

The maps of predicted classified bird stopover use during spring highlight consistent high emigrant density along forested regions at higher elevation in the west during both early and late years (Figure 9). The late year's model shows a very strong elevational gradient of increasing emigrant density with elevation. This is likely due, in part, to overestimation of emigrant densities at extreme western longitudes where the model extrapolated beyond the range of the training data.

GAMs for both seasons using the subset of grid cells that contained LiDAR-derived canopy heights found positive relationships between canopy height and mean VIR and, except for spring of early years, negative relationships between canopy height and CV VIR after controlling for all the other covariates. We present here just the marginal response functions for the late fall years as an example (Figure 10).

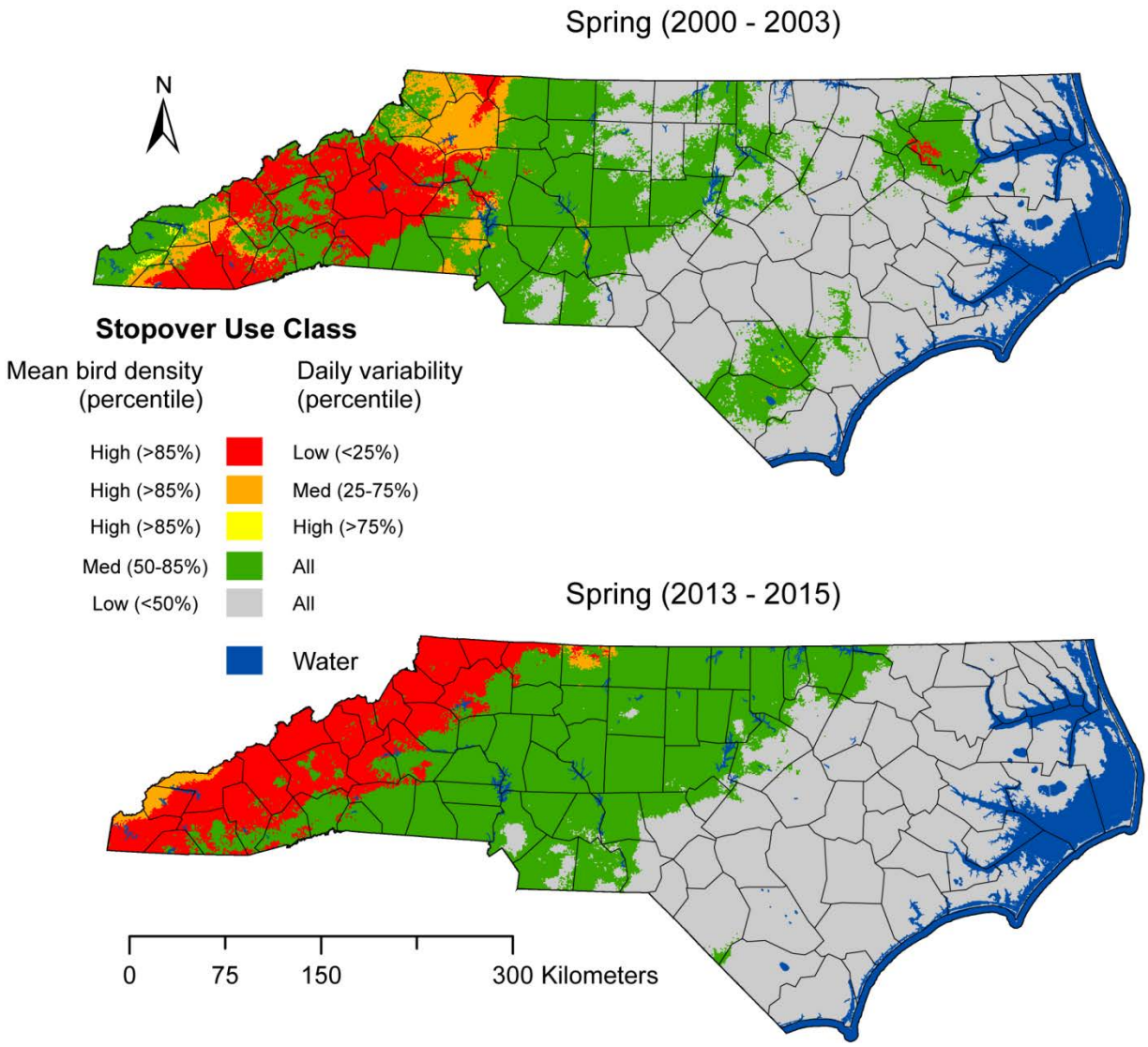

Figure 9. Classified stopover use maps based on predicted bird densities during spring of early (top panel) and late (bottom panel) years.

Decadal changes: There was a 7.8% net change in land cover among the nine major cover types from years 2001-2011 within 100 km range of the five radars. The majority of these land cover changes can be attributed to increased shrub cover, increased urban development, and decreased pine forest (Table 4).

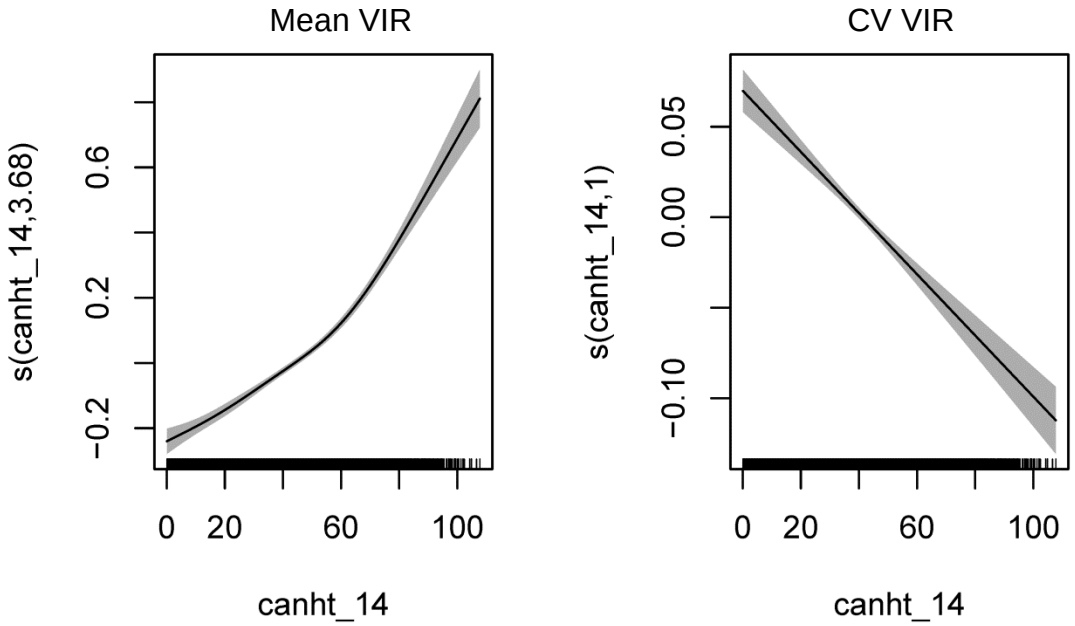

Figure 10. Marginal response functions of mean and CV VIR on canopy height from GAMs during late fall years (2013-2014).

Table 4. Net percent change in area of various land cover types between 2001 and 2011 based on NLCD for the region within 100 km of 5 NEXRAD stations that cover portions of North Carolina.

Land cover type	Net change (%)
Urban	0.96
Hardwood forest	-0.61
Pine forest	-1.91
Mixed forest	-0.28
Shrub	1.75
Grassland	0.61
Agriculture	-0.54
Woody wetlands	-0.40
Marsh	0.32

Overall, emigrant densities declined by 29% (early mean VIR = 2.20 cm^2/ha; late mean VIR = 1.57 cm^2/ha) between time periods during fall and increased by 5% (early mean VIR = 0.87 cm^2/ha; late mean VIR = 0.91 cm^2/ha) during spring. In fall, the overall decline in emigrant densities occur broadly throughout the state (Figure 11). See Appendix C for individual radar

maps depicting emigrant density changes. Most of the areas of increased emigrant density are around KAKQ, along the coast near KMHX, and the southern extent of the KGSP radar.

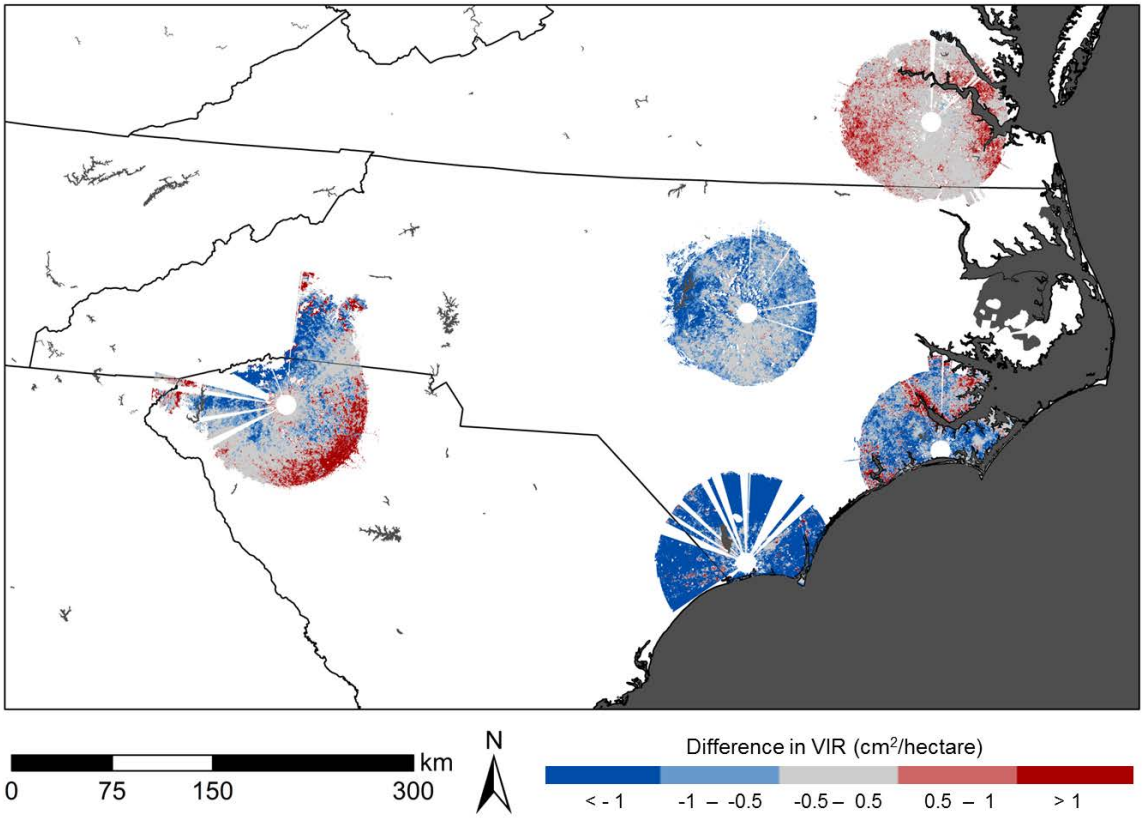

Figure 11. Emigrant density changes from early (2000-2002) to late (2013-2014) years across five radars in the fall season.

Emigrant densities did not change appreciably for most areas between early and late years during spring. However, there were broadscale decreases in emigrant density occurred along the coastal radars, KMHX and KLTX (Figure 12; see Appendix B for individual radar maps). Increases in emigrant density occurred in the northwest region of KRAX and on the fringes of the KGSP radar.

Fine scale (i.e., measured at the sample volume) changes in emigrant densities were not closely associated with land cover changes via visual inspection. For example, we found some urbanized areas that were associated with decreases in migrant use while others were not (Figure

13). Moreover, some areas the changed in migrant use occurred where there was no net change in land cover. However, when summarized across sample volumes, we found trends in the "noise" of the fine scale data. During both seasons, increasing fraction of afforestation trended positively with increasing emigrant density (Table 5). Conversely, increasing fraction of deforestation and urbanization trended positively with decreasing emigrant density.

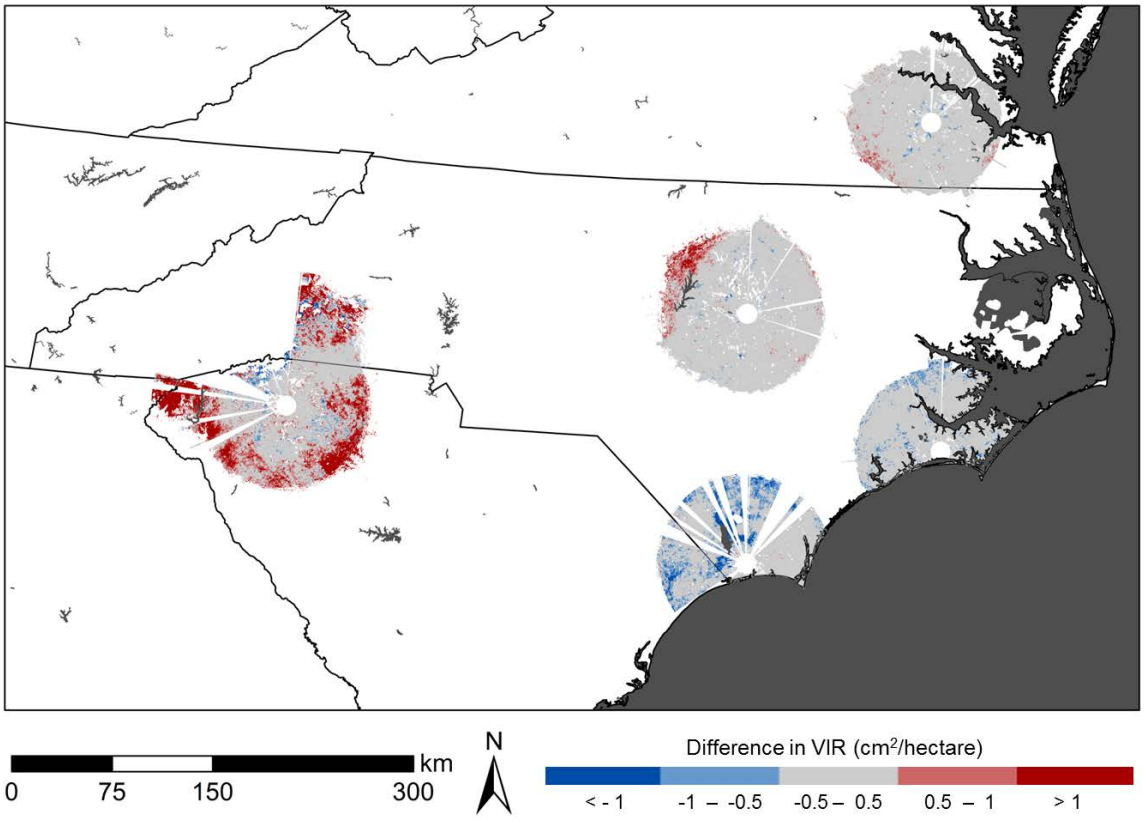

Figure 12. Emigrant density changes from early (2000-2003) to late (2013-2015) years across five radars in the spring season.

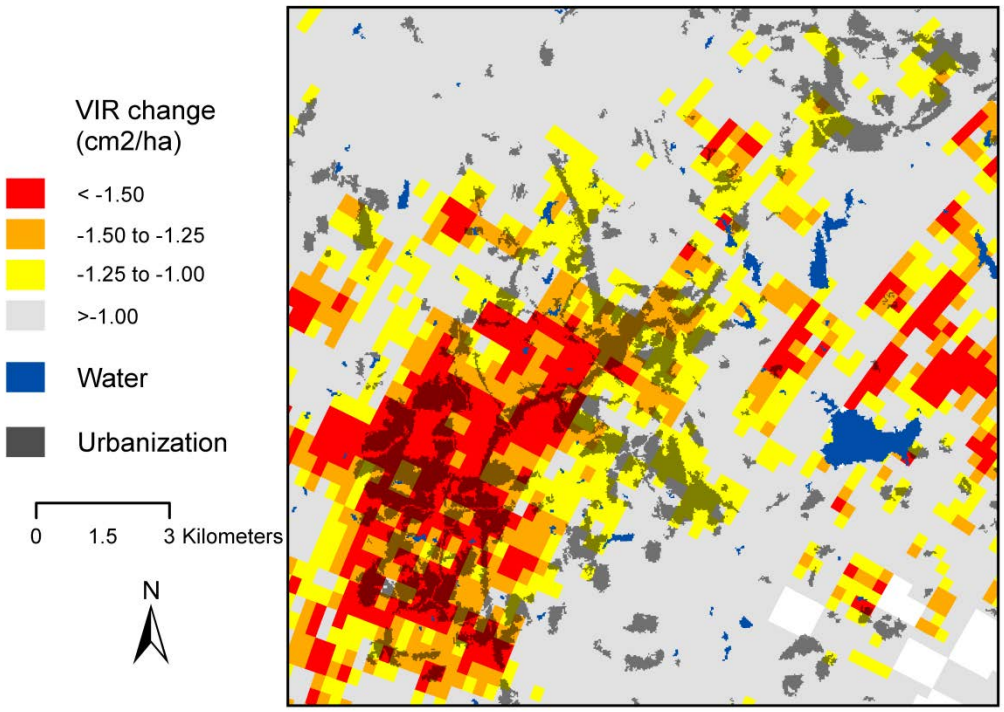

Figure 13. Example maps depicting decreased emigrant densities (i.e. change in mean VIR) between early and late years associated with urbanization near KRAX during the fall season.

Table 5. Overall percent of land area within sample volumes that underwent a change in land cover by type separated by observed changes in emigrant density between early and late years for fall and spring seasons.

Season	Emigrant density change	Percent of land area experiencing change		
		Urbanization	Deforestation	Afforestation
Spring	Decrease	1.17	7.11	1.54
	No change	1.25	5.82	1.61
	Increase	0.87	4.02	2.13
Fall	Decrease	1.76	6.29	1.23
	No change	1.19	5.90	1.65
	Increase	0.79	5.40	2.30

When modeled at the broader 1-km-grid scale, geographic position and changes in landscape composition largely explained changes in emigrant density between years (Appendix D). Again, local scale factors were rather uninformative and consistently ranked lowest in relative influence. Modeling responses appeared to behave erratically at extreme limits of

observed predictor values, so we focus our interpretation of marginal responses to the inner 90th percentile range of predictor values.

In both seasons, emigrant densities increased to the west and north and with greater proximity to the coast. Distance to bright lights decreased for most areas in the late years. This change in proximity to bright lights had a greater relative influence during spring and weak influence during the fall. In spring, decreases in emigrant density were strongest for areas that were 5 to 10 km closer to bright lights. Areas that were even closer to bright lights increased in emigrant density.

With respect to changes in landscape composition, as more pine forest in the surrounding landscape disappeared, the more emigrant density declined. In contrast, greater decreases in agricultural lands in the surrounding landscape during spring led to greater increases in emigrant density. Responses to changes in hardwood and urban cover in the landscape, while relatively influential, were less consistent among and within seasons.

DISCUSSION

Weather surveillance radars provided direct comprehensive observations of the spatio-temporal patterns of stopover use of migrating birds across nearly a quarter of the land area within the state of North Carolina. These observations can serve as a baseline of the status and aggregate distribution of migratory landbird species, many of which are of conservation concern, and may facilitate long-term monitoring and fill critical data gaps. Classified by the mean and variability of emigrant density within seasons, we were able to map areas of the greatest importance for landbird stopover during spring and fall in North Carolina. Areas characterized by consistently-high bird density may represent the greatest return on conservation dollars spent

regardless of the quality of resources or function of different areas for migrants (Mehlman et al. 2005).

At the outset, it's important to keep in mind that while the maps of discretely classified migrant stopover density we produced can be powerfully effective at focusing conservation efforts, they can also oversimplify the dynamics of bird migration and the function of any particular area for stopover. Our stopover use classification scheme was intentionally coarse and simplified. The unclassified data include more precise measures of migrant stopover density at finer temporal scales and can better elucidate dynamics of bird use. Additionally, the function of particular stopover areas may not be closely tied to the density of bird use and likely varies among migrants at a site within and among days. Yet, even without understanding the underlying mechanisms driving stopover habitat use, the comprehensive observation of bird distributions by radar provides for visual interpretation of the aggregate patterns of stopover habitat use by migrant landbirds.

We also caution against relying too heavily on our state-wide predictive maps to assess the relative importance of sites outside of radar-sampled areas. The predicted bird densities within radar-sampled areas agreed quite well with radar-observed densities, but the accuracy of predicted bird densities elsewhere remains unvalidated. The use of GAM models can allow for extrapolation to new scenarios or values outside those used to build the models. For example, the most extreme western regions of the state are outside of the longitudes used to build the models. However any extrapolation risks magnifying error in the accuracy of response functions which may become exaggerated beyond the range of the training data. Thus, the state-wide map should be viewed as a guide for conservation purposes. Confidence in the predictive model can be improved with further evaluation and testing; for eaxmaple, through field surveys to ground-truth

the predicted patterns. That being said, there are important patterns in stopover use that we discuss below that are robust to the modeling approach that we used and provide important evidence of the nature of bird stopover distributions to their habitat.

Our results emphasize the hierarchy of factors extrinsic and intrinsic to specific stopover sites that can influence migrant distributions across multiple spatial scales as has been well demonstrated by others and previous efforts by our lab (Hutto 1985, Kelly et al. 1999, Moore et al. 2005, Buler et al. 2007, Buler and Moore 2011, Buler and Dawson 2014). At a broad geographic scale, migrants occurred at greater density along latitudinal and longitudinal gradients to the south and west, and, during fall, in closer proximity to the Atlantic Ocean coastline. In spring, coastal concentrations of migrants were not evident. At a landscape scale, emigrant densities were related to land cover composition, with the most consistent and highest bird stopover densities were positively associated with the amount forested and urban habitats in the landscape and negatively to the amount of agriculture. Furthermore, migrants occurred at greater densities in habitats with taller canopy and higher primary productivity. Strong general patters such as proximity to the coast and positive association with tall and productive habitats are both intuitive and supported by a growing body of stopover habitat literature (Buler et al. 2007, Bonter et al. 2009, Buler and Moore 2011, Buler and Dawson 2014). For example, Mcfarland et al. (2012) found positive relationships between bird density and NDVI, and Osborne et al. (2001) found NDVI to be helpful in predictive modeling of bird habitat when combined with other landscape variables.

In the fall, the dominance of forest-dwelling migrants that are concentrated into coastal areas likely masks the habitat affinities of marshbirds to marsh habitat. This is supported by the negative relationship of emigrant density to marsh in the landscape in the fall. In contrast, there

was a positive relationship between emigrant density and emergent marsh in the surrounding landscape during the spring. This is consistent with the idea that since most migrants are concentrated in the mountains during spring, the radar measures in coastal areas are likely dominated by obligate marshbirds. Additionally, fall migrations have a higher recruitment due to the large flux of juvenile individuals in the population. This may also affect the dispersal of birds due to the fact that juveniles tend to follow coastlines more heavily in the fall season and can also get disoriented more easily than adults of the same species (Ralph 1978).

The difference in seasonal concentrations of migrants near the coast in fall and in the mountains in spring also highlights broad scale differences in migratory routes of migrants between seasons. The radar observations are consistent with evidence of clockwise looped trajectories of migrants to the east in fall and to the west during spring from extensive eBird data (Sorte et al. 2016), and highlights the generalized nature of such migration strategies. It seems the importance of coastal stopover sites is greater during the fall and stopover sites within the Appalachian mountains is greater during the spring.

It is not surprising that local scale habitat composition had weaker effects than landscape level factors in explaining bird stopover distributions across such a broad geographic area since hierarchical processes at broad scales can limit smaller scale processes (Hutto 1985, Wiens 1989). Unfortunately, the resolution of the radar data is not fine enough to measure airspace over pure land cover types and resolve cleanly fine-scale patterns in habitat use. Thus, there is noise in the data from sampling of mixed habitat types.

This is the first study to assess decadal changes in migrant distributions with radar that we are aware of. Changes in emigrant distributions occurred at broad geographic scales likely due to stochasticity in weather patterns that could dynamically shift migrant trajectories (e.g.,

Gauthreaux et al. 2005, LaFleur et al. 2016). The strongest patterns indicate a stronger dichotomy in the changing distributions of migrants. Migrant densities have increased at both the extreme western portion of the state and in areas close to the coast. Additionally, migrant densities have declined in both seasons in the southern portion of the state. Future analyses of annual variability in stopover distributions patterns tied to measures of weather systems and wind fields would help elucidate these mechanisms. Changes in bird distributions were only weakly associated with fine-scale land cover changes, which is not surprising given the relatively small scale at which land cover changes occur relative to resolution of the radar and when looking at a state-wide scale.

At a landscape scale, losses of pine forest and increases in agriculture have led to declines in emigrant densities. The increase in early successional upland habitats and most of the decline in forests could tie directly to the cutting and regrowth of forests from timber industry, which is quite active in North Carolina. Although soft and hardwood forest are now timbered at similar or lower rates than in the early 2000's, regrowth is a slow process and trees do not replace themselves as quickly as deforestation occurs (Brown and Vogt 2015).

We found that although emigrant densities were positively associated with urban development at a landscape scale, the relationship with proximity to brightly-lit areas (i.e., major cities) varied between time periods. Previous radar mapping studies have also revealed high-density use of forested areas in human- dominated landscapes, particularly urban parks within large cities (Bonter et al. 2009, Buler and Dawson 2014b). Migrant stopover use of human-dominated landscapes in the USA is consistent with large-scale citizen-science survey efforts (La Sorte et al. 2014). These urban forest sites can provide resources for migrants to refuel during their stopovers (Seewagen and Slayton 2008). Interestingly, forest patches may be particularly

sought after by migrants who find themselves in human-dominated landscapes since the strongest positive relationships between bird stopover density and forest cover occurred in areas with low amounts of forest cover in the landscape like cities (Buler and Dawson 2014). Moreover, the same study found that bird density was positively related to the amount of human development in the landscape near large cities. Thus, large cities actually had relatively greater bird densities within them after accounting for the amount of forest cover and other factors shaping migrant distributions. This supports the hypothesis that migrating birds may actually be attracted to large urban areas at a landscape scale.

A possible mechanism for the greater migrant densities in landscape with greater urban development could be phototaxis of migrants to the artificial light glow of big cities when they are migrating at night (Gauthreaux and Belser 2006), which has also been cited as an explanation for altitudinal shifts in migrants during flight (Bowlin et al. 2015). This led us to consider proximity to brightly lit areas as a predictor of migrant densities. Interestingly, we found that migrants appeared to avoid brightly lit areas in the early years, but show attraction to bright lights in the later years. This early evidence of such broad-scale response to bright lights of cities for migrating birds from radar observations is exciting, but needs further development. It is hard to interpret these findings in isolation of other field data to better understand these patterns. We are cautious to suggest that migrants may be evolving their response to being more attracted to bright areas in more recent years, but that is a possibility given the evidence. Alternatively, spurious relationships or confounding factors could be vetted with more comprehensive time series analysis of this relationship rather than relying on just two time points for comparison.

Future research should be focused on better understanding changes in migrant distributions over longer time scales (e.g., the radar data archive began in1995 for most radars)

and with greater frequency (e.g., annually) within landscapes with high turn-over (i.e., regions with active timber industry) in order to address questions about behavioral shifts in habitat use and population regulation patterns in response to landscape-change, weather, and climate drivers.

It is important that we improve our understanding of important stopover areas in order to more effectively conserve songbirds. These data can be useful to achieve this goal by quantifying what habitats birds generally favor as well as where local bird populations are changing densities in relation to land cover changes. This will aid to promote wise use land development as well as protecting areas where birds are consistently stopping over at high densities.

ACKNOWLEDGEMENTS

We thank Emily Slingerland for assistance with radar data screening and Deanna Dawson for assistance with radar data screening and providing helpful discussions about study design and analysis. We also thank John Carpenter for helpful discussions about study design and analysis. Doug Newcomb provided LiDAR data on canopy heights.

LITERATURE CITED

Åkesson, S., T. Alerstam, and A. Hedenström. 1996. Flight initiation of nocturnal passerine migrants in relation to celestial orientation conditions at twilight. J Avian Biol 27.

Bonter, D. N., S. A. Gauthreaux, and T. M. Donovan. 2009. Characteristics of important stopover locations for migrating birds: Remote sensing with radar in the Great Lakes Basin. Conservation Biology 23:440–448.

Bowlin, M. S., D. A. Enstrom, B. J. Murphy, E. Plaza, P. Jurich, and J. Cochran. 2015. Unexplained altitude changes in a migrating thrush: Long-flight altitude data from radio-telemetry. The Auk 132:808–816.

Brown, M. J., and J. T. ; Vogt. 2015. North Carolina's forests, 2013.

Brown, S., C. Hickey, B. Harrington, and R. Gill. 2001. The U.S. shorebird conservation plan, 2nd edition. Manomet Center for Conservation Sciences, Manomet, Massachusetts.

Browning, K. A., and R. Wexler. 1968. The determination of kinematic properties of a wind field using Doppler radar. J Appl Meteorol 7.

Buler, J. J., and D. K. Dawson. 2014. Radar analysis of fall bird migration stopover sites in the northeastern U.S. The Condor: Ornithological Applications 116:357–370.

Buler, J. J., and R. H. Diehl. 2009. Quantifying bird density during migratory stopover using weather surveillance radar. IEEE Transactions on Geoscience and Remote Sensing 47:2741–2751.

Buler, J. J., V. Lakshmanan, and D. La Puma. 2012a. Improving weather radar data processing for biological research applications: final report. USGS Patuxent Wildlife Research Center, Laurel, MD, USA.

Buler, J. J., and F. R. Moore. 2011. Migrant–habitat relationships during stopover along an ecological barrier: extrinsic constraints and conservation implications. Journal of Ornithology 152:S101–S112.

Buler, J. J., F. R. Moore, and S. Woltmann. 2007. A multi-scale examination of stopover habitat use by birds. Ecology 88:1789–1802.

Buler, J. J., L. A. Randall, J. P. Fleskes, W. C. Barrow, T. Bogart, and D. Kluver. 2012b. Mapping wintering waterfowl distributions using weather surveillance radar. PLoS ONE 7:e41571.

Farnsworth, A., D. Sheldon, J. Geevarghese, J. Irvine, B. Van Doren, K. Webb, T. Dietterich, and S. Kelling. 2014. Reconstructing velocities of migrating birds from weather radar - A case study in computational sustainability. AI Magazine 35:31–48.

Gauthreaux, S. A., and C. G. Belser. 1998. Displays of bird movements on the WSR-88D: patterns and quantification. Weather and Forecasting 13:453–464.

Gauthreaux, S. A., and C. G. Belser. 2006. Effects of artificial night lighting on migrating birds. Pages 67–93*in* C. Rich and T. Longcore, editors.Ecological consequences of artificial night lighting. Island Press, Washington, D. C.

Gauthreaux, S. A., J. E. Michi, and C. G. Belser. 2005. The temporal and spatial structure of the atmosphere and its influence on bird migration strategies. Pages 182–196*in* R. Greenberg and P. P. Marra, editors.Birds of two worlds. Smithsonian Institution, Washington, D. C.

Guisan, A., T. C. Edwards Jr, and T. Hastie. 2002. Generalized linear and generalized additive models in studies of species distributions: setting the scene. Ecological Modelling 157:89–100.

Hijmans, R. J., S. Phillips, J. R. Leathwick, and J. Elith. 2015. Package “dismo”. Species distribution modeling.

Hutto, R. L. 1985. Habitat selection by nonbreeding, migratory land birds. Pages 455–476*in* M. L. Cody, editor.Habitat selection in birds. Academic Press, Inc., Orlando.

Kelly, J. F., R. Smith, D. M. Finch, F. R. Moore, and W. Yong. 1999. Influence of summer biogeography on wood warbler stopover abundance. Condor 101:76–85.

Kushlan, J., M. Steinkamp, K. Parsons, J. Capp, M. Acosta Cruz, M. C. Coulter, I. Davidson, L. Dickson, N. Edelson, R. Elliot, R. Erwin, S. Hatch, S. Kress, R. Milko, S. Miller, K. Mills, R. Paul, R. Phillips, J. Saliva, W. J. Sydeman, J. Trapp, J. Wheeler, and K. Wohl. 2002. Waterbird Conservation for the Americas: The North American Waterbird Conservation Plan, Version 1. Waterbird Conservation for the Americas. Washington, DC, USA.

La Sorte, F. A., M. W. Tingley, and A. H. Hurlbert. 2014. The role of urban and agricultural areas during avian migration: an assessment of within-year temporal turnover. Global Ecology and Biogeography 23:1225–1234.

LaFleur, J. M., J. J. Buler, and F. R. Moore. 2016. Geographic position and landscape composition explain regional patterns of migrating landbird distributions during spring stopover along the northern coast of the Gulf of Mexico. Landscape Ecology:1–13.

Larkin, R. P. 1991. Flight speeds observed with radar, a correction: slow "birds" are insects. Behavioral Ecology and Sociobiology 29:221–224.

Larkin, R. P., W. R. Evans, and R. H. Diehl. 2002. Nocturnal flight calls of Dickcissels and Doppler radar echoes over South Texas in spring. Journal of Field Ornithology 73:2–8.

Li, J. 2016. Assessing spatial predictive models in the environmental sciences: Accuracy measures, data variation and variance explained. Environmental Modelling & Software 80:1–8.

Mcfarland, T. M., C. Van Riper, and G. E. Johnson. 2012. Evaluation of NDVI to assess avian abundance and richness along the upper San Pedro River. Journal of Arid Environments 77:45–53.

Moore, F. R., M. S. Woodrey, J. J. Buler, S. Woltmann, and T. R. Simons. 2005. Understanding the stopover of migratory birds: a scale dependent approach. Pages 684–689*in* C. J. Ralph and T. D. Rich, editors.Bird Conservation Implementation and Integration in the Americas: Proceedings of the Third International Partners in Flight Conference. USDA Forest Service, Gen. Tech. Rep. PSW-GTR-191.

Newton, I. 2004. Population limitation in migrants. Ibis 146:197–226.

North Carolina Wildlife Resources Commission. 2005. North Carolina Wildlife Action Plan. Raleigh, NC.

Osborne, P. E., J. C. Alonso, and R. G. Bryant. 2001. Modelling landscape-scale habitat use using GIS and remote sensing: a case study with great bustards. Journal of applied ecology 38:458–471.

Ralph, C. J. 1978. Disorientation and possible fate of young passerine coastal migrants. Bird Banding 49:237–247.

Rich, T. D., C. J. Beardmore, H. Berlanga, P. J. Blancher, M. S. W. Bradstreet, G. S. Butcher, D. W. Demarest, E. H. Dunn, W. C. Hunter, E. E. Iñigo-Elias, J. A. Kennedy, A. M. Martell, A. O. Panjabi, D. N. Pashley, K. V. Rosenberg, C. M. Rustay, J. S. Wendt, and T. C. Will. 2004. Partners in Flight North American Landbird Conservation Plan. Cornell Lab of Ornithology, Ithaca, NY.

Richardson, W. J. 1978. Timing and amount of bird migration in relation to weather: A review. Oikos 30:224–272.

Seewagen, C. L., and E. J. Slayton. 2008. Mass changes of migratory landbirds during stopovers in a New York city park. The Wilson Journal of Ornithology 120:296–303.

Sillett, T. S., and R. T. Holmes. 2002. Variation in survivorship of a migratory songbird throughout its annual cycle. Journal of Animal Ecology 71:296–308.

Sorte, F. A. L., D. Fink, W. M. Hochachka, and S. Kelling. 2016. Convergence of broad-scale migration strategies in terrestrial birds. Proc. R. Soc. B 283:20152588.

Valcu, M., and B. Kempenaers. 2010. Spatial autocorrelation: an overlooked concept in behavioral ecology. Behavioral Ecology 21:902–905.

Wiens, J. A. 1989. Spatial scaling in ecology. Functional Ecology 3:385–397.

Wood, S. N. 2011. Fast stable restricted maximum likelihood and marginal likelihood estimation of semiparametric generalized linear models. Journal of the Royal Statistical Society: Series B (Statistical Methodology) 73:3–36.

APPENDIX A. Locally classified bird stopover density during fall of early (2000-2002; n=31) and late (2013-2014; n=18) years from KAKQ (Wakefield, VA).

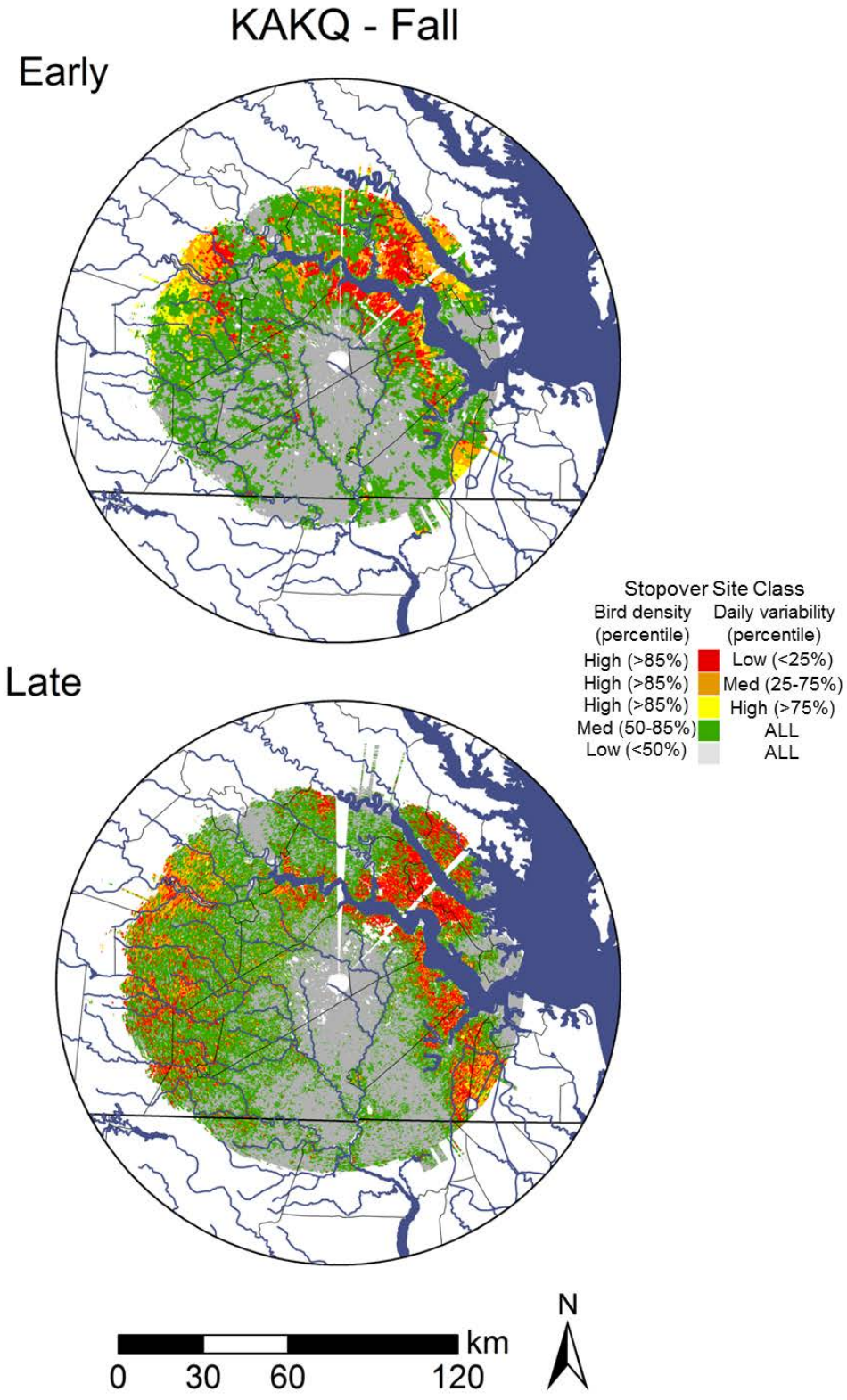

APPENDIX A. (continued). Locally classified bird stopover density during **spring** of early (2000-2003; n=38) and late (2013-2015; n=52) years from **KAKQ** (Wakefield, VA).

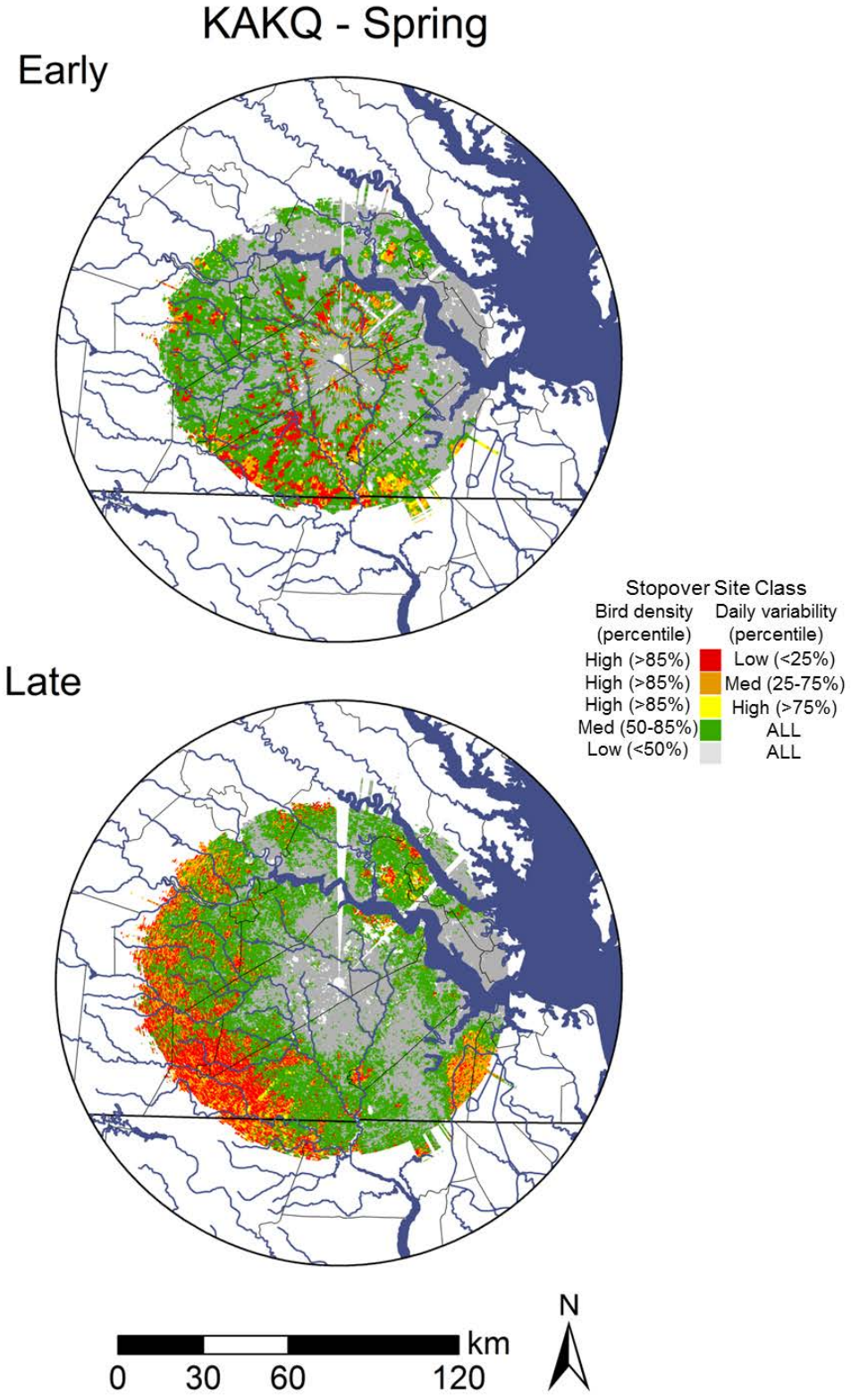

APPENDIX A. (continued). Locally classified bird stopover density during **fall** of early (2000-2002; n=51) and late (2013-2014; n=50) years from **KGSP** (Greer, SC).

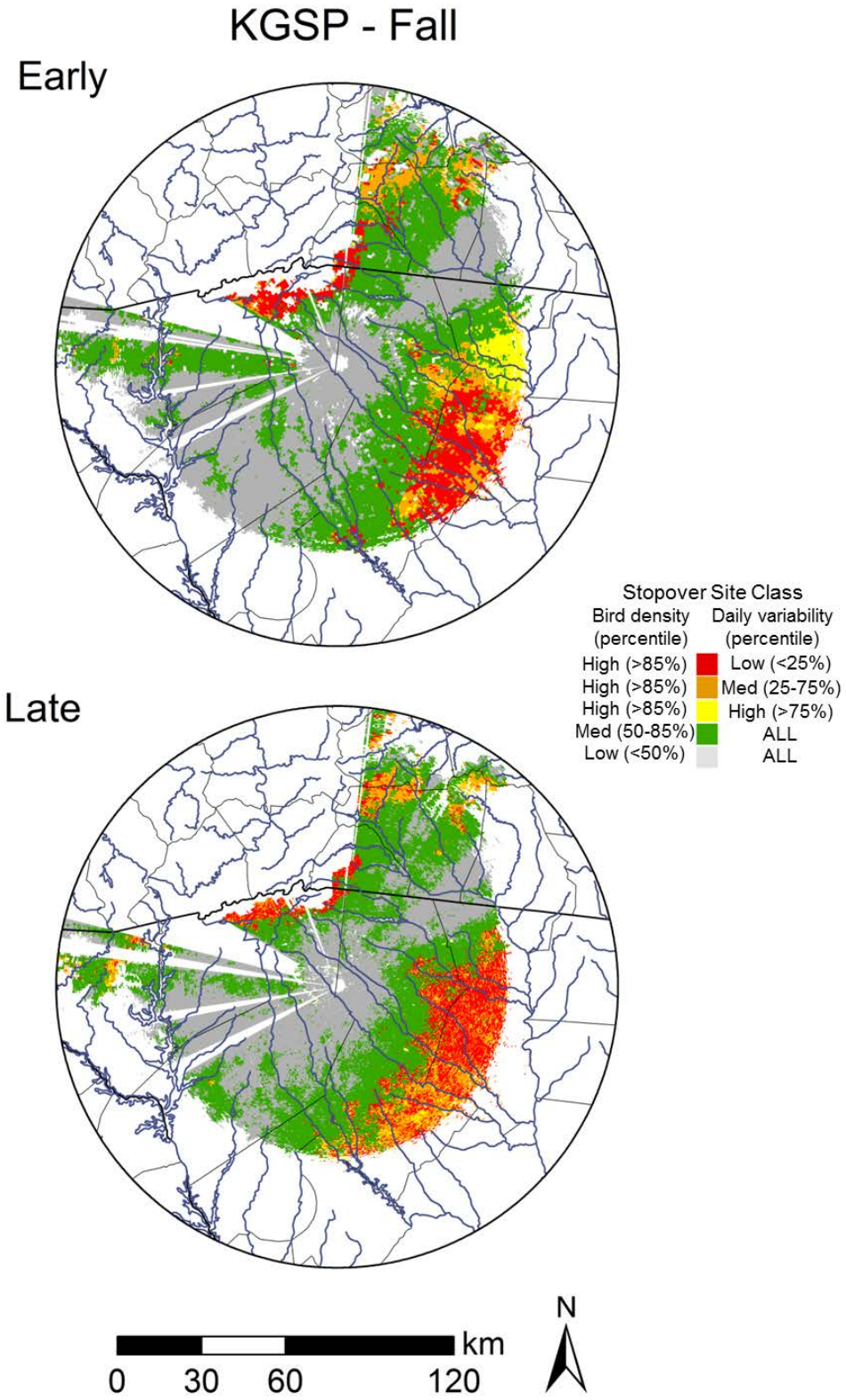

APPENDIX A. (continued). Locally classified bird stopover density during **spring** of early (2000-2003; n=70) and late (2013-2015; n=52) years from **KGSP** (Greer, SC).

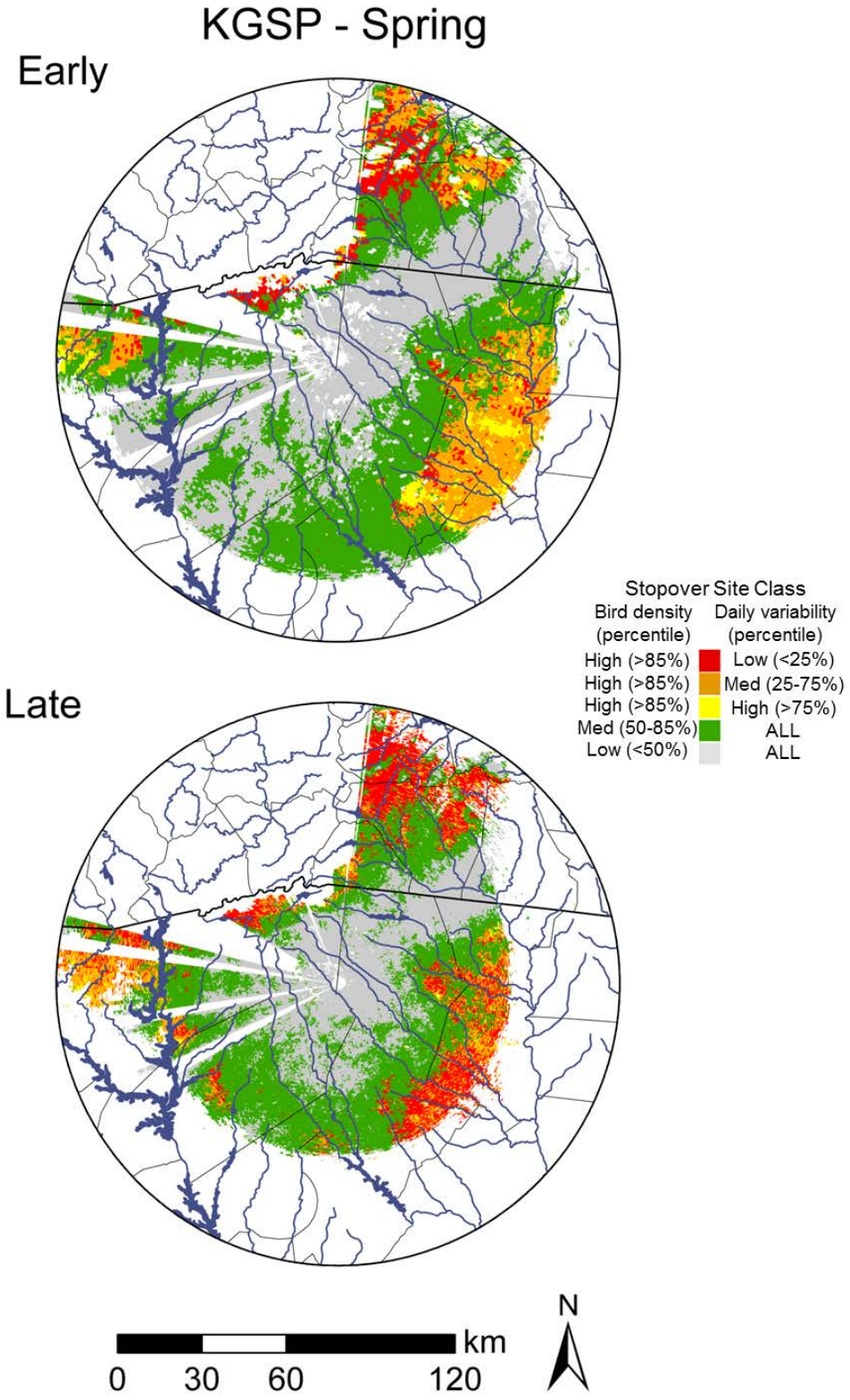

APPENDIX A. (continued). Locally classified bird stopover density during **fall** of early (2000-2002; n=26) and late (2013-2014; n=32) years from **KLTX** (Wilmington, NC).

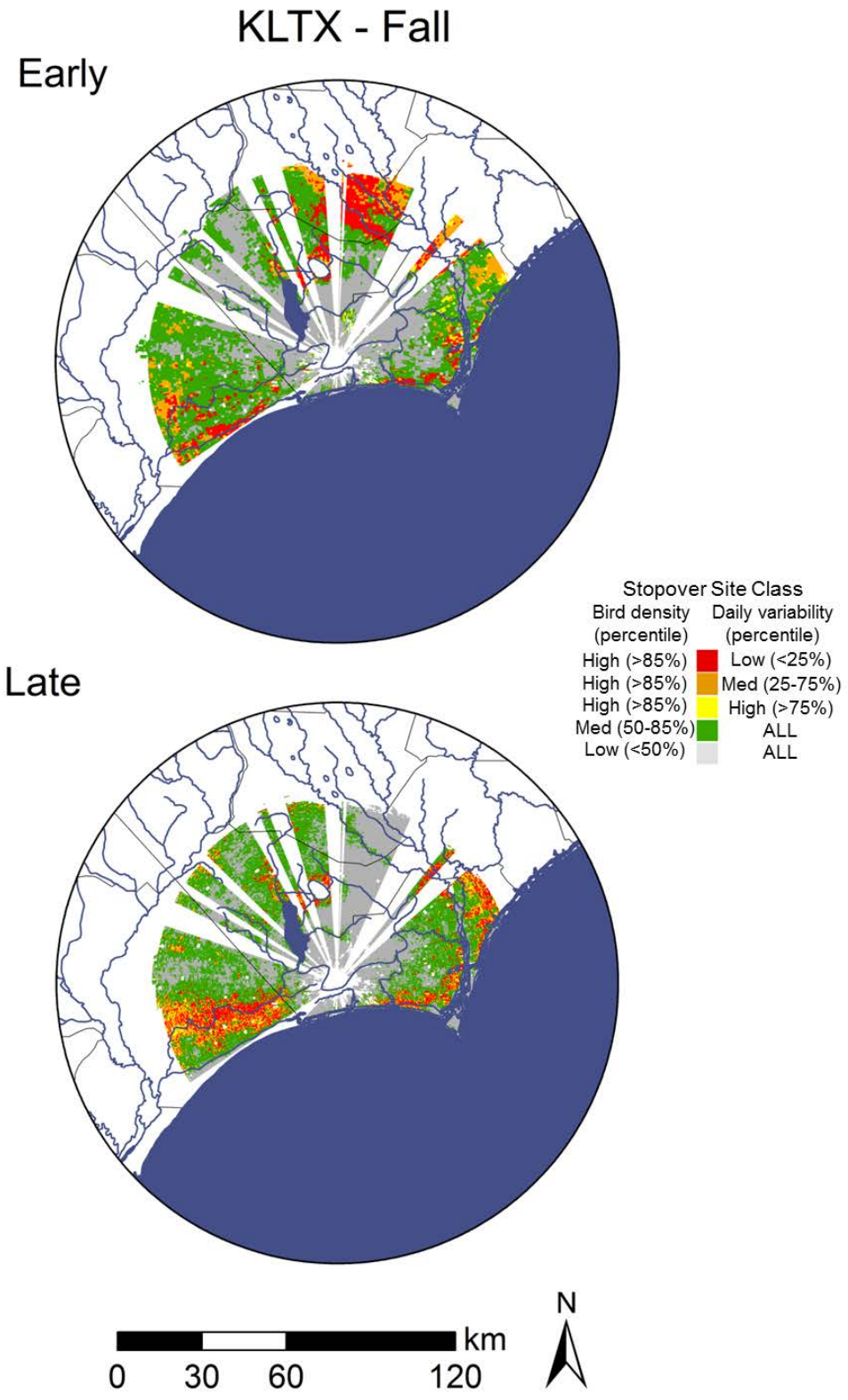

APPENDIX A. (continued). Locally classified bird stopover density during **spring** of early (2000-2003; n=28) and late (2013-2015; n=35) years from **KLTX** (Wilmington, NC).

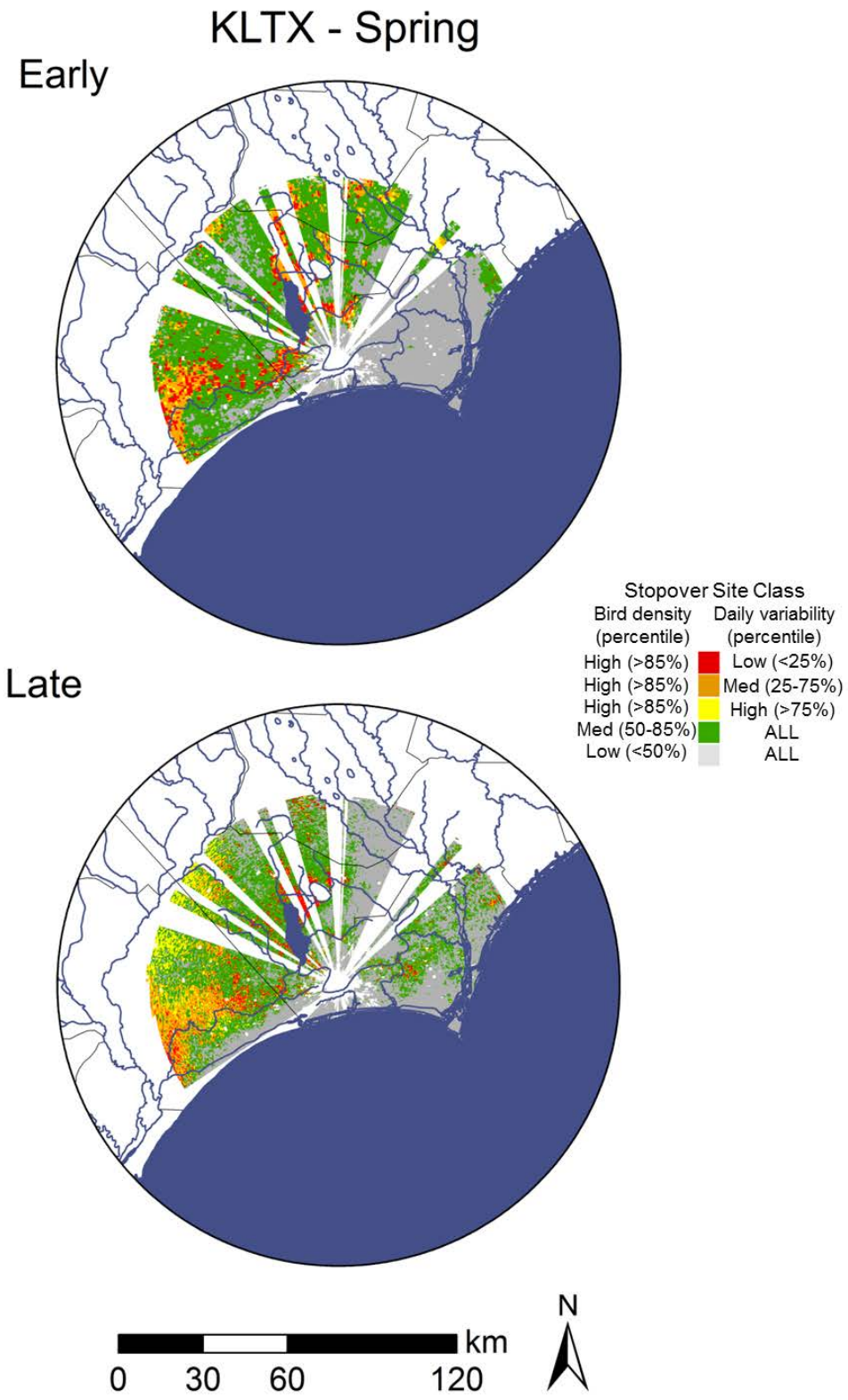

APPENDIX A. (continued). Locally classified bird stopover density during **fall** of early (2000-2002; n=44) and late (2013-2014; n=13) years from **KMHX** (Morehead City, NC).

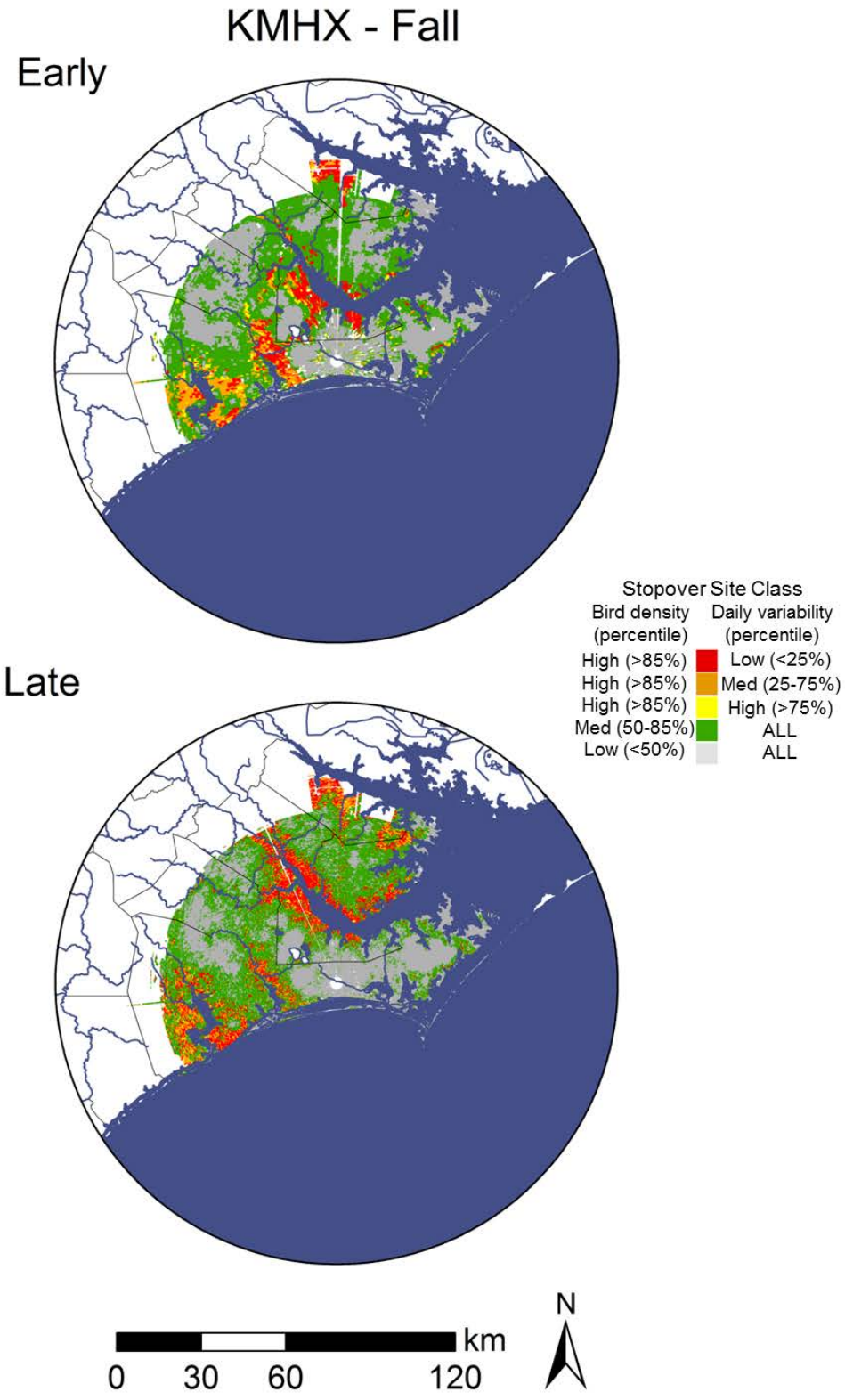

APPENDIX A. (continued). Locally classified bird stopover density during **spring** of early (2000-2003; n=15) and late (2013-2015; n=30) years from **KMHX** (Morehead City, NC).

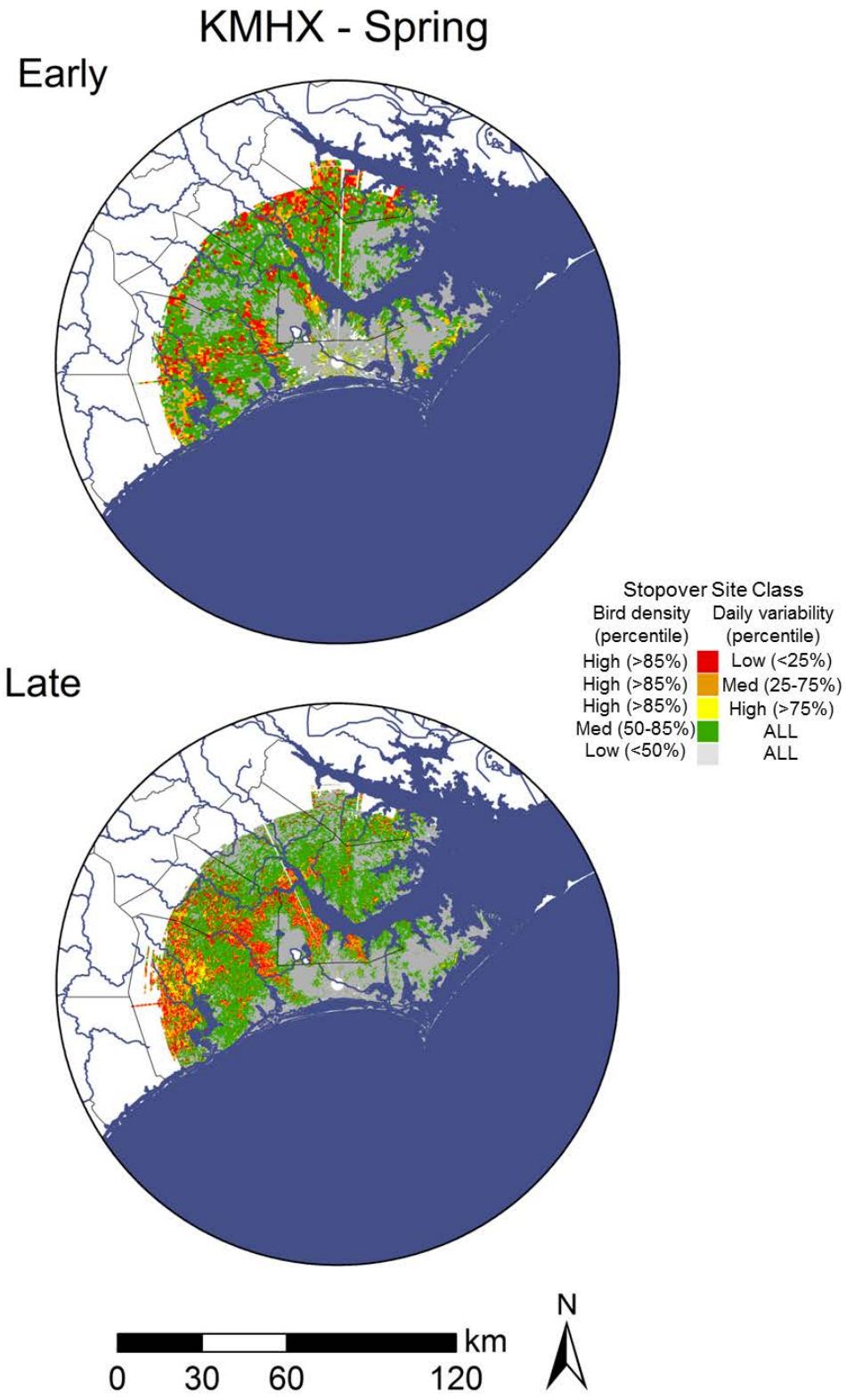

APPENDIX A. (continued). Locally classified bird stopover density during **fall** of early (2000-2002; =60) and late (2013-2014; n=44) years from **KRAX** (Raleigh, NC).

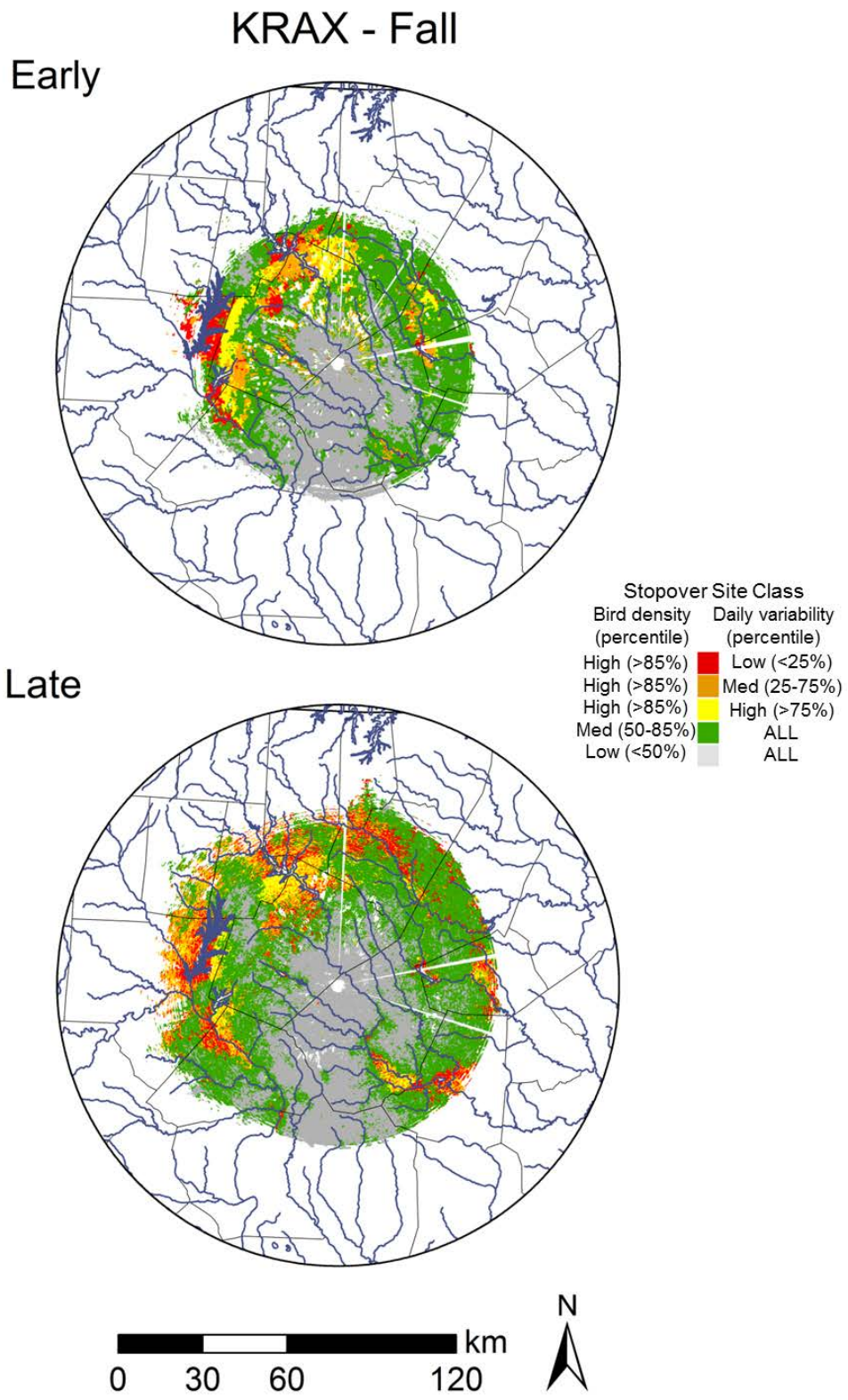

APPENDIX A. (continued). Locally classified bird stopover density during **spring** of early (2000-2003; n=26) and late (2013-2015; n=33) years from **KRAX** (Raleigh, NC).

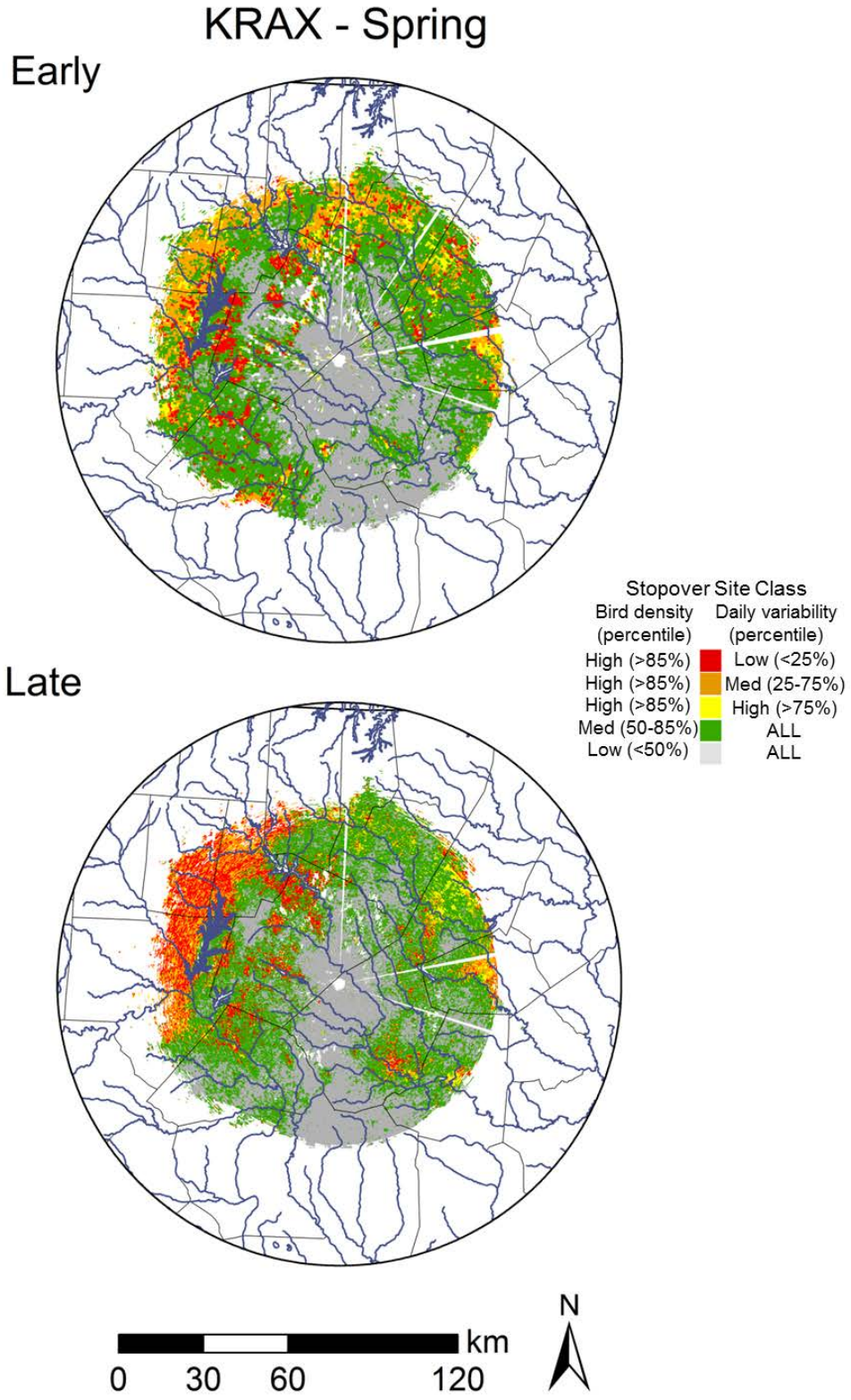

APPENDICES B1-B8. The following pages present a series of outputs of marginal response plots and summaries of Generalized Additive Models predicting the log of geometric mean VIR (i.e., mean VIR) and Coefficient of Variation of geometric mean VIR (i.e., CV VIR) of relative bird stopover density for each one square kilometer cell within North Carolina. Effective degrees of freedom of spline functions are denoted in parentheses on y-axis labels of plots. Responses for log of mean VIR are backtransformed onto original scale of measurement (cm2/ha).

APPENDIX B.1. Marginal response plots and summary of GAM model fit for **mean VIR during spring of early years** (2000-2003).

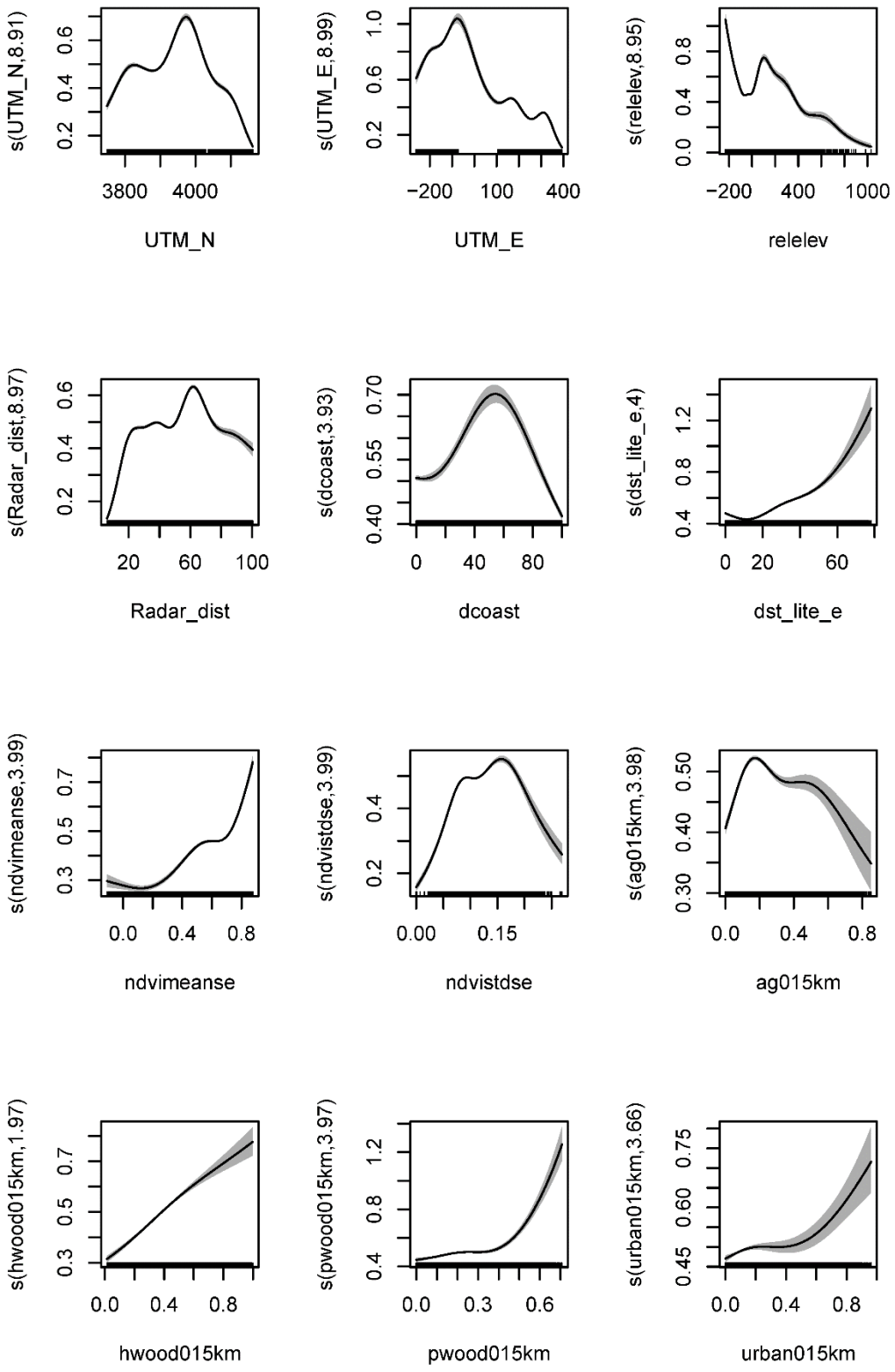

APPENDIX B.1. (continued)

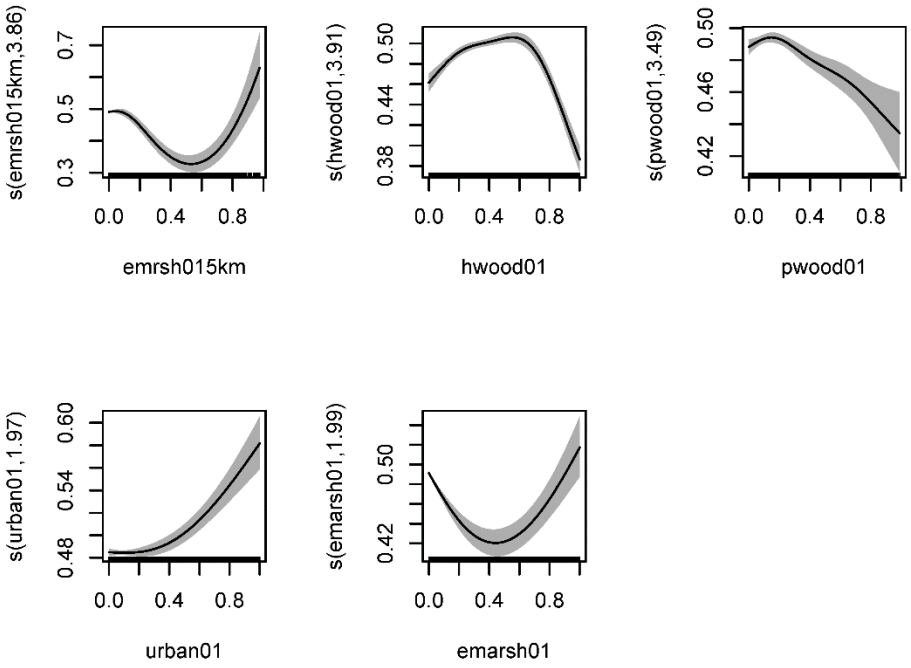

APPENDIX B.1. (continued)

```
Early years spring mean VIR
Family: gaussian
Link function: identity

Formula:
lgeo ~ s(UTM_N, k = 10) + s(UTM_E, k = 10) + s(relelev, k = 10) +
    s(Radar_dist, k = 10) + s(dcoast, k = 5) + s(dst_lite_e,
    k = 5) + s(ndvimeanse, k = 5) + s(ndvistdse, k = 5) + s(ag015km,
    k = 5) + s(hwood015km, k = 3) + s(pwood015km, k = 5) + s(urban015km,
    k = 5) + s(emrsh015km, k = 5) + s(hwood01, k = 5) + s(pwood01,
    k = 5) + s(urban01, k = 3) + s(emarsh01, k = 3)

Parametric coefficients:
             Estimate Std. Error t value Pr(>|t|)
(Intercept) -0.539564   0.001778  -303.4   <2e-16 ***
---
Signif. codes:  0 ‘***’ 0.001 ‘**’ 0.01 ‘*’ 0.05 ‘.’ 0.1 ‘ ’ 1

Approximate significance of smooth terms:
                edf Ref.df       F  p-value
s(UTM_N)      8.913  8.998  537.86  < 2e-16 ***
s(UTM_E)      8.991  9.000 1123.91  < 2e-16 ***
s(relelev)    8.953  8.999  293.75  < 2e-16 ***
s(Radar_dist) 8.972  9.000  939.00  < 2e-16 ***
s(dcoast)     3.926  3.996  286.62  < 2e-16 ***
s(dst_lite_e) 3.999  4.000  458.21  < 2e-16 ***
s(ndvimeanse) 3.993  4.000  356.96  < 2e-16 ***
s(ndvistdse)  3.990  4.000  301.63  < 2e-16 ***
s(ag015km)    3.981  4.000  157.35  < 2e-16 ***
s(hwood015km) 1.969  1.999  290.30  < 2e-16 ***
s(pwood015km) 3.970  3.999  109.33  < 2e-16 ***
s(urban015km) 3.661  3.935   18.17 1.43e-12 ***
s(emrsh015km) 3.864  3.989   46.66  < 2e-16 ***
s(hwood01)    3.913  3.995   86.50  < 2e-16 ***
s(pwood01)    3.487  3.855   10.48 3.60e-08 ***
s(urban01)    1.973  1.999   37.56  < 2e-16 ***
s(emarsh01)   1.993  2.000   53.70  < 2e-16 ***
---
Signif. codes:  0 ‘***’ 0.001 ‘**’ 0.01 ‘*’ 0.05 ‘.’ 0.1 ‘ ’ 1

R-sq.(adj) =  0.799   Deviance explained =   80%
GCV = 0.16939  Scale est. = 0.16913   n = 53472
```

APPENDIX B.2. Marginal response plots and summary of GAM model fit for **CV VIR during spring of early years** (2000-2003).

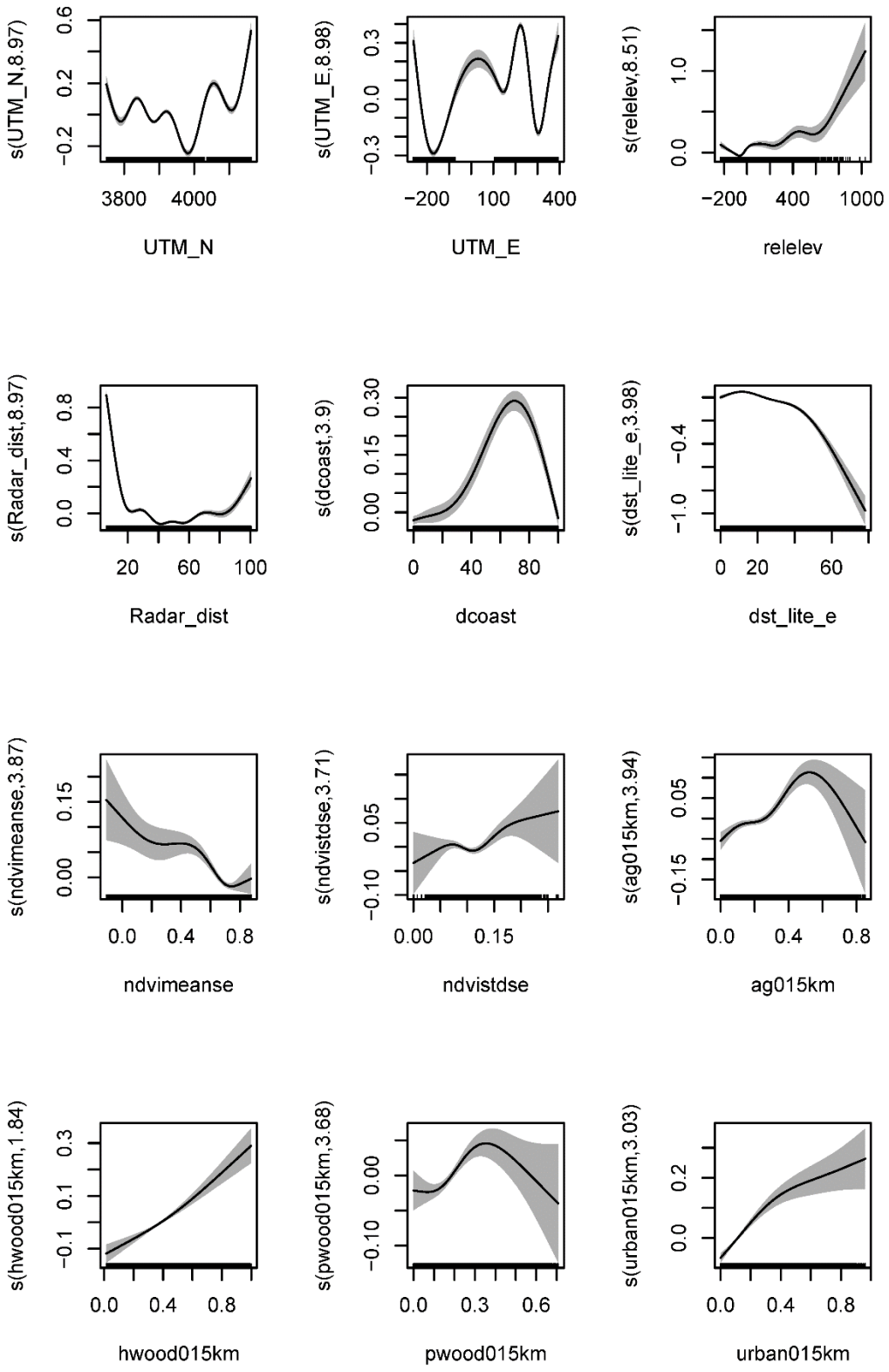

APPENDIX B.2. (continued)

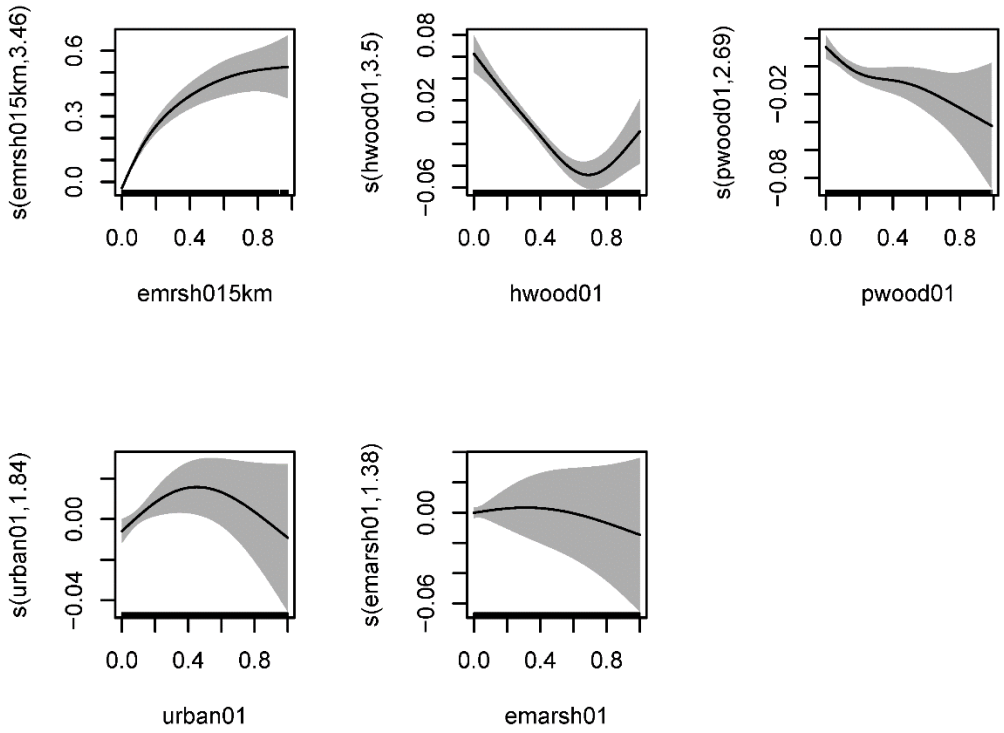

APPENDIX B.2. (continued)

```
Early years spring cv
Family: gaussian
Link function: identity

Formula:
es_cvros ~ s(UTM_N, k = 10) + s(UTM_E, k = 10) + s(relelev, k = 10) +
    s(Radar_dist, k = 10) + s(dcoast, k = 5) + s(dst_lite_e,
    k = 5) + s(ndvimeanse, k = 5) + s(ndvistdse, k = 5) + s(ag015km,
    k = 5) + s(hwood015km, k = 3) + s(pwood015km, k = 5) + s(urban015km,
    k = 5) + s(emrsh015km, k = 5) + s(hwood01, k = 5) + s(pwood01,
    k = 5) + s(urban01, k = 3) + s(emarsh01, k = 3)

Parametric coefficients:
            Estimate Std. Error t value Pr(>|t|)
(Intercept) 1.409238   0.001662     848   <2e-16 ***
---
Signif. codes:  0 ‘***’ 0.001 ‘**’ 0.01 ‘*’ 0.05 ‘.’ 0.1 ‘ ’ 1

Approximate significance of smooth terms:
                edf Ref.df       F  p-value
s(UTM_N)      8.973  9.000 175.592  < 2e-16 ***
s(UTM_E)      8.982  9.000 535.216  < 2e-16 ***
s(relelev)    8.514  8.932  27.683  < 2e-16 ***
s(Radar_dist) 8.967  9.000 476.418  < 2e-16 ***
s(dcoast)     3.901  3.993 153.349  < 2e-16 ***
s(dst_lite_e) 3.977  4.000 122.943  < 2e-16 ***
s(ndvimeanse) 3.870  3.990  20.057  < 2e-16 ***
s(ndvistdse)  3.708  3.956   6.353 0.000162 ***
s(ag015km)    3.944  3.998  23.267  < 2e-16 ***
s(hwood015km) 1.844  1.973  44.205  < 2e-16 ***
s(pwood015km) 3.680  3.945  11.814 2.42e-09 ***
s(urban015km) 3.026  3.543  29.245  < 2e-16 ***
s(emrsh015km) 3.455  3.833  67.524  < 2e-16 ***
s(hwood01)    3.500  3.863  30.431  < 2e-16 ***
s(pwood01)    2.693  3.234   4.342 0.003585 **
s(urban01)    1.837  1.970   4.323 0.021121 *
s(emarsh01)   1.384  1.618   0.233 0.670695
---
Signif. codes:  0 ‘***’ 0.001 ‘**’ 0.01 ‘*’ 0.05 ‘.’ 0.1 ‘ ’ 1

R-sq.(adj) =  0.333   Deviance explained = 33.4%
GCV = 0.14789  Scale est. = 0.14768   n = 53472
```

APPENDIX B.3. Marginal response plots and summary of GAM model fit for **mean VIR during spring of late years** (2013-2015).

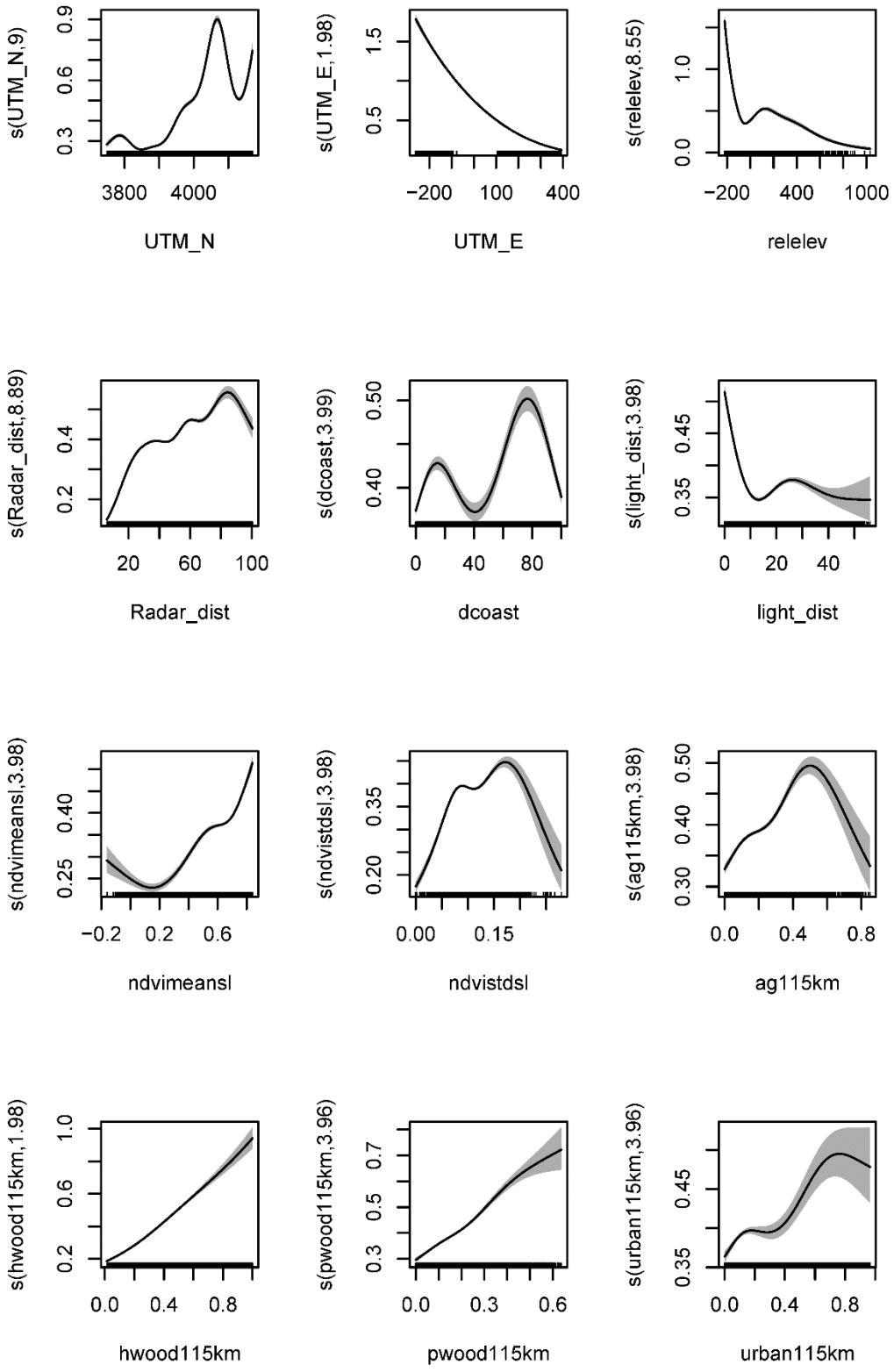

APPENDIX B.3. (continued)

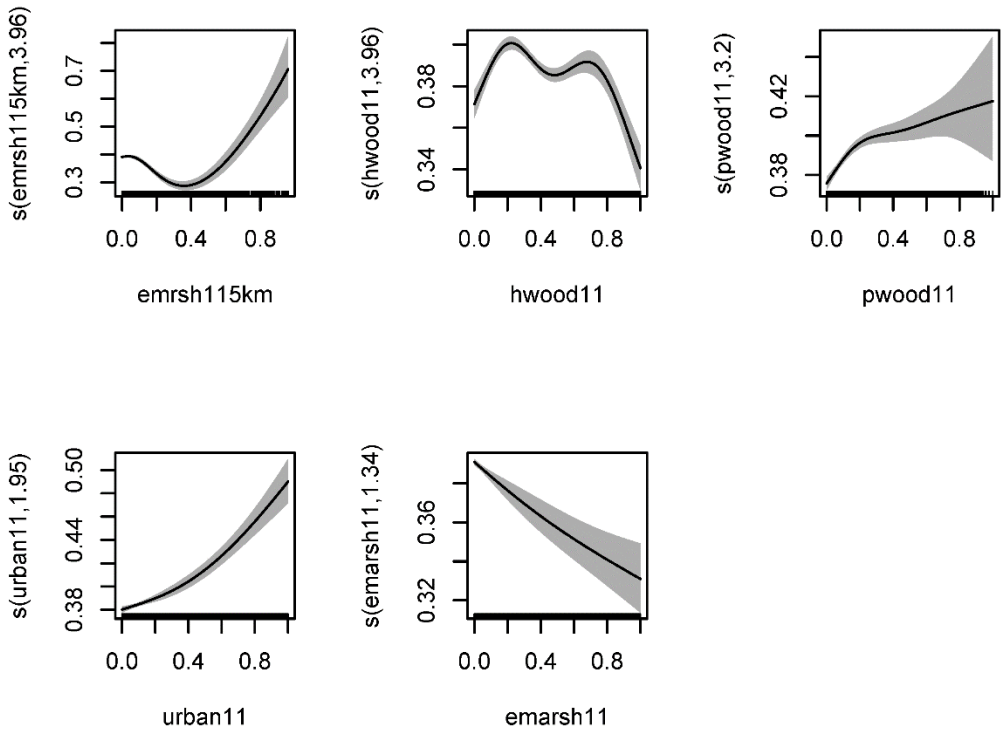

APPENDIX B.3. (continued)

```
Late years spring mean VIR
Family: gaussian
Link function: identity

Formula:
lgeo ~ s(UTM_N, k = 10) + s(UTM_E, k = 3) + s(relelev, k = 10) +
    s(Radar_dist, k = 10) + s(dcoast, k = 5) + s(light_dist,
    k = 5) + s(ndvimeansl, k = 5) + s(ndvistdsl, k = 5) + s(ag115km,
    k = 5) + s(hwood115km, k = 3) + s(pwood115km, k = 5) + s(urban115km,
    k = 5) + s(emrsh115km, k = 5) + s(hwood11, k = 5) + s(pwood11,
    k = 5) + s(urban11, k = 3) + s(emarsh11, k = 3)

Parametric coefficients:
             Estimate Std. Error t value Pr(>|t|)
(Intercept) -0.693895   0.001848  -375.4   <2e-16 ***
---
Signif. codes:  0 ‘***’ 0.001 ‘**’ 0.01 ‘*’ 0.05 ‘.’ 0.1 ‘ ’ 1

Approximate significance of smooth terms:
                edf Ref.df        F  p-value
s(UTM_N)      8.998  9.000  1704.54  < 2e-16 ***
s(UTM_E)      1.981  2.000 13406.60  < 2e-16 ***
s(relelev)    8.548  8.943   699.32  < 2e-16 ***
s(Radar_dist) 8.890  8.996  1100.02  < 2e-16 ***
s(dcoast)     3.991  4.000   111.85  < 2e-16 ***
s(light_dist) 3.976  4.000   270.24  < 2e-16 ***
s(ndvimeansl) 3.982  4.000   252.13  < 2e-16 ***
s(ndvistdsl)  3.982  4.000   187.75  < 2e-16 ***
s(ag115km)    3.979  4.000   103.04  < 2e-16 ***
s(hwood115km) 1.985  2.000  1095.20  < 2e-16 ***
s(pwood115km) 3.956  3.999   194.46  < 2e-16 ***
s(urban115km) 3.962  3.999    29.23  < 2e-16 ***
s(emrsh115km) 3.956  3.999   100.89  < 2e-16 ***
s(hwood11)    3.961  3.999    31.16  < 2e-16 ***
s(pwood11)    3.199  3.672    21.09 1.36e-15 ***
s(urban11)    1.949  1.997    77.90  < 2e-16 ***
s(emarsh11)   1.340  1.564    30.69 1.28e-09 ***
---
Signif. codes:  0 ‘***’ 0.001 ‘**’ 0.01 ‘*’ 0.05 ‘.’ 0.1 ‘ ’ 1

R-sq.(adj) =  0.856   Deviance explained = 85.6%
GCV = 0.17624  Scale est. = 0.17598   n = 51521
```

APPENDIX B.4. Marginal response plots and summary of GAM model fit for **CV VIR during spring of late** years (2013-2015).

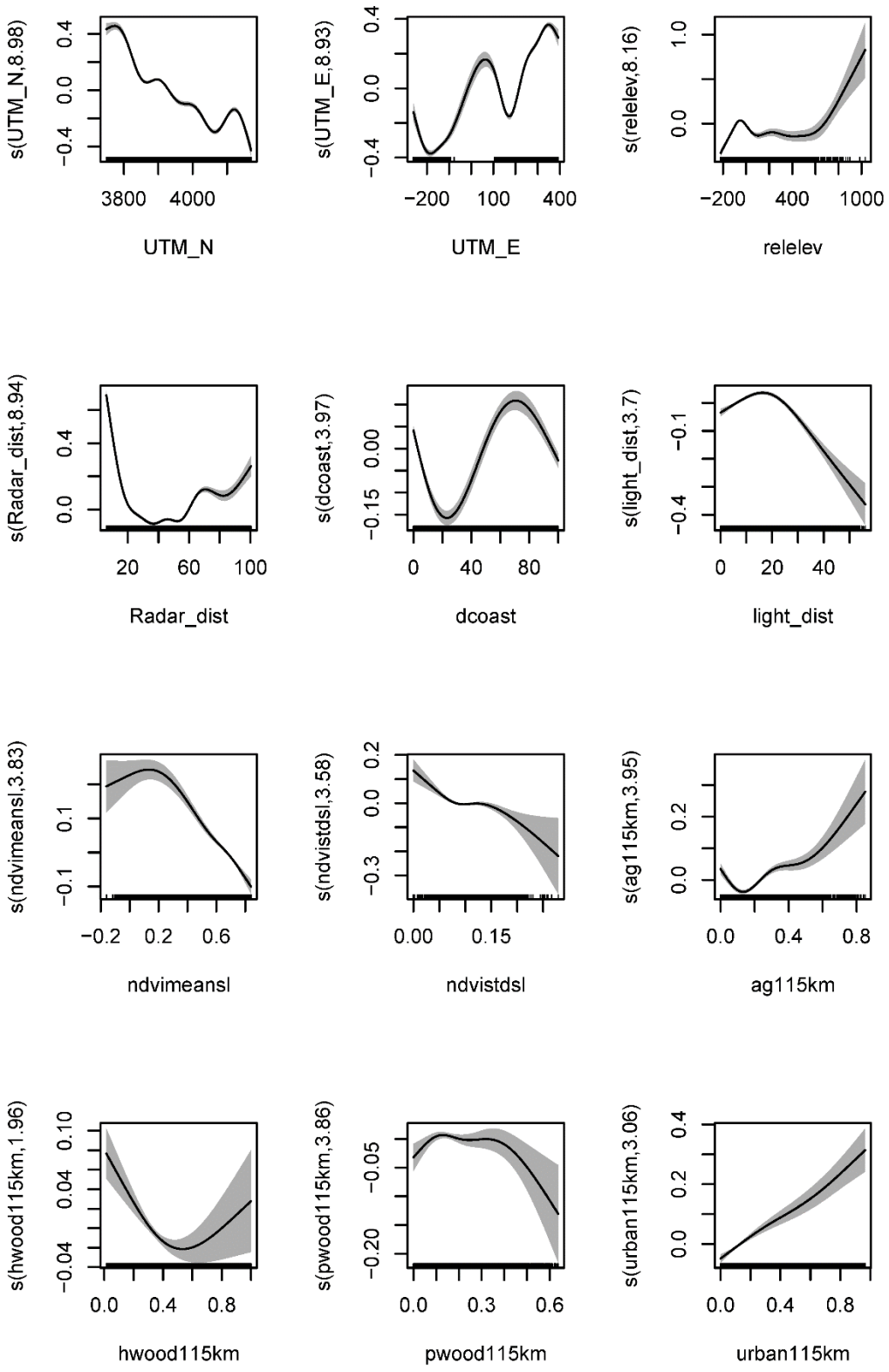

APPENDIX B.4. (continued)

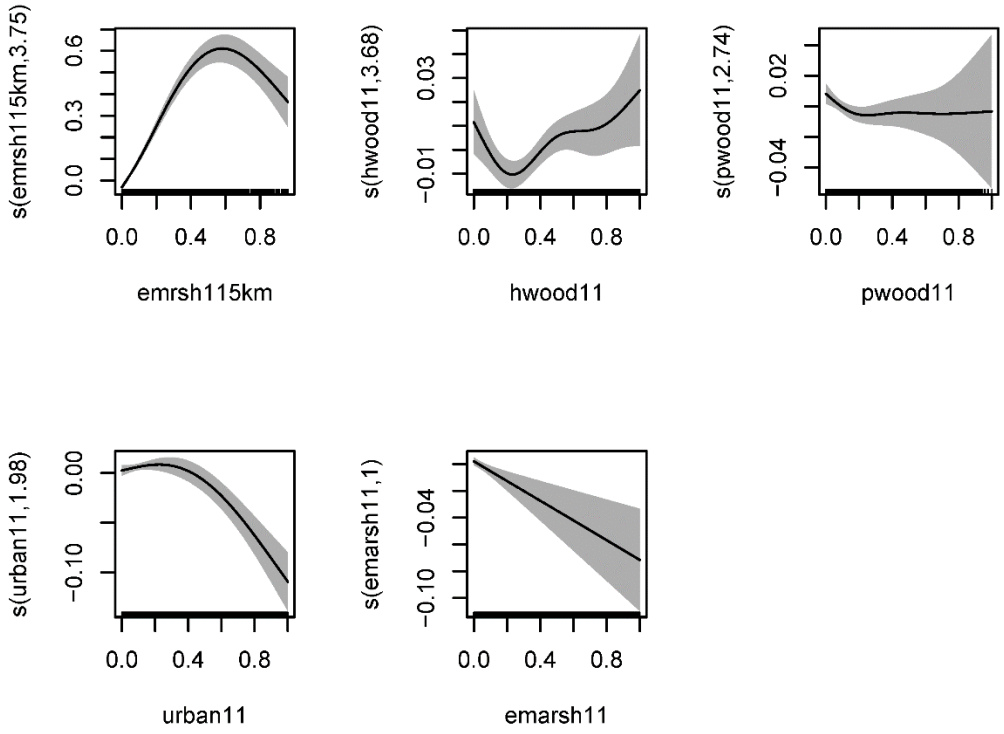

APPENDIX B.4. (continued)

```
Late years spring CV
Family: gaussian
Link function: identity

Formula:
ls_cvros ~ s(UTM_N, k = 10) + s(UTM_E, k = 10) + s(relelev, k = 10) +
    s(Radar_dist, k = 10) + s(dcoast, k = 5) + s(light_dist,
    k = 5) + s(ndvimeansl, k = 5) + s(ndvistdsl, k = 5) + s(ag115km,
    k = 5) + s(hwood115km, k = 3) + s(pwood115km, k = 5) + s(urban115km,
    k = 5) + s(emrsh115km, k = 5) + s(hwood11, k = 5) + s(pwood11,
    k = 5) + s(urban11, k = 3) + s(emarsh11, k = 3)

Parametric coefficients:
            Estimate Std. Error t value Pr(>|t|)
(Intercept)   1.7821     0.0014    1273   <2e-16 ***
---
Signif. codes:  0 ‘***’ 0.001 ‘**’ 0.01 ‘*’ 0.05 ‘.’ 0.1 ‘ ’ 1

Approximate significance of smooth terms:
               edf Ref.df       F  p-value
s(UTM_N)      8.976  9.000 324.929  < 2e-16 ***
s(UTM_E)      8.932  8.998 601.264  < 2e-16 ***
s(relelev)    8.161  8.813  64.550  < 2e-16 ***
s(Radar_dist) 8.937  8.999 609.708  < 2e-16 ***
s(dcoast)     3.969  3.999 178.319  < 2e-16 ***
s(light_dist) 3.696  3.950  90.719  < 2e-16 ***
s(ndvimeansl) 3.831  3.984 108.275  < 2e-16 ***
s(ndvistdsl)  3.578  3.906  15.241 1.61e-11 ***
s(ag115km)    3.950  3.998  55.373  < 2e-16 ***
s(hwood115km) 1.961  1.998  22.757 2.71e-10 ***
s(pwood115km) 3.860  3.988   5.011 0.000484 ***
s(urban115km) 3.059  3.580  25.263  < 2e-16 ***
s(emrsh115km) 3.745  3.961 138.711  < 2e-16 ***
s(hwood11)    3.683  3.942   4.273 0.001271 **
s(pwood11)    2.740  3.281   2.223 0.070411 .
s(urban11)    1.980  1.999  28.411 3.10e-13 ***
s(emarsh11)   1.000  1.000  14.100 0.000174 ***
---
Signif. codes:  0 ‘***’ 0.001 ‘**’ 0.01 ‘*’ 0.05 ‘.’ 0.1 ‘ ’ 1

R-sq.(adj) =   0.56   Deviance explained = 56.1%
GCV = 0.10108  Scale est. = 0.10093   n = 51521
```

APPENDIX B.5. Marginal response plots and summary of GAM model fit for **mean VIR during fall of early years** (2000-2002).

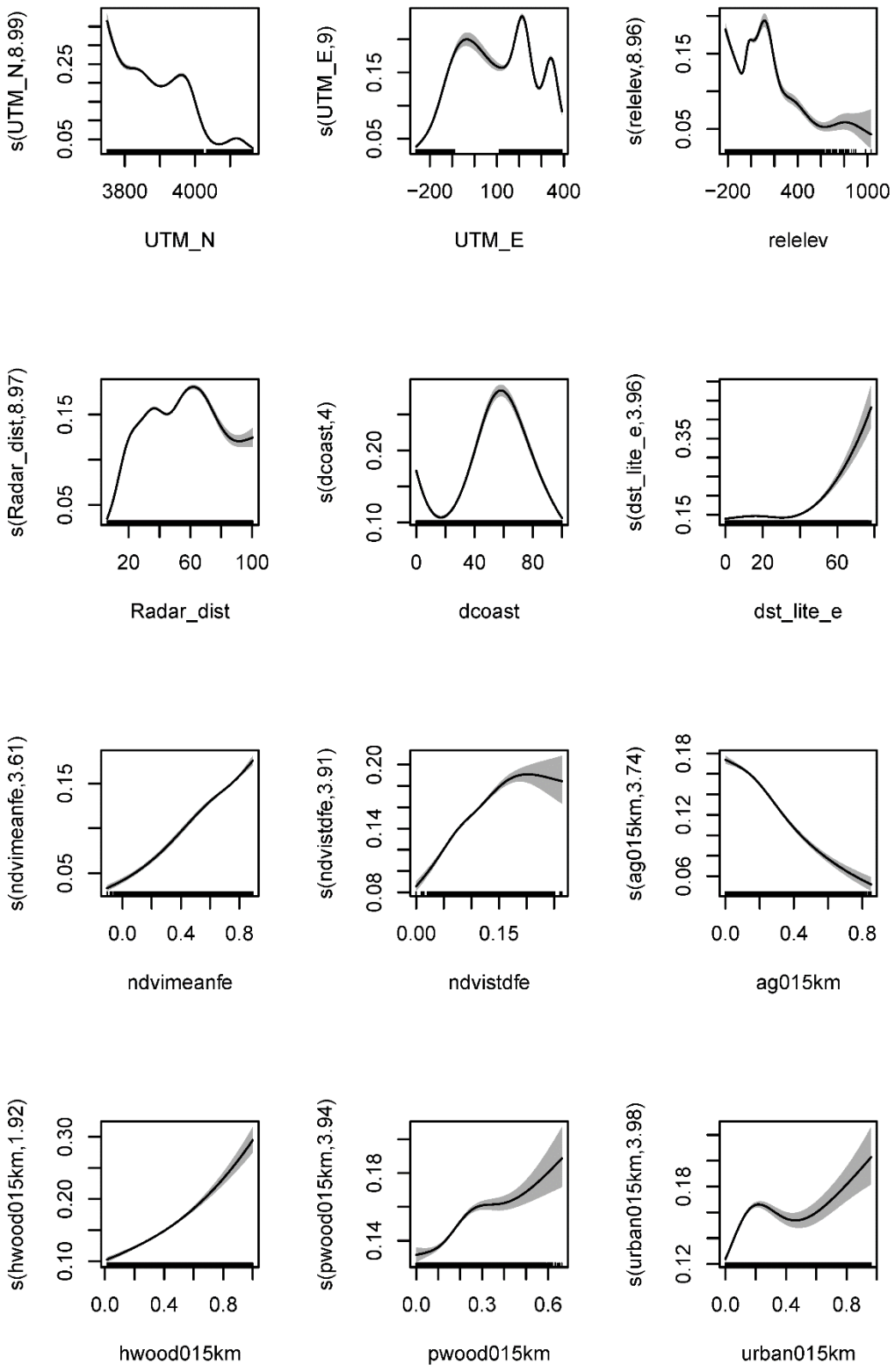

APPENDIX B.5. (continued)

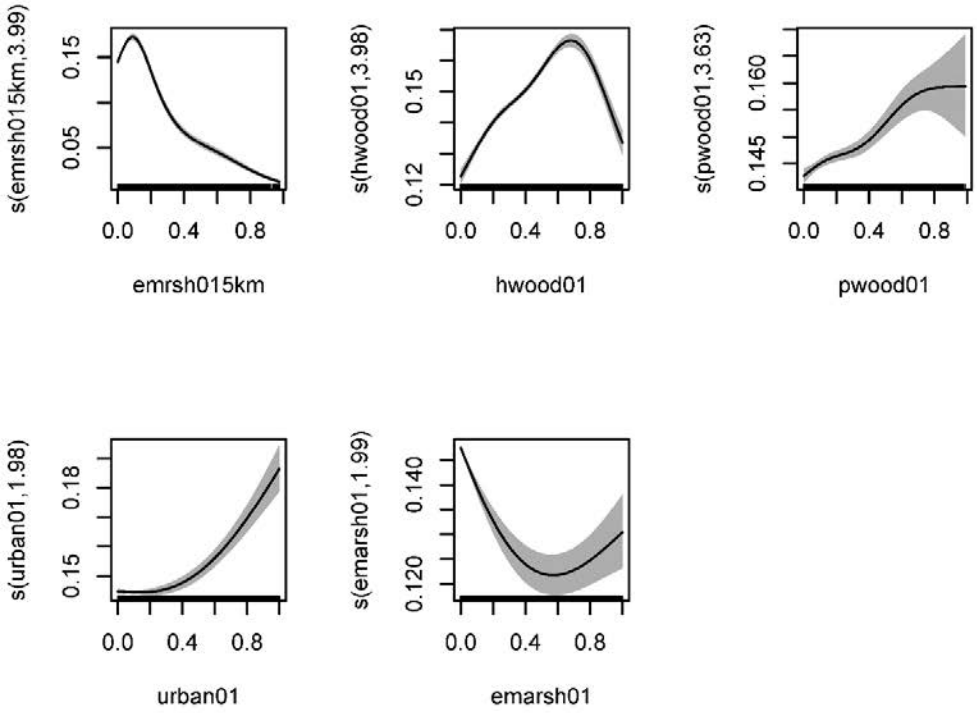

APPENDIX B.5. (continued)

```
Early years fall mean VIR
Family: gaussian
Link function: identity

Formula:
lgeo ~ s(UTM_N, k = 10) + s(UTM_E, k = 10) + s(relelev, k = 10) +
    s(Radar_dist, k = 10) + s(dcoast, k = 5) + s(dst_lite_e,
    k = 5) + s(ndvimeanfe, k = 5) + s(ndvistdfe, k = 5) + s(ag015km,
    k = 5) + s(hwood015km, k = 3) + s(pwood015km, k = 5) + s(urban015km,
    k = 5) + s(emrsh015km, k = 5) + s(hwood01, k = 5) + s(pwood01,
    k = 5) + s(urban01, k = 3) + s(emarsh01, k = 3)

Parametric coefficients:
            Estimate Std. Error t value Pr(>|t|)
(Intercept) 0.412989   0.001758   234.9   <2e-16 ***
---
Signif. codes:  0 ‘***’ 0.001 ‘**’ 0.01 ‘*’ 0.05 ‘.’ 0.1 ‘ ’ 1

Approximate significance of smooth terms:
                edf Ref.df       F  p-value
s(UTM_N)      8.992  9.000 2775.66  < 2e-16 ***
s(UTM_E)      8.999  9.000 1054.19  < 2e-16 ***
s(relelev)    8.956  8.999  313.76  < 2e-16 ***
s(Radar_dist) 8.966  9.000 1213.19  < 2e-16 ***
s(dcoast)     3.997  4.000 1498.36  < 2e-16 ***
s(dst_lite_e) 3.963  3.999  102.27  < 2e-16 ***
s(ndvimeanfe) 3.609  3.920  543.71  < 2e-16 ***
s(ndvistdfe)  3.907  3.995  293.25  < 2e-16 ***
s(ag015km)    3.741  3.963  302.82  < 2e-16 ***
s(hwood015km) 1.918  1.993  278.19  < 2e-16 ***
s(pwood015km) 3.941  3.998   54.23  < 2e-16 ***
s(urban015km) 3.979  4.000  159.52  < 2e-16 ***
s(emrsh015km) 3.995  4.000  586.48  < 2e-16 ***
s(hwood01)    3.981  4.000  215.69  < 2e-16 ***
s(pwood01)    3.625  3.920   15.19 3.55e-12 ***
s(urban01)    1.984  2.000   68.33  < 2e-16 ***
s(emarsh01)   1.987  2.000   62.93  < 2e-16 ***
---
Signif. codes:  0 ‘***’ 0.001 ‘**’ 0.01 ‘*’ 0.05 ‘.’ 0.1 ‘ ’ 1

R-sq.(adj) =  0.805   Deviance explained = 80.6%
GCV = 0.15182  Scale est. = 0.15156   n = 49038
```

APPENDIX B.6. Marginal response plots and summary of GAM model fit for **CV VIR during fall of early** years (2000-2002).

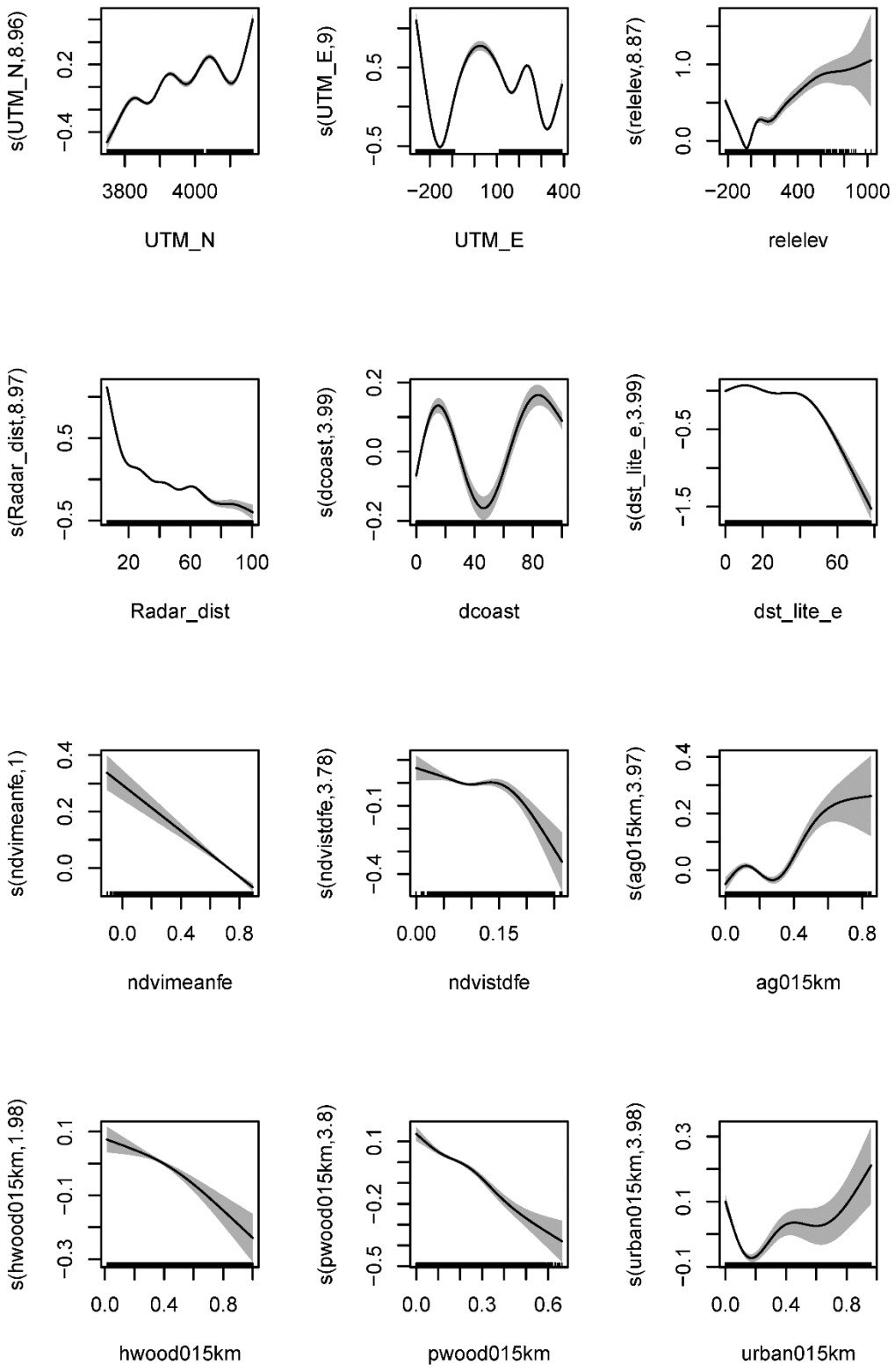

APPENDIX B.6. (continued)

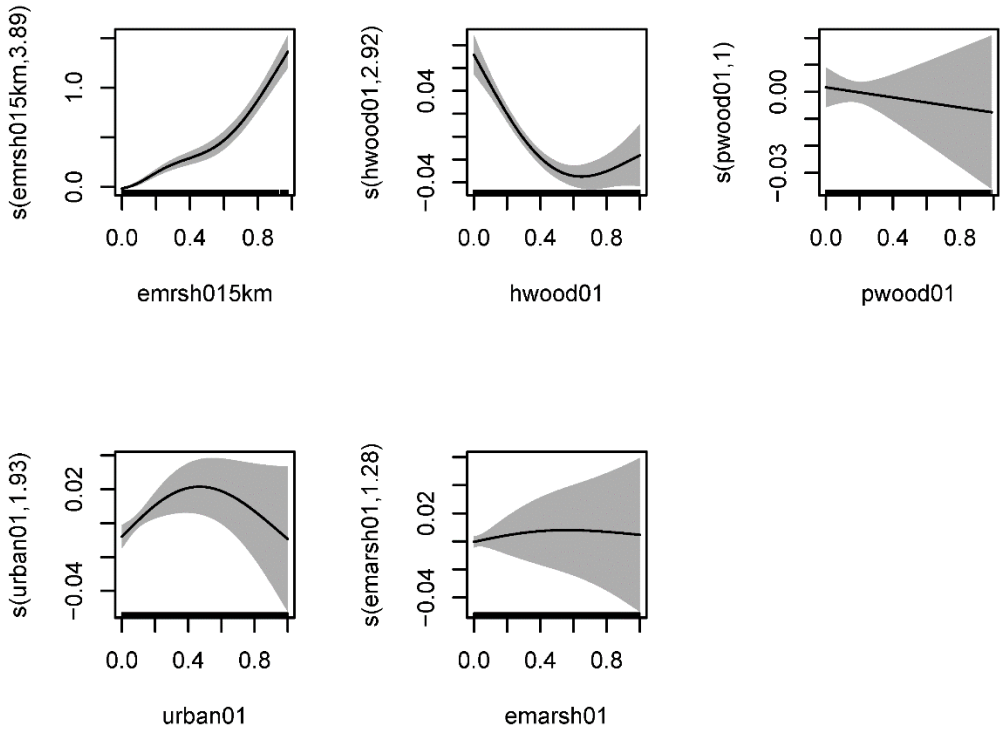

APPENDIX B.6. (continued)

```
Early years fall cv
Family: gaussian
Link function: identity

Formula:
ef_cvros ~ s(UTM_N, k = 10) + s(UTM_E, k = 10) + s(relelev, k = 10) +
    s(Radar_dist, k = 10) + s(dcoast, k = 5) + s(dst_lite_e,
    k = 5) + s(ndvimeanfe, k = 5) + s(ndvistdfe, k = 5) + s(ag015km,
    k = 5) + s(hwood015km, k = 3) + s(pwood015km, k = 5) + s(urban015km,
    k = 5) + s(emrsh015km, k = 5) + s(hwood01, k = 5) + s(pwood01,
    k = 5) + s(urban01, k = 3) + s(emarsh01, k = 3)

Parametric coefficients:
            Estimate Std. Error t value Pr(>|t|)
(Intercept) 1.406249   0.001903     739   <2e-16 ***
---
Signif. codes:  0 ‘***’ 0.001 ‘**’ 0.01 ‘*’ 0.05 ‘.’ 0.1 ‘ ’ 1

Approximate significance of smooth terms:
                edf Ref.df        F  p-value
s(UTM_N)      8.965  9.000  150.060  < 2e-16 ***
s(UTM_E)      8.995  9.000 1082.948  < 2e-16 ***
s(relelev)    8.872  8.995  157.993  < 2e-16 ***
s(Radar_dist) 8.971  9.000  564.803  < 2e-16 ***
s(dcoast)     3.988  4.000  118.532  < 2e-16 ***
s(dst_lite_e) 3.995  4.000  155.721  < 2e-16 ***
s(ndvimeanfe) 1.000  1.000  124.744  < 2e-16 ***
s(ndvistdfe)  3.782  3.974    9.670 4.98e-08 ***
s(ag015km)    3.969  3.999   62.638  < 2e-16 ***
s(hwood015km) 1.981  1.999   20.321 1.26e-09 ***
s(pwood015km) 3.805  3.979   49.933  < 2e-16 ***
s(urban015km) 3.979  4.000   71.638  < 2e-16 ***
s(emrsh015km) 3.894  3.993   74.998  < 2e-16 ***
s(hwood01)    2.917  3.452   31.090  < 2e-16 ***
s(pwood01)    1.000  1.000    0.287  0.59192
s(urban01)    1.929  1.994    5.129  0.00757 **
s(emarsh01)   1.277  1.476    0.304  0.75867
---
Signif. codes:  0 ‘***’ 0.001 ‘**’ 0.01 ‘*’ 0.05 ‘.’ 0.1 ‘ ’ 1

R-sq.(adj) =  0.466   Deviance explained = 46.7%
GCV = 0.17785  Scale est. = 0.17758   n = 49038
```

APPENDIX B.7. Marginal response plots and summary of GAM model fit for **mean VIR during fall of late years** (2013-2014).

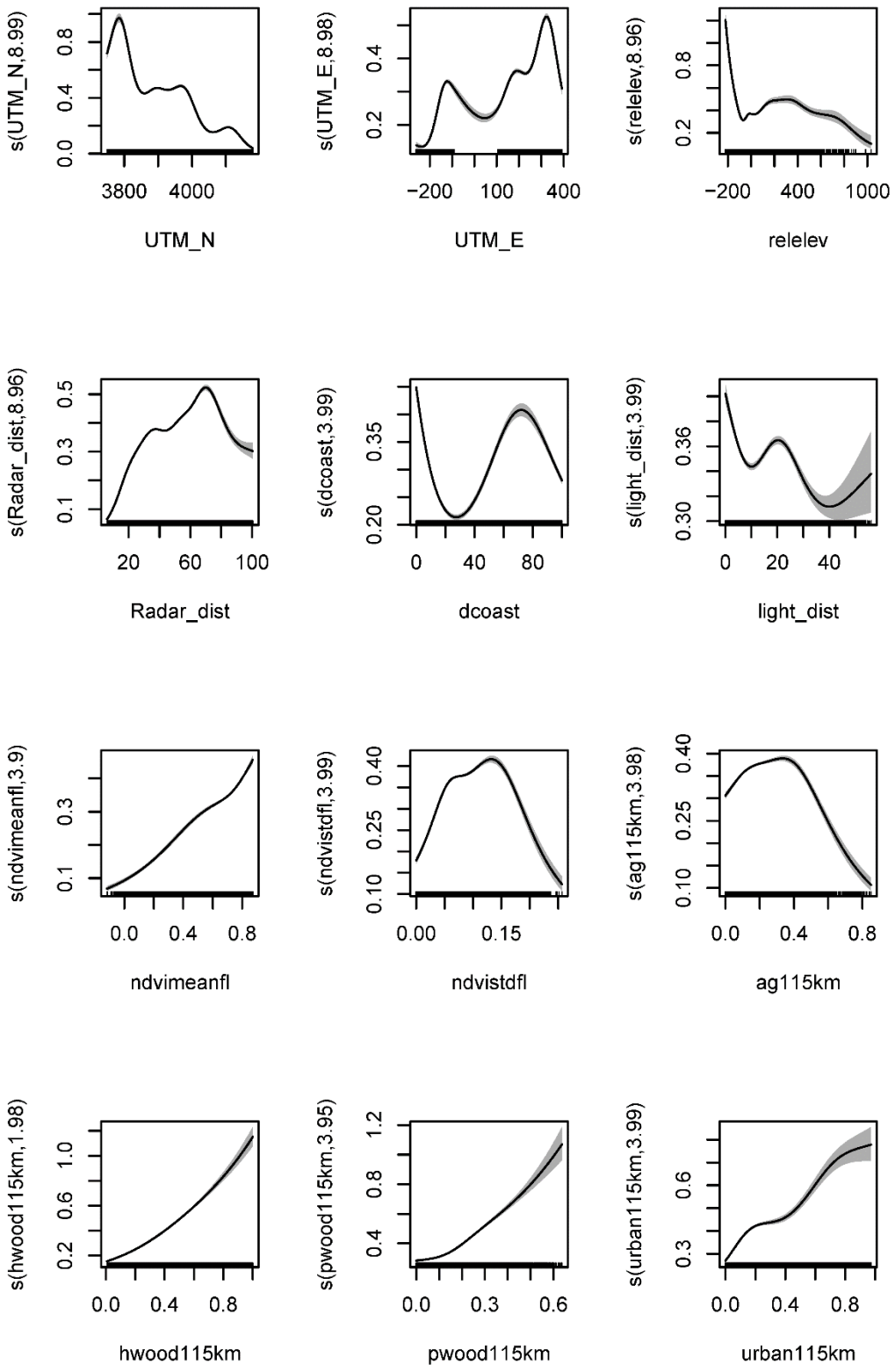

APPENDIX B.7. (continued)

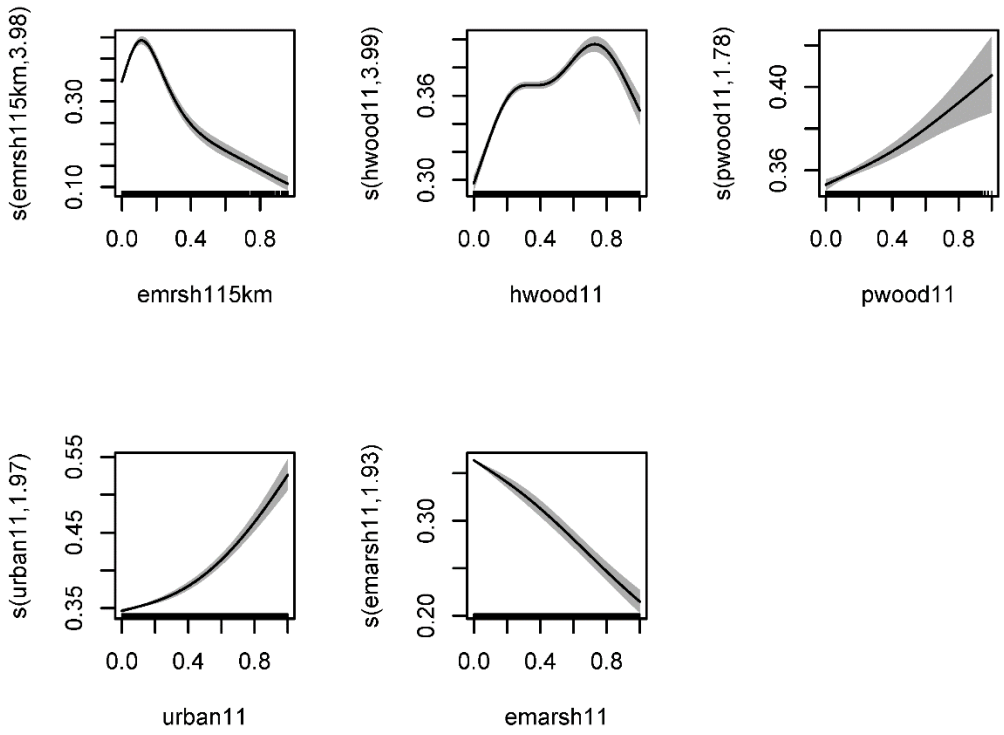

APPENDIX B.7. (continued)

```
Late years fall mean VIR
Family: gaussian
Link function: identity

Formula:
lgeo ~ s(UTM_N, k = 10) + s(UTM_E, k = 10) + s(relelev, k = 10) +
    s(Radar_dist, k = 10) + s(dcoast, k = 5) + s(light_dist,
    k = 5) + s(ndvimeanfl, k = 5) + s(ndvistdfl, k = 5) + s(ag115km,
    k = 5) + s(hwood115km, k = 3) + s(pwood115km, k = 5) + s(urban115km,
    k = 5) + s(emrsh115km, k = 5) + s(hwood11, k = 5) + s(pwood11,
    k = 5) + s(urban11, k = 3) + s(emarsh11, k = 3)

Parametric coefficients:
            Estimate Std. Error t value Pr(>|t|)
(Intercept)  0.17007    0.00177   96.09   <2e-16 ***
---
Signif. codes:  0 ‘***’ 0.001 ‘**’ 0.01 ‘*’ 0.05 ‘.’ 0.1 ‘ ’ 1

Approximate significance of smooth terms:
                edf Ref.df       F  p-value
s(UTM_N)      8.990  9.000 1590.37  < 2e-16 ***
s(UTM_E)      8.983  9.000  879.53  < 2e-16 ***
s(relelev)    8.957  8.999  331.84  < 2e-16 ***
s(Radar_dist) 8.962  9.000 1874.98  < 2e-16 ***
s(dcoast)     3.987  4.000 1218.51  < 2e-16 ***
s(light_dist) 3.985  4.000   77.49  < 2e-16 ***
s(ndvimeanfl) 3.904  3.995  633.60  < 2e-16 ***
s(ndvistdfl)  3.992  4.000  408.37  < 2e-16 ***
s(ag115km)    3.982  4.000  228.68  < 2e-16 ***
s(hwood115km) 1.980  2.000 1478.63  < 2e-16 ***
s(pwood115km) 3.947  3.998  447.19  < 2e-16 ***
s(urban115km) 3.993  4.000  269.32  < 2e-16 ***
s(emrsh115km) 3.981  4.000  322.47  < 2e-16 ***
s(hwood11)    3.986  4.000  145.00  < 2e-16 ***
s(pwood11)    1.781  2.225   23.58 1.17e-11 ***
s(urban11)    1.975  1.999  201.17  < 2e-16 ***
s(emarsh11)   1.928  1.995  184.51  < 2e-16 ***
---
Signif. codes:  0 ‘***’ 0.001 ‘**’ 0.01 ‘*’ 0.05 ‘.’ 0.1 ‘ ’ 1

R-sq.(adj) =  0.715   Deviance explained = 71.5%
GCV = 0.16456  Scale est. = 0.16431   n = 52450
```

APPENDIX B.8. Marginal response plots and summary of GAM model fit for **CV VIR during fall of late** years (2013-2014).

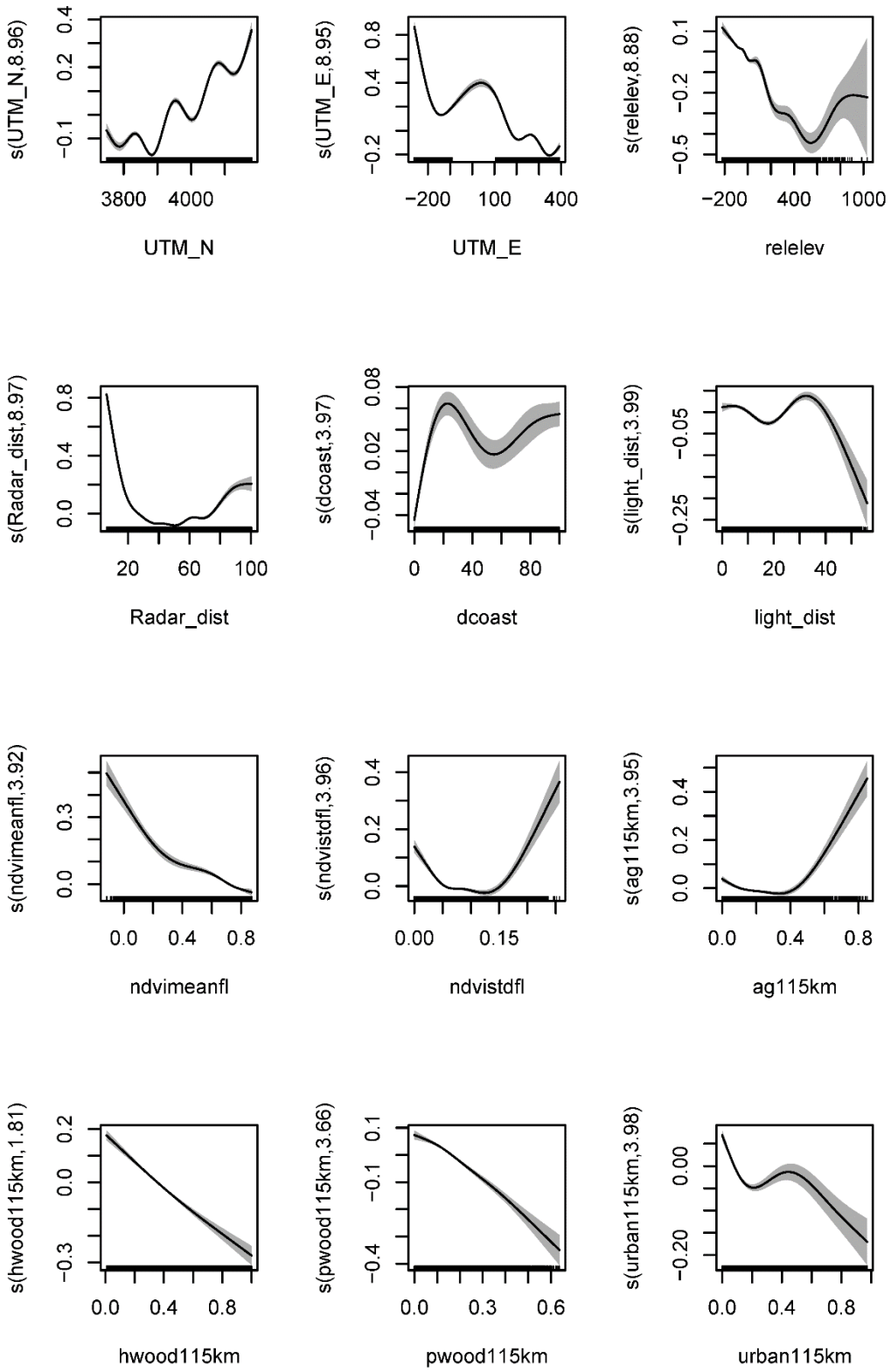

APPENDIX B.8. (continued)

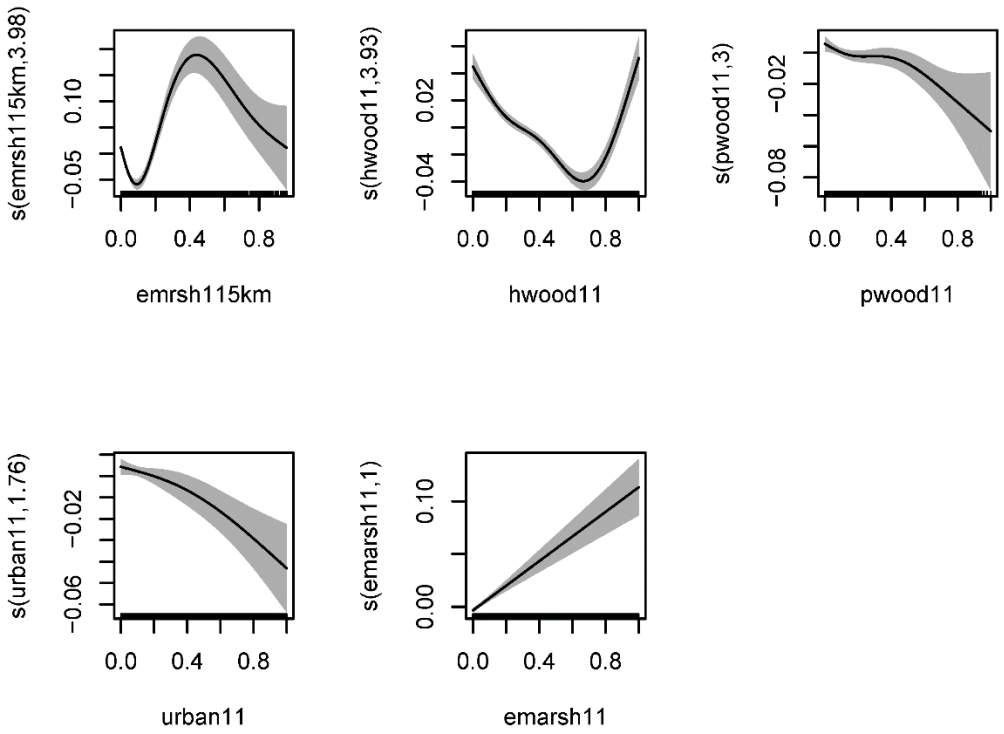

APPENDIX B.8. (continued)

```
Late years fall cv
Family: gaussian
Link function: identity

Formula:
lf_cvros ~ s(UTM_N, k = 10) + s(UTM_E, k = 10) + s(relelev, k = 10) +
    s(Radar_dist, k = 10) + s(dcoast, k = 5) + s(light_dist,
    k = 5) + s(ndvimeanfl, k = 5) + s(ndvistdfl, k = 5) + s(ag115km,
    k = 5) + s(hwood115km, k = 3) + s(pwood115km, k = 5) + s(urban115km,
    k = 5) + s(emrsh115km, k = 5) + s(hwood11, k = 5) + s(pwood11,
    k = 5) + s(urban11, k = 3) + s(emarsh11, k = 3)

Parametric coefficients:
             Estimate Std. Error t value Pr(>|t|)
(Intercept) 1.4441602  0.0009721    1486   <2e-16 ***
---
Signif. codes:  0 ‘***’ 0.001 ‘**’ 0.01 ‘*’ 0.05 ‘.’ 0.1 ‘ ’ 1

Approximate significance of smooth terms:
               edf Ref.df        F  p-value
s(UTM_N)     8.956  8.999  509.582  < 2e-16 ***
s(UTM_E)     8.945  8.999  768.131  < 2e-16 ***
s(relelev)   8.883  8.996   74.480  < 2e-16 ***
s(Radar_dist) 8.965  9.000 1544.133  < 2e-16 ***
s(dcoast)    3.970  3.999   92.113  < 2e-16 ***
s(light_dist) 3.987  4.000   63.283  < 2e-16 ***
s(ndvimeanfl) 3.918  3.996  131.150  < 2e-16 ***
s(ndvistdfl)  3.957  3.999   65.849  < 2e-16 ***
s(ag115km)   3.948  3.998   78.649  < 2e-16 ***
s(hwood115km) 1.807  1.962  245.422  < 2e-16 ***
s(pwood115km) 3.662  3.939  100.993  < 2e-16 ***
s(urban115km) 3.976  4.000   97.268  < 2e-16 ***
s(emrsh115km) 3.976  4.000  107.847  < 2e-16 ***
s(hwood11)   3.935  3.997   75.029  < 2e-16 ***
s(pwood11)   3.000  3.512    4.403 0.002414 **
s(urban11)   1.756  1.939    8.331 0.000184 ***
s(emarsh11)  1.000  1.000   72.230  < 2e-16 ***
---
Signif. codes:  0 ‘***’ 0.001 ‘**’ 0.01 ‘*’ 0.05 ‘.’ 0.1 ‘ ’ 1

R-sq.(adj) =  0.449   Deviance explained =   45%
GCV = 0.049636  Scale est. = 0.049561  n = 52450
```

APPENDIX C. Changes in bird stopover density between early and late years during spring and fall from the KAKQ (Wakefield, VA) radar station.

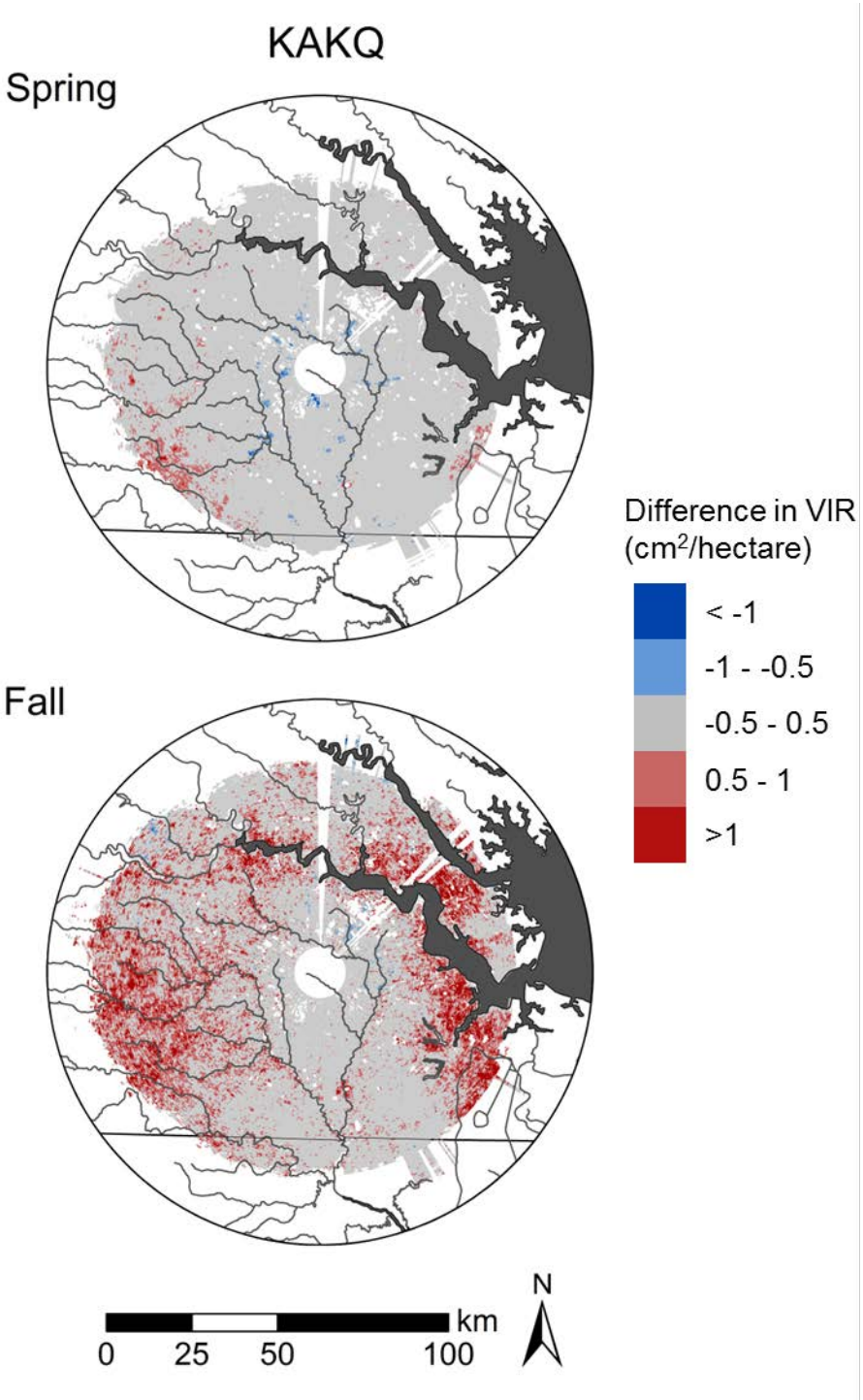

APPENDIX C (continued). Changes in bird stopover density between early and late years during spring and fall from the KGSP (Greer, SC) radar station.

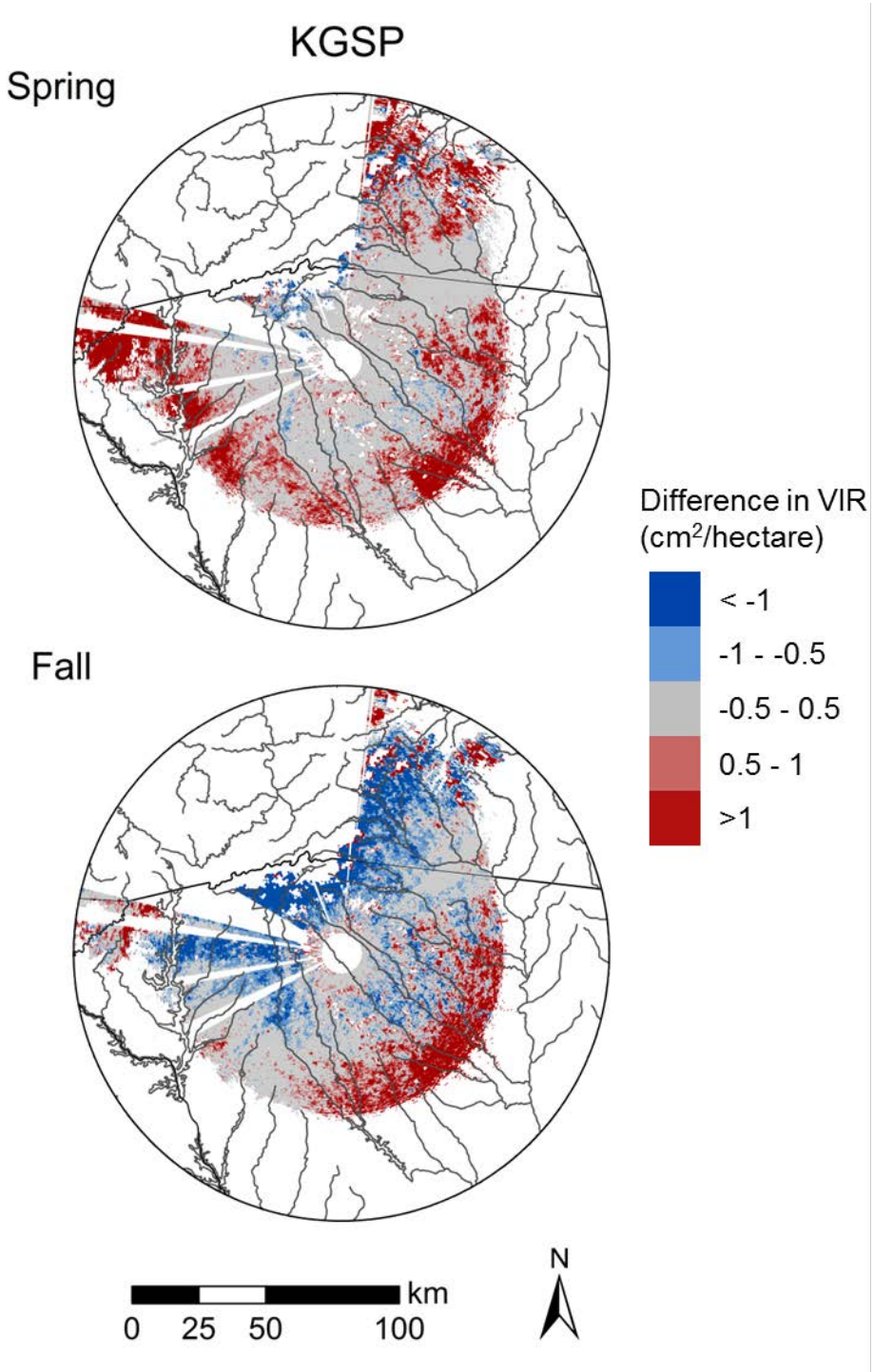

APPENDIX C (continued). Changes in bird stopover density between early and late years during spring and fall from the KLTX (Wilmington, NC) radar station.

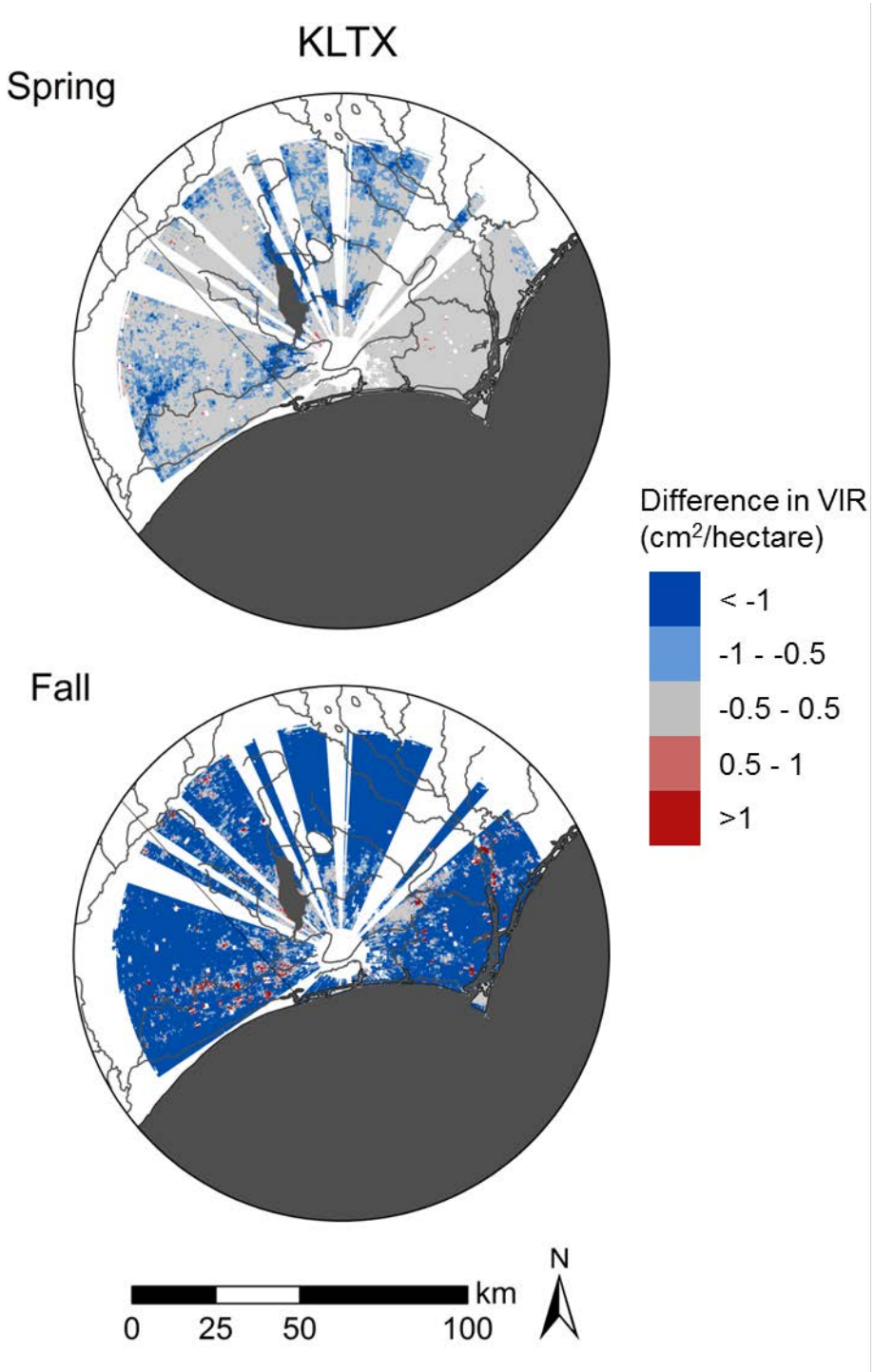

APPENDIX C (continued). Changes in bird stopover density between early and late years during spring and fall from the KMHX (Morehead City, NC) radar station.

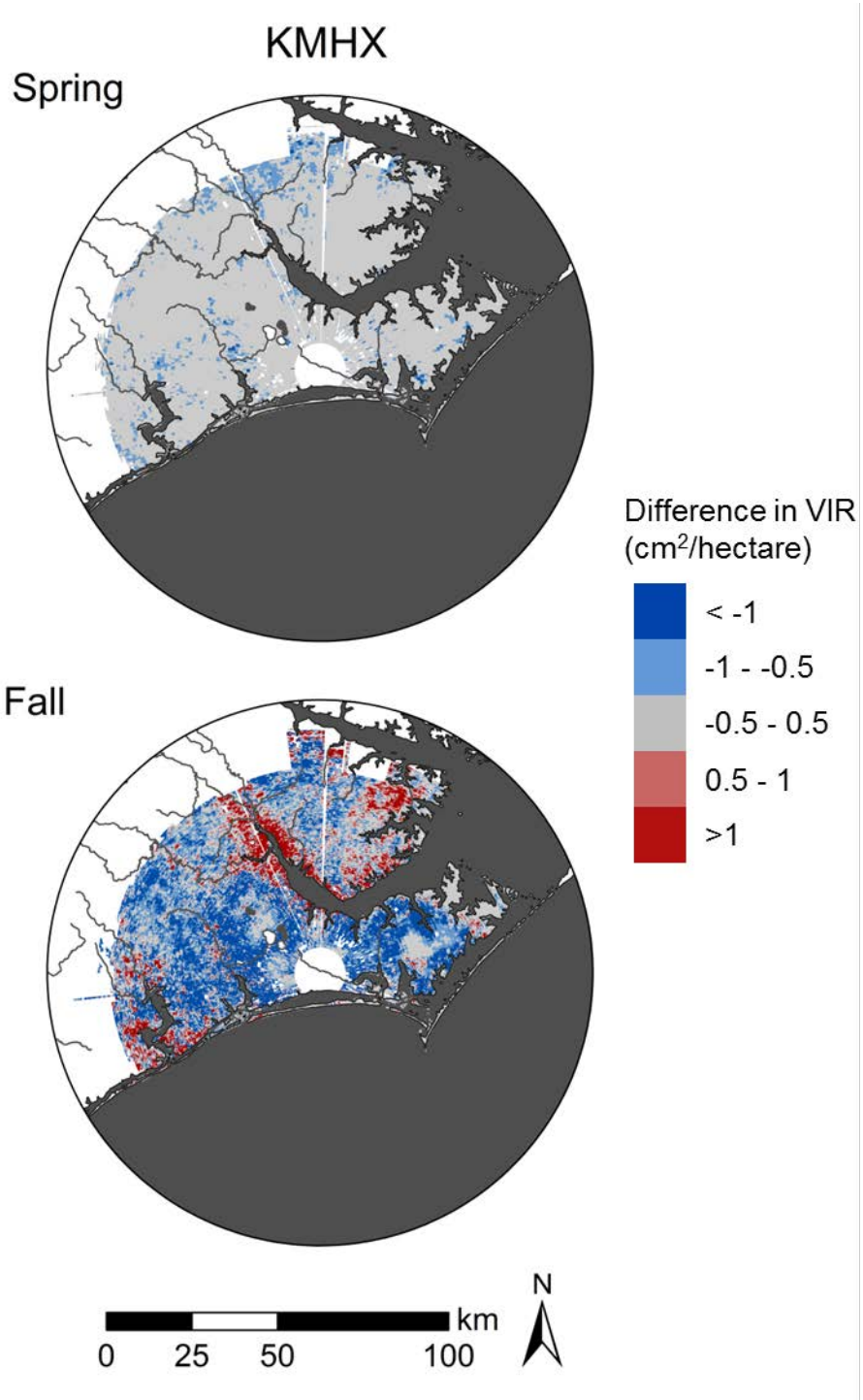

APPENDIX C (continued). Changes in bird stopover density between early and late years during spring and fall from the KRAX (Raleigh, NC) radar station.

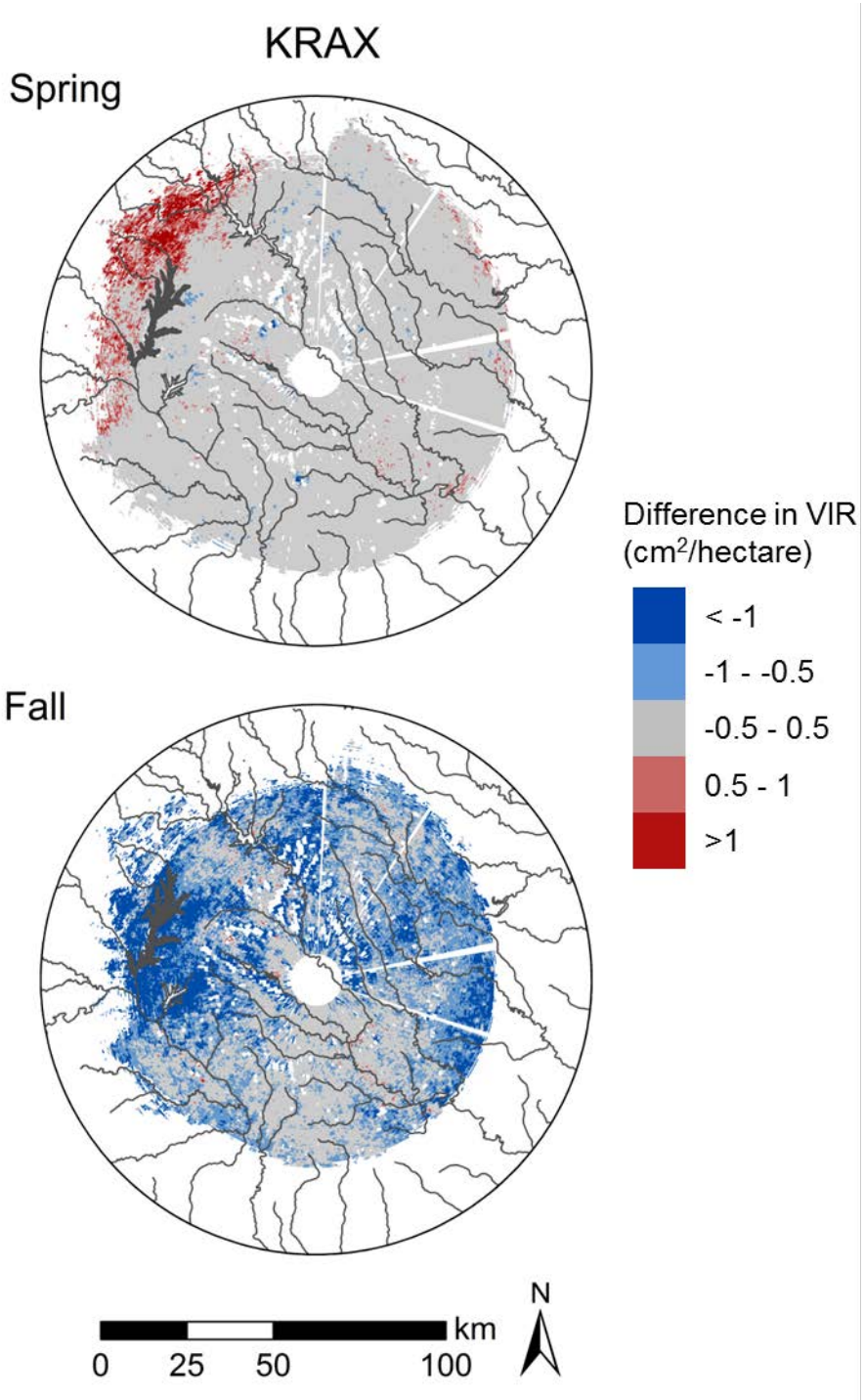

APPENDIX D. Summary of Boosted Regression Tree (BRT) model to predict the change in mean Vertically-Integrated Reflectivity (VIR) within one square kilometer polygons within North Carolina at the onset of nocturnal bird migration for early years (2001-2003) and late years (2013-2015) during **fall** migration. Two series of smoothed marginal response plots are presented for predictors with relative influence above 3%. The first series shows responses across the full range of predictor values. Rug plots on the x-axes denote percentiles at 5% intervals. The second series shows responses for only the inner 90th quantile of predictor values (outer 5% of observations trimmed) so as to eliminate unreliable responses at extreme values of the predictors.

```
GBM STEP - version 2.9

Performing cross-validation optimisation of a boosted regression tree model
for NA and using a family of gaussian
Using 46883 observations and 13 predictors
creating 10 initial models of 100 trees
fitting final gbm model with a fixed number of 900 trees

folds are unstratified
total mean deviance =  3.4132
tolerance is fixed at  0.0034


mean total deviance = 3.413
mean residual deviance = 0.264

estimated cv deviance = 0.54 ; se = 0.021

training data correlation = 0.961
cv correlation =  0.918 ; se = 0.002


                          var    rel.inf
UTM_N                   UTM_N 35.6877702
UTM_E                   UTM_E 19.6003690
dcoast                 dcoast 18.9062146
hwoodchange5km hwoodchange5km  6.3109346
pwoodchange5km pwoodchange5km  4.8577341
urbanchange5km urbanchange5km  3.4387436
diffdistlight   diffdistlight  3.4095799
agchange5km       agchange5km  2.2526413
ndvichangef       ndvichangef  1.6961255
forestchange     forestchange  1.4635988
lightchange       lightchange  1.1359556
urbanchange       urbanchange  0.6462553
agchange             agchange  0.5940777
```

APPENDIX D (continued). Marginal response plots for all observations.

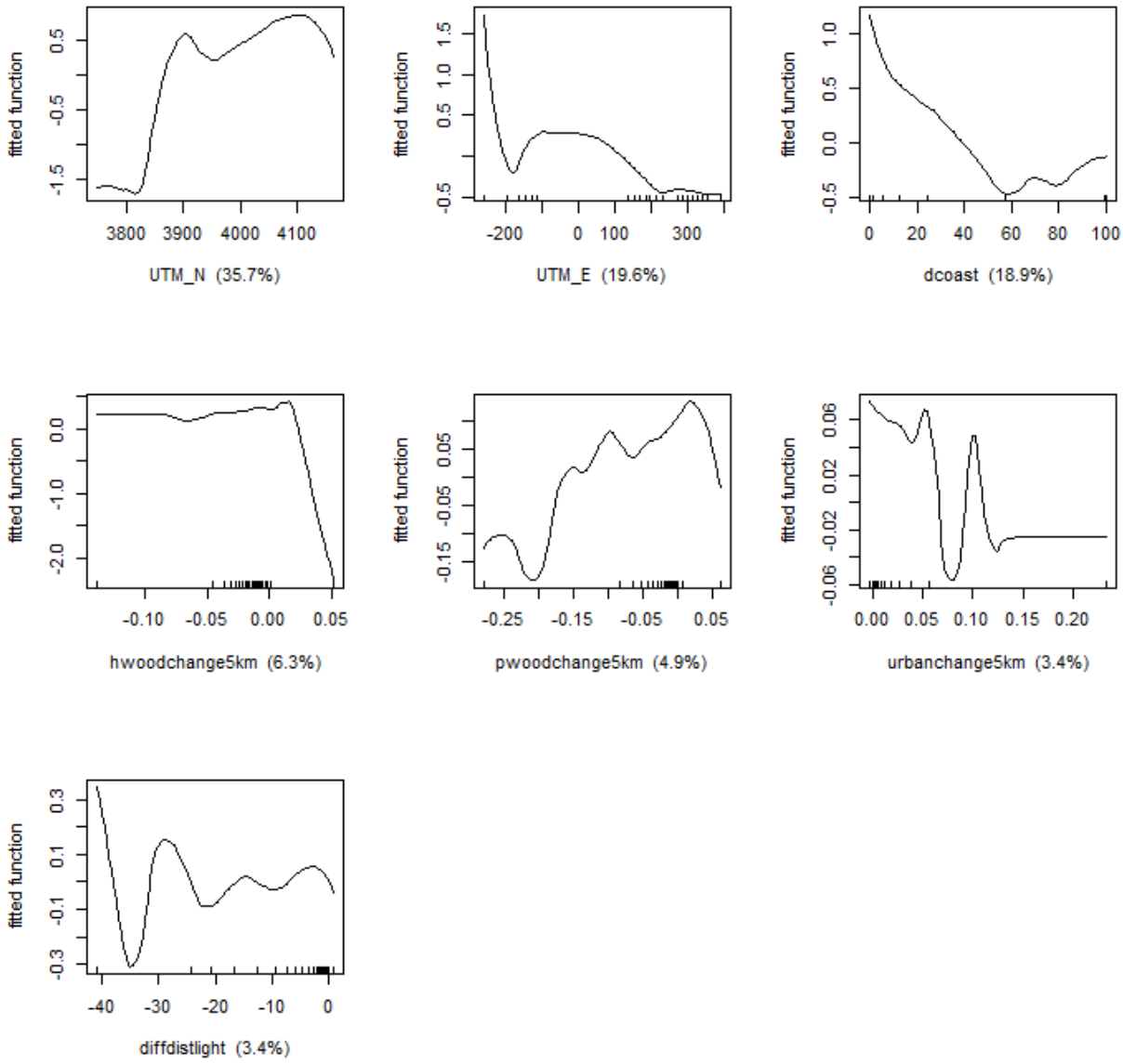

APPENDIX D (continued). Marginal response plots for observations within 90% inner-quantile range of predictor values

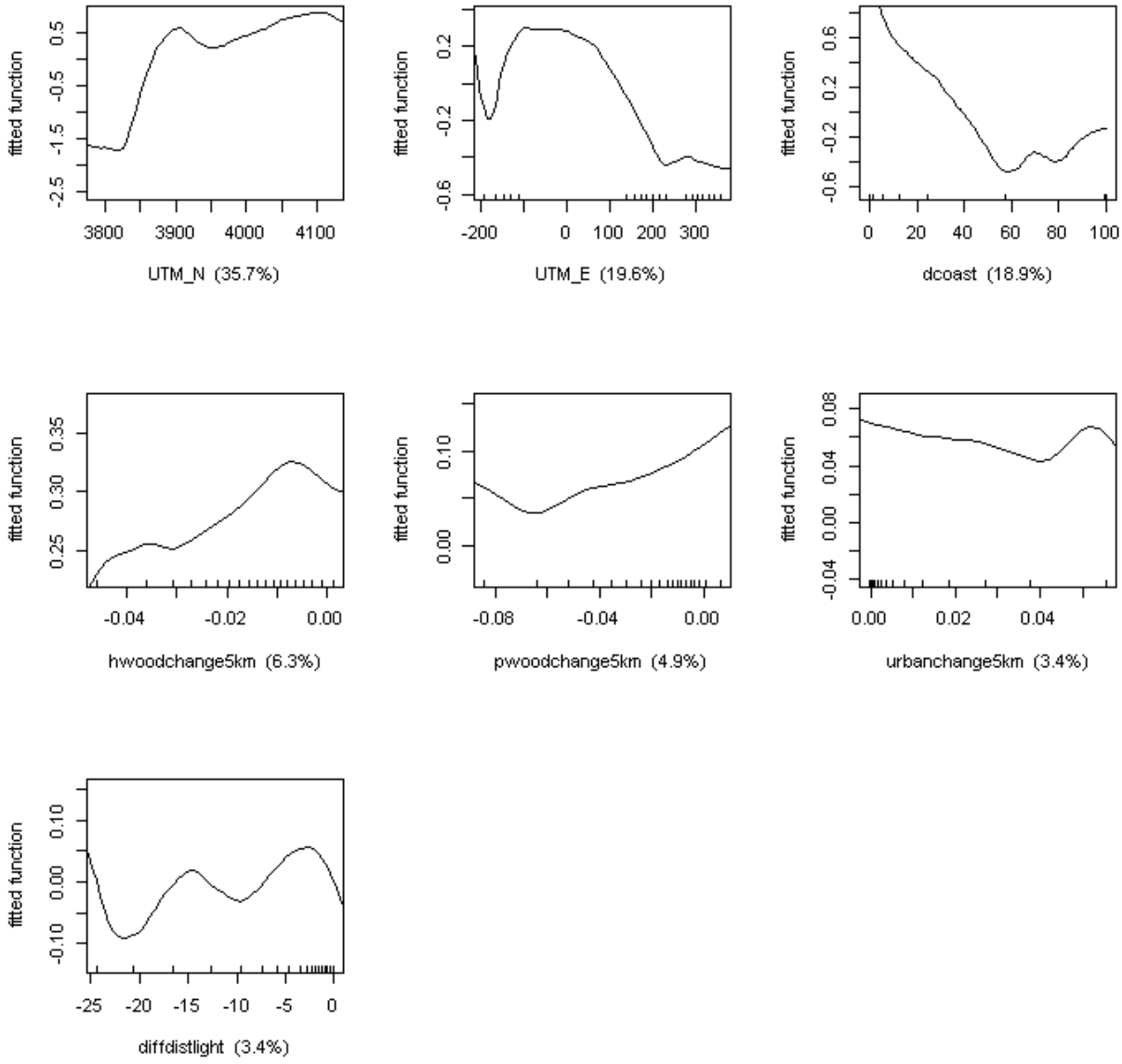

APPENDIX E. Summary of Boosted Regression Tree (BRT) model to predict the change in mean Vertically-Integrated Reflectivity (VIR) within one square kilometer polygons within North Carolina at the onset of nocturnal bird migration for early years (2001-2003) and late years (2013-2015) during **spring** migration. Two series of smoothed marginal response plots are presented for predictors with relative influence above 3%. The first series shows responses across the full range of predictor values. Rug plots on the x-axes denote percentiles at 5% intervals. The second series shows responses for only the inner 90th quantile of predictor values (outer 5% of observations trimmed) so as to eliminate unreliable responses at extreme values of the predictors.

```
GBM STEP - version 2.9

Performing cross-validation optimisation of a boosted regression tree model
for NA and using a family of gaussian
Using 48235 observations and 13 predictors
creating 10 initial models of 100 trees

folds are unstratified
total mean deviance =  0.5209
tolerance is fixed at  5e-04
fitting final gbm model with a fixed number of 1000 trees for NA

mean total deviance = 0.521
mean residual deviance = 0.052

estimated cv deviance = 0.145 ; se = 0.004

training data correlation = 0.948
cv correlation =  0.852 ; se = 0.004

                          var    rel.inf
UTM_E                   UTM_E 35.1320187
UTM_N                   UTM_N 18.3575272
diffdistlight   diffdistlight  8.6230464
pwoodchange5km pwoodchange5km  7.9358741
dcoast                 dcoast  7.0496201
urbanchange5km urbanchange5km  5.2219639
agchange5km       agchange5km  4.8794450
hwoodchange5km hwoodchange5km  4.3861694
ndvichanges       ndvichanges  2.5977010
lightchange       lightchange  1.9001357
forestchange     forestchange  1.8338361
urbanchange       urbanchange  1.1282674
agchange             agchange  0.9543949
```

APPENDIX E (continued). Marginal response plots for all observations

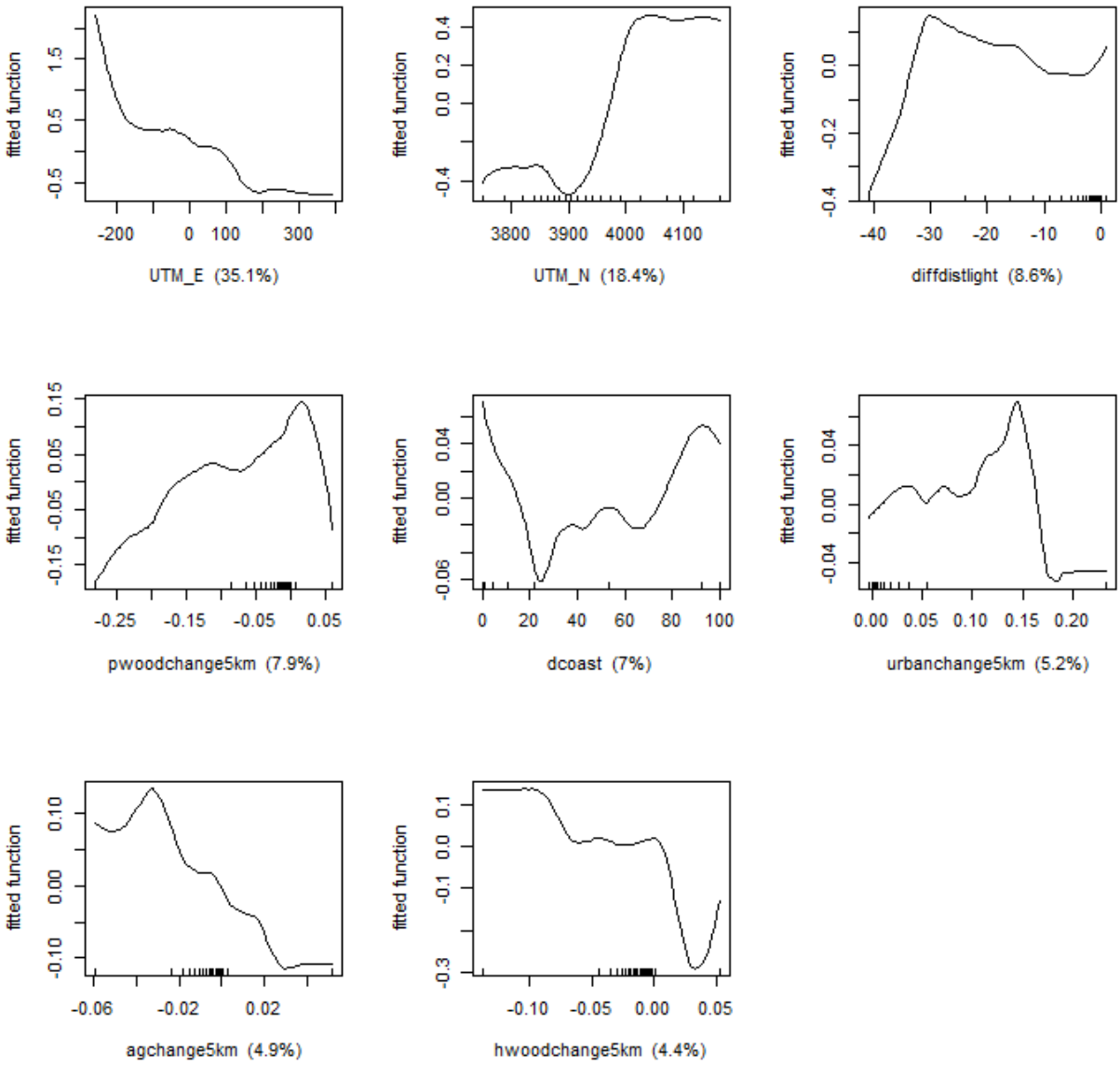

APPENDIX E (continued). Marginal response plots for observations within 90% inner-quantile range of predictor values